

PISTON RING DESIGN FOR REDUCED FRICTION IN MODERN INTERNAL COMBUSTION ENGINES

by

Grant Smedley

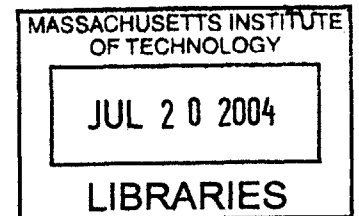
B.Eng., Mechanical Engineering
McGill University, 2002

Submitted to the Department of Mechanical Engineering
in Partial Fulfillment of the Requirements of the Degree of

Master of Science in Mechanical Engineering
at the
Massachusetts Institute of Technology

May 2004

© 2004 Massachusetts Institute of Technology. All rights reserved.



Signature of Author: _____
Department of Mechanical Engineering
May 7, 2004

Certified by: _____
Dr. Tian Tian
Lecturer, Department of Mechanical Engineering
Thesis Supervisor

Certified by: _____
Dr. Victor W. Wong
Lecturer, Department of Mechanical Engineering
Thesis Supervisor

Accepted by: _____
Ain A. Sonin
Chairman, Department Committee on Graduate Studies
Department of Mechanical Engineering

BARKER

(This page was intentionally left blank)

PISTON RING DESIGN FOR REDUCED FRICTION IN MODERN INTERNAL COMBUSTION ENGINES

by

Grant Smedley

Submitted to the Department of Mechanical Engineering
on May 7, 2004 in Partial Fulfillment of the
Requirements for the Degree of Master of Science in
Mechanical Engineering

Abstract

Piston ring friction losses account for approximately 20% of the total mechanical losses in modern internal combustion engines. A reduction in piston ring friction would therefore result in higher efficiency, lower fuel consumption and reduced emissions. The goal of this study was to develop low-friction piston ring designs to improve engine efficiency, without adversely affecting oil consumption, blowby, wear, or cost. These are desirable objectives for today's engine manufacturers as they strive to improve engine performance while trying to meet increasingly stringent emissions regulations.

Using an existing piston ring friction and lubrication model, the main contributors to friction in modern internal combustion engines were identified as the top ring around top dead center of the compression/expansion strokes and the oil control ring throughout the engine cycle. Model predictions indicated that the top ring friction could be reduced by implementing a skewed barrel profile design or an upward piston groove tilt design, and oil control ring friction could be reduced by decreasing ring tension. An increase in groove wear was predicted to occur with the upward piston groove tilt design, which could be eliminated by the introduction of a positive static twist on the top ring. An increase in oil consumption was predicted to occur with the low-tension oil control ring design, which could be mitigated either by the introduction of a negative static twist on the second ring, or by the implementation of the skewed barrel top ring design.

Model predictions indicated that by combining the low-friction designs, a reduction in piston ring pack friction of 30-35% could be achieved, without an increase in blowby, wear, or oil consumption. Experimental results conducted on a full-scale natural gas power generation engine supported the model predictions for the low-tension oil control ring design. The predicted reduction in piston ring friction would translate to a 0.5-1% increase in brake thermal efficiency, which would result in a significant improvement in fuel economy and a substantial reduction in emissions over the life of the engine.

Thesis Supervisors:

Dr. Tian Tian (Lecturer, Department of Mechanical Engineering)

Dr. Victor W. Wong (Lecturer, Department of Mechanical Engineering)

(This page was intentionally left blank)

Acknowledgements

During my time at MIT, I have met a number of people who have contributed to making my experience here rewarding and enjoyable from both a personal and professional standpoint.

First and foremost, I would like to thank my advisors, Dr. Tian Tian and Dr. Victor Wong for their contributions to both my work as well as my personal and professional development throughout my time in the Sloan Automotive Lab. I would like to thank Tian for all of the technical insight he has provided on numerous occasions throughout the duration of the project. I have come to greatly admire his approach to research and the balance that he has been able to achieve between his work and his personal life. I would like to thank Dr. Wong for giving me the opportunity to take on a significant amount of responsibility in our project, and for encouraging me to write technical publications and attend conferences. I believe that these experiences have played an instrumental role in my professional development during my time at MIT.

I would like to thank our project partners, Waukesha Engine, Dresser Inc. and Colorado State University, as well as the members of MIT's Lubrication Consortium for their support and insight in this study. I would also like to acknowledge the United States Department of Energy for their financial support of this program.

I would like to thank several people from the Sloan Automotive Lab who have made technical contributions to my work through numerous useful discussions: Jeff Jocsak, Fiona McClure, Liang Liu, Vince Costanzo, Brian Hallgren, Tiffany Groode, Kevin Lang, Oscar Lopez, and last but certainly not least, Yeunwoo Cho, who has also armed me with some excellent Korean expressions.

I would also like to thank Jean Collin and Mathieu Bernier, who have contributed significantly to my work both in graduate school and throughout my undergraduate education. I consider both their technical and personal advice to have been invaluable throughout the time that we have known each other.

Finally, last but not least, I would like to thank my family for their support throughout my time here, and my girlfriend, Janine Pierce, for giving me a very important reason to be happy that I decided to come to MIT.

(This page was intentionally left blank)

Table of Contents

Abstract.....	3
Acknowledgements	5
List of Figures.....	11
List of Tables	13
1. Introduction.....	15
1.1. Sources of Friction in Modern Internal Combustion Engines	15
1.2. Overview of the Piston Ring-Liner System	15
1.2.1. Description of the Piston Ring-Liner System	15
1.2.2. Typical Piston Ring Designs.....	17
1.2.3. Dynamic Phenomena in the Piston Ring-Liner System.....	19
1.3. Previous Piston Ring Friction Studies	20
1.3.1. Historical Perspective	20
1.3.2. Early Piston Ring Friction and Lubrication Work.....	20
1.3.3. Recent Friction Studies	21
1.4. Objectives and Approach used in the Present Study	23
2. Fundamentals of Friction and Lubrication in the Piston Ring Pack.....	25
2.1. Modes of Lubrication in the Piston Ring-Liner System	25
2.1.1. Pure Hydrodynamic Friction.....	26
2.1.2. Pure Boundary Friction.....	29
2.1.3. Mixed Friction	30
2.2. Governing Equations for Piston Ring Friction and Lubrication	30
2.2.1. The Reynolds Equation.....	30
2.2.2. Radial Force Balance	31
2.2.3. Conservation of Mass	32
2.2.4. Boundary Conditions	32
2.3. Effect of Dynamic Phenomena in the Piston Ring Pack.....	32
2.4. Model Formulation	33
2.4.1. Overview of Modeling Tools.....	33
2.4.2. Solution of Governing Equations.....	34
2.4.3. Additional Modeling Considerations.....	36
3. Primary Sources of Friction in the Piston Ring Pack.....	39
3.1. Effect of Engine Operating Conditions on Sources of Friction.....	39
3.1.1. Modern Internal Combustion Engine Operating Conditions	39
3.1.2. Effect of Engine Speed	40
3.1.3. Effect of Engine Load.....	41
3.1.4. Illustration of Effect of Speed and Load on Piston Ring Friction	42
3.1.5. Effect of Oil Supply on Piston Ring Friction.....	47
3.1.6. Summary of the Effect of Engine Operating Conditions on Piston Ring Friction	53
3.2. Physical Insight into Primary Sources of Friction in High Load, Low Speed Engines.....	55

3.2.1.	Top Ring around TDC of Compression.....	55
3.2.2.	Oil Control Ring Throughout Engine Cycle.....	56
4.	Friction Reduction Strategies	59
4.1.	Top Ring	59
4.1.1.	Skewed Barrel Profile	60
4.1.2.	Top Ring Groove Upward Tilt.....	60
4.1.3.	Reduced Top Ring Axial Height.....	61
4.2.	Oil Control Ring	62
4.2.1.	Reduced Tension Oil Control Ring.....	62
4.3.	Adverse Effects of Reduced Friction Designs	62
4.3.1.	Reduced Ring Life	62
4.3.2.	Increased Top Ring Groove Wear	62
4.3.3.	Increased Oil Consumption.....	63
4.4.	Designs to Compensate for Adverse Effects	64
4.4.1.	Effect of Top Ring Static Twist on Top Ring Groove Wear	64
4.4.2.	Effect of Second Ring Design on Oil Consumption.....	65
4.4.3.	Effect of Oil Control Ring Conformability on Oil Consumption.....	68
4.5.	Additional Design Limitations.....	69
4.5.1.	Manufacturing Limitations	69
4.5.2.	Transition to Boundary Lubrication at Midstroke	69
5.	Application of Reduced Friction Design Strategies to a Natural Gas Power Generation Engine	71
5.1.	Description of Engine and Relevant Specifications.....	71
5.2.	Reduced Friction Designs and Model Predictions.....	72
5.2.1.	Reduced Tension OCR	72
5.2.2.	Skewed Barrel Top Ring.....	73
5.2.3.	Reduced Axial Height Top Ring.....	75
5.2.4.	Upward Top Ring Groove Tilt.....	76
5.3.	Experimental Validation	82
5.3.1.	General Description of Experimental Setup	83
5.3.2.	Description of Instrumentation	84
5.3.3.	Experimental Procedure.....	85
5.3.4.	Variability and Repeatability of Measured Data	87
5.2.5.	Comparison of Pressure Data.....	89
5.3.6.	Baseline Test Results	92
5.3.7.	Results for Reduced Tension Oil Control Ring	93
5.3.8.	Results for Skewed Barrel Top Ring	94
5.3.9.	Results for Combined System.....	96
6.	Further Opportunities for Friction Reduction.....	99
6.1.	Liner Roughness	99
6.2.	Piston Land Height Reduction	100
6.3.	Further Insights into Potential Designs for Reduced Top Ring Friction at Midstroke from Nondimensionalization of Governing Equations	102
7.	Summary and Recommendations.....	109
	References.....	113
	Appendix A: Derivation of Fundamental Equations.....	117

A.1.	Shear Stress Between the Ring and the Liner and Volumetric Flow Rate of Oil	117
A.2.	Derivation of the Reynolds Equation.....	119
Appendix B: Metrics for Evaluating Friction Reduction.....		121
B.1.	Determination of FMEP in the Friction Model.....	121
B.2.	Determination of FMEP from the Experimental Results.....	122
B.3.	Error Analysis of the Experimental Results.....	124
B.4.	Comparison of FMEP between Model and Experiment.....	128
Appendix C: Metrics for Assessment of Results		129
C.1.	Brake Thermal Efficiency.....	129
C.2.	Fuel Cost.....	130

(This page was intentionally left blank)

List of Figures

Figure 1-1: The Piston Ring Pack.....	16
Figure 1-2: Effect of Taper Face Profile on Oil Transport.....	17
Figure 2-1: Typical Lubrication Conditions Encountered by Piston Rings.....	25
Figure 2-2: Hydrodynamic Lubrication Between the Ring and the Liner.....	27
Figure 2-3: Illustration of the Fully-Flooded Inlet Condition.....	28
Figure 2-4: Illustration of the Two Sources of Oil Supply to the Second Ring During Downstrokes	37
Figure 3-1: Friction Power Loss Contributions in the Piston Ring Pack.....	42
Figure 3-2: FMEP Contributions in the Piston Ring Pack.....	43
Figure 3-3: Friction Power Loss Contributions of the Ring Pack at Lower Load Condition.....	44
Figure 3-4: FMEP Contributions of the Ring Pack at Lower Load Condition.....	44
Figure 3-5: Friction Power Losses in the Piston Ring Pack at Low Load, High Speed..	45
Figure 3-6: FMEP Contributions in the Ring Pack at Low Load, High Speed	46
Figure 3-7: Illustration of the Dry Region	47
Figure 3-8: Evolution of the Dry Region.....	49
Figure 3-9: Evolution of the Dry Region with Nonzero Initial Oil Film Thickness.....	51
Figure 3-10: Friction Power Losses in Dry Region with Nonzero Initial Oil Film Thickness	52
Figure 3-11: FMEP Contributions in Dry Region with Nonzero Initial Oil Film Thickness	52
Figure 3-12: Illustration of the Top Ring near TDC of Compression	55
Figure 3-13: Illustration of Effect of Oil Control Ring Tension on Oil Film Thickness.	56
Figure 4-1: Illustration of Skewed Barrel Profile Design.....	60
Figure 4-2: Illustration of Top Ring Upward Groove Tilt Design.....	61
Figure 4-3: Illustration of Reduced Axial Height Design.....	61
Figure 4-4: Effect of Upward Top Ring Groove Tilt.....	63
Figure 4-5: Effect of Top Ring Static Twist.....	65
Figure 4-6: Top Ring Reverse Flutter.....	66
Figure 4-7: Second Ring Collapse	67
Figure 4-8: Second Ring with Negative Static Twist	68
Figure 5-1: Effect of Oil Control Ring Tension on Oil Control Ring FMEP	72
Figure 5-2: Effect of Oil Control Ring Tension on Total Ring Pack FMEP	73
Figure 5-3: Effect of Skewed Barrel Profile on Top Ring FMEP	74
Figure 5-4: Effect of Skewed Barrel Profile on Total Ring Pack FMEP.....	74
Figure 5-5: Effect of Top Ring Axial Height on Top Ring FMEP.....	75
Figure 5-6: Effect of Top Ring Axial Height on Total Ring Pack FMEP	75
Figure 5-7: Effect of Top Ring Groove Upward Tilt on Top Ring FMEP	77
Figure 5-8: Effect of Upward Top Ring Groove Tilt on Top Ring FMEP	77
Figure 5-9: Effect of Groove Tilt on Top Ring Dynamic Twist.....	78
Figure 5-10: Top Ring Moments and Twist	79
Figure 5-11: Illustration of Moments due to Ring-Liner Interaction.....	80

Figure 5-12: Effect of Groove Tilt on Oil Squeezing	81
Figure 5-13: Experimental Setup	84
Figure 5-14: Distribution of IMEP Measurements	88
Figure 5-15: Experimental Pressure Data	90
Figure 5-16: Magnified View of Pressure Data around TDC of Compression	90
Figure 5-17: Comparison of Pressure Data between Model and Experiment	92
Figure 6-1: Effect of Liner Roughness on Total Ring Pack FMEP	100
Figure 6-2: Effect of Land Heights on Total Ring Pack FMEP	101
Figure 6-3: Top Ring Hydrodynamic Friction Map	107

List of Tables

Table 2-1: Summary of Method of Solution of Governing Equations	35
Table 3-1: Summary of Main Contributors to Friction for Different Engine Operating Conditions	53
Table 5-1: Waukesha Engine Specifications	71
Table 5-2: Test Matrix	82
Table 5-3: Results for the Baseline Case	93
Table 5-4: Results for Reduced Tension Oil Control Ring.....	94
Table 5-5: Results for Skewed Barrel Profile Top Ring.....	95
Table 5-6: Results for Combined System	97
Table B-1: Data Summary	126

(This page was intentionally left blank)

1. Introduction

1.1. Sources of Friction in Modern Internal Combustion Engines

Mechanical losses due to friction account for between 4 and 15% of the total energy consumed in modern internal combustion engines [1]. 40-55% of those total mechanical losses occur in the power cylinder [2], and half of the power cylinder friction losses come from friction generated by the piston rings [1,3,4]. As a result, a reduction in piston ring friction has the potential to improve engine efficiency, lower fuel consumption and reduce emissions. These are important objectives for today's engine manufacturers, who are striving to improve engine performance while trying to meet increasingly stringent emission standards.

1.2. Overview of the Piston Ring-Liner System

1.2.1. Description of the Piston Ring-Liner System

The piston ring pack in an internal combustion engine typically consists of three circular rings located in grooves in the piston, as shown in Figure 1-1. The rings move with the piston along the cylinder liner during engine operation. The primary function of the rings is to prevent high-pressure gases from leaking through the piston-liner interface, which would result in power losses. Effective sealing is thus needed between the rings and the liner. However, without lubrication, this close contact between the ring and the liner would result in large friction power losses. As a result, the other main objective of the piston rings is to effectively distribute lubricant along the ring-liner interface, without allowing excessive oil to pass the interface and leak into the combustion chamber where it could be consumed. A third function of the piston rings that is particularly important for the top ring is the dissipation of heat from the piston to the cylinder liner.

In order for the system to effectively achieve these overall objectives, each piston ring has a unique role. The top ring seals the ring-liner interface in order to prevent high-pressure gas from escaping from the cylinder into the lower parts of the ring pack. The oil control ring regulates the amount of oil that passes the ring-liner interface to lubricate the upper rings. A second ring is also present in most engines. This ring scrapes down excessive oil that passes the oil control ring-liner interface. The second ring-groove interface thus provides a barrier against oil flow into the top ring groove from the lower parts of the piston, which reduces oil consumption. Since the second ring only serves to control excess oil that passes the oil control ring-liner interface, its presence is not critical and it may not be used in certain types of engines depending on their purpose. In racing engines where minimizing weight is a critical objective and life expectancy is low, no second ring is used because this reduces the required piston height, decreasing the overall engine weight. In larger diesel engines where long life is desired and high pressures are generally reached in order to provide high torque, reducing oil consumption is a critical objective, and thus two second rings are sometimes used to control oil flow more effectively.

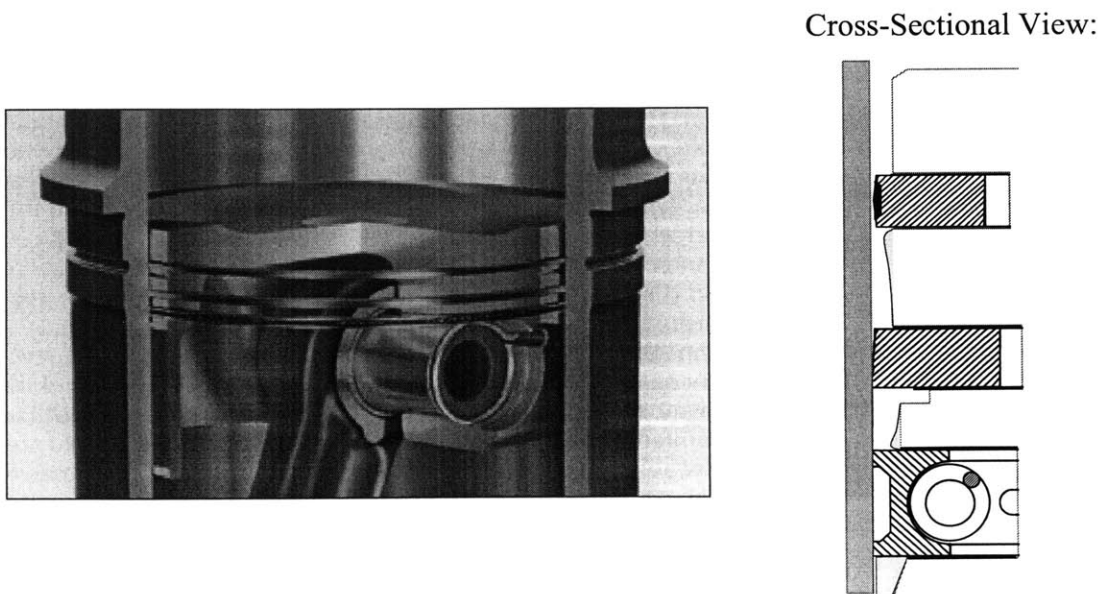


Figure 1-1: The Piston Ring Pack

1.2.2. Typical Piston Ring Designs

As can be seen in Figure 1-1, the cross-section of each of the rings is different. The different designs reflect the unique purpose of each of the rings.

The top two rings are designed with a diameter that is larger than the size of the cylinder bore in which they are to be installed. They are made with a gap in their circumference so that they can be compressed to fit into the cylinder bore during installation. Once they are installed, their own tension allows them to maintain an effective seal against the liner.

The top ring has a barrel-shaped face profile, which has been shown to be most effective for lubrication [5]. Sufficient lubrication is critical for the top ring as it is subjected to the high cylinder pressures, which can result in large radial forces acting on the back of the ring. If there is no lubrication between the top ring and the liner, large contact pressures can be generated, and this can result in significant wear and an increase in the top ring gap over time. This will result in higher power losses due to the larger amount of high-pressure gases in the cylinder that can escape through the larger gap.

The second ring, also called the scraper ring, has a tapered face so that it cannot accumulate oil on its upper edge to scrape it in the upward direction towards the combustion chamber. However, it can very effectively accumulate oil on its lower edge to scrape it down toward the crankcase to prevent excessive oil from reaching the top ring. This idea is illustrated below in Figure 1-2.

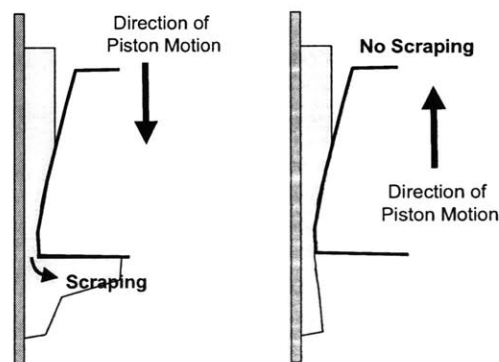


Figure 1-2: Effect of Taper Face Profile on Oil Transport

The design of the oil control ring is quite different from that of the compression rings. There are several design variations that exist for different types of engines. The focus of this study was on the twin-land oil control ring, which is typically used in large diesel engines. This ring consists of a spring mounted inside two rails to ensure adequate conformability to the liner. The circumferential length of the spring determines the tension of the oil control ring once installed in the cylinder bore. The high tension force from the ring on the liner created by the spring is necessary to achieve adequate conformability when thermal and mechanical deformation of the cylinder bore occurs during engine operation. The design takes advantage of the high unit pressure exerted on the oil film by the large tension force acting on the small lands, which results in a reduction in oil film thickness, controlling oil more effectively. Two lands are used because it is believed that at least one of the lands will control oil at any given time in the engine cycle, depending on the relative angle between the ring and the liner.

The rings are manufactured with different materials depending on the type of engine in which they are to be installed. In larger diesel engines, the rings are typically made of ductile cast iron due to the high thermal stability of the material, which makes it suitable to the high operating temperatures in these engines. Steel is the more popular material for rings to be used in smaller gasoline engines because it is stronger than cast iron, and therefore, the size of the rings can be reduced and conformability improved without a reduction in ring life. Cast iron ring faces are typically coated with a chrome layer for wear reduction, although considerable research is currently being devoted to the identification and development of materials and face coatings for reduced friction and wear [2,4]. Some studies have been conducted in which steel rings were investigated for larger diesel engines [6]. These rings showed promise for use in this type of engine, except for temperature limitations and some significant wear observed with certain steel materials used in articulated pistons.

The function and performance of the piston rings is significantly affected by the dynamics of the piston ring-liner system. These dynamic phenomena are introduced in the section that follows.

1.2.3. Dynamic Phenomena in the Piston Ring-Liner System

There is a small clearance between the rings and their respective piston grooves, which is present as a result of manufacturing tolerances in the ring and groove axial heights.

Although this clearance is only on the order of 100 microns, it can cause strong gas flows and create significant pressure differences. The gas dynamics and pressure variations throughout the engine cycle cause the rings to undergo significant axial lift and twist relative to their grooves. These ring dynamics play an important role in the determination of the amount of oil between the rings and the liner as well as the amount of friction generated between them.

Several other factors also affect ring-liner lubrication as well as the ability of the rings to seal the ring-liner interface. Bore distortion occurs because of mechanical stresses and thermal expansion due to the temperature gradient along the liner in the direction of piston motion. This overall bore distortion is comprised of radial expansion and circumferential out-of-roundness, and it is therefore a complex 3-D phenomenon that can significantly affect the conformability of the piston rings to the liner. Ring-liner lubrication is also significantly affected by the asymmetric geometry of the crank and connecting rod. As a result of this asymmetry and the various forces encountered during the engine cycle, the piston will tend to tilt about the axis of the piston pin throughout the engine cycle, which will affect angle between the ring and the liner.

The dynamics that arise due to the clearances between the ring and the grooves, combined with bore distortion and piston tilt, ultimately determine the ring-liner relative angle. This angle significantly affects the lubrication between the ring and the liner, and the friction generated by their interaction. The link between these dynamic phenomena and piston ring friction and lubrication is discussed in more detail in Chapter 2.

1.3. Previous Piston Ring Friction Studies

1.3.1. Historical Perspective

Sealing the interface between the piston and the cylinder bore has been a challenge since the advent of the internal combustion engine. Significant advances were made in this area during the development of the steam engine, when James Watt bolted a tightly packed hemp matrix to the piston in order to prevent high-pressure gas leakage. It was not until 1797 that Rev. Edward Cartright proposed the use of metallic rings in place of the shorter-lasting hemp gasket. However, methods to ensure adequate sealing using these metal rings required complex assemblies, which typically involved springs mounted in elaborate configurations. In the mid 19th century, John Ramsbottom proposed an ingeniously simple design that would eliminate all need for such complex assemblies. Ramsbottom's ring was designed to be 10% greater in diameter than the cylinder in which it would be installed, so that its own elasticity could be used to seal the piston-liner interface. By the 1920's, these metallic Ramsbottom rings were used extensively, and there was no real need for further development in this area because of the mild operating conditions of internal combustion engines at the time. However, as internal combustion engine performance continued to improve, sealing and heat transfer became more important issues, and efforts were needed to optimize the ring designs for minimal friction and wear. In addition, adequate oil control became a more critical objective, as the system required a sufficient amount of lubricant in order to withstand the harsher environment. More detailed piston ring friction and lubrication studies thus began [7].

1.3.2. Early Piston Ring Friction and Lubrication Work

In 1935, Hawkes and Hardy identified fundamental nature of lubrication along the piston stroke. Specifically, their study revealed the predominant modes of lubrication throughout the different parts of the engine cycle [7]. In 1960, Faro-Barros and Dyson expanded on this work and measured friction force variation along the stroke length,

which confirmed this trend. This work was supported by Furhama et al. in the 1950's with his movable bore experiment [3].

In 1979, Rohde, Whitaker and McAllister studied the effect of piston ring design variables on friction. Specifically, they investigated the effect of varying the face profile and ring tension on friction and oil film thickness. Their assumed ring profile was very different than the parabolic profile assumed today, but this was necessary to allow them to carry out numerical computations. Their study also ignored some important effects and assumed lubrication conditions that were not entirely realistic. Nevertheless, it was one of the first studies of its kind and was an important contribution to this field [8]. In 1982, Kovach et al. ranked major contributors to friction in the engine using motored friction results and showed that the largest contributors were the piston and piston rings. They also suggested reducing tension and optimizing the face profile of the rings to further reduce friction [3]. In a comprehensive review paper released in 1985, Ting identified the optimization of ring pack design to minimize friction and oil losses without compromising sealing efficiency as an area for further study [3]. Several such studies would follow.

1.3.3. Recent Friction Studies

In 1984, Hill and Newman initiated a project to develop reduced friction piston rings. Based on some simple analysis, they determined five design features that could be altered to reduce friction, which included axial width, surface pressure, number of rings, effective face profile of the rings and geometry of the ring and bore. They found that rings with a smaller axial width reduced friction, but this friction reduction was accompanied by a reduction in axial stiffness. Different materials were investigated to compensate for this effect, but they found that steel rings (the leading candidate) suffered from side face wear from the aluminum piston grooves. They concluded that surface pressure should be reduced for low-friction, but that this would result in higher levels of oil consumption and blowby. They developed a simple expression in which

conformability was shown to be inversely proportional to radial width cubed, and therefore this factor was deemed most important for the purposes of maximizing conformability. They left the ring profile, bore macrogeometry, and the 2-ring set design for future investigation [4].

In 1992, Jeng developed two models for piston ring lubrication analysis, incorporating realistic boundary conditions and oil transport predictions. In this work, he also performed a parametric study to examine the effects of some engine parameters on tribological performance. Specifically, he considered the effect of the bore-stroke ratio, surface roughness, ring tension, ring-groove position, ring offset, ring crown height (barrel drop), and ring width on friction. His results were largely qualitative (only power loss graphs were shown, and no specific quantitative results were given), and were not validated experimentally [9].

In 1995, Nakada et al. released a study that focused on surface treatments to reduce friction and wear. He also suggested removing one ring to reduce friction. As in the previous study, no significant quantitative conclusions were drawn in his work [2].

In 1997, Cullen and Frodsham investigated reduced cross-section compression rings made of steel rather than cast iron. They found that steel rings with a significantly larger free gap could be used because of the higher strength of steel compared to cast iron. The larger free gap increased ring tension, improving conformability of the ring to the liner. They also found that ring radial width should be minimized to reduce the ring's moment of inertia and to improve conformability. Friction was reduced by implementing a skewed barrel profile on the top ring. They measured lower oil consumption and blowby in several test conditions using the new ring designs. They noted that steel could not be used if top ring temperature exceeded 260°C due to the higher thermal relaxation resistance of steel compared to cast iron [6].

In 1998, Richardson reviewed several methods for reducing friction that had been investigated by different companies and research institutions. He also reviewed models

that were being developed and methods for measuring friction. He specifically investigated the effect of using a skewed barrel profile, a larger barrel drop, reduced ring width, and the combination of these on friction. He did not investigate the manufacturing feasibility of barrel drops or skewed barrel profiles. In this work, no real quantitative conclusions were drawn, as only the reduction of the peak value of friction power loss was given [1].

In 2000, Tomanik et al. performed a study in which they reduced oil ring tension such that unit pressure decreased from 1.1 to 0.8 N/mm². This resulted in a 30% reduction in friction power losses according to predictions from a Ricardo friction model. Unfortunately, their experimental work focused on a combination of several changes for reduced friction (including bearings, etc.), and therefore they did not isolate the effect of the individual changes implemented to reduce friction for the purposes of comparison with the model [10].

From these most relevant studies, it can be clearly seen that most of the previous work has focused exclusively on reduction of piston ring friction, and relatively little emphasis has been placed on ensuring that other adverse effects are minimized. This is due to the complexity of these concomitant effects, which has prevented the development of accurate models to predict these effects quantitatively.

1.4. Objectives and Approach used in the Present Study

The goal of the present study was to develop designs to reduce piston ring friction, without increasing oil consumption, blowby, and wear. Achieving this objective was facilitated to a great extent by the use of the extensive modeling tools developed at MIT over the past decade. An experimental evaluation of the designs was also conducted to validate the model predictions and to evaluate certain effects that could not be predicted quantitatively by the model. The use of this combined approach with the goal of developing an optimized piston ring pack in which friction is reduced without adverse

effects on oil consumption, blowby and wear, is what distinguishes this work from many of the previous studies that have been conducted in this area.

It should also be emphasized that efforts were focused on developing designs that would not increase cost or introduce any need for major modification of current engine components. As a result, changes in ring materials, the introduction of face coatings, and changes in the type of lubricant used in the engine were considered to be outside the scope of the present study and were not considered as a result.

The following approach was used this study. The modeling tools developed at MIT were first used to identify the primary sources of friction in the piston ring packs of modern internal combustion engines. Reduced friction design strategies were then developed and model predictions were obtained for the friction reduction potential of each of the designs. The design strategies were then applied to redesign the piston rings of a large-bore natural gas power generation engine. The reduced friction rings were manufactured and tested on the full-scale natural gas engine in the Engine and Energy Conversion Lab at Colorado State University to validate the model predictions.

Chapter 2 presents an overview of the fundamentals of friction and lubrication in the piston ring pack, and introduces the modeling tools that were used in this study. Chapter 3 details the application of the modeling tools to identify the primary sources of friction in the piston ring pack. Chapter 4 presents several general design strategies to reduce piston ring friction. In Chapter 5, these general strategies are applied to redesign the piston rings in a Waukesha natural gas power generation engine, and model predictions and experimental results are obtained to predict the performance of these new ring designs. Chapter 6 presents several potential areas for future investigation, and a complete summary of this study as well as future recommendations are given in Chapter 7.

2. Fundamentals of Friction and Lubrication in the Piston Ring Pack

2.1. Modes of Lubrication in the Piston Ring-Liner System

Due to the variation in oil supply to the different piston rings throughout the engine cycle, each ring encounters different modes of lubrication while traveling along the liner. If a sufficient amount of oil exists on the liner to support a load, hydrodynamic lubrication conditions are present. Otherwise, the load from the ring on the liner is supported by contact between the asperities on the two surfaces and boundary lubrication conditions are said to be present. As will be seen in later sections, these modes of lubrication have a profound effect on the magnitude of the friction force generated by the motion of the rings along the liner.

A schematic of a typical lubrication condition between the ring and the liner is shown below in Figure 2-1. As can be seen in the figure, due to the roughness of the surfaces in contact, it is possible for certain portions of the two surfaces to have asperity contact and for other parts to be sufficiently lubricated such that the ring is supported by the load from the oil film. To simplify this situation, the modes of lubrication are typically characterized by the spacing between nominal lines that define smooth surfaces representing the average of the asperities.

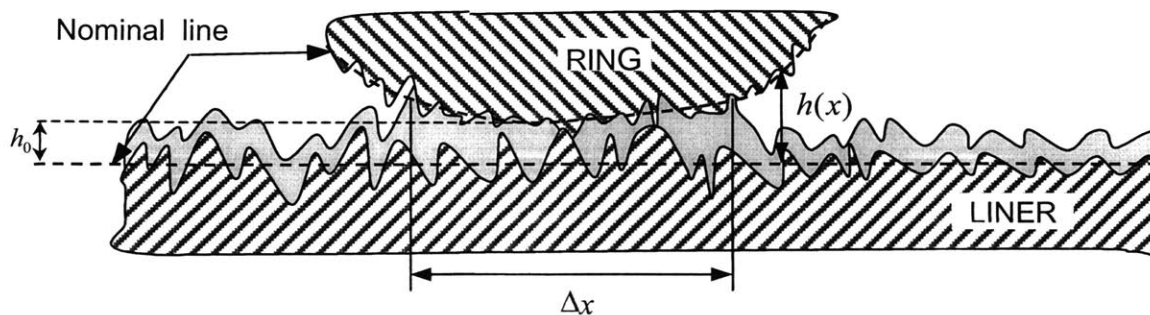


Figure 2-1: Typical Lubrication Conditions Encountered by Piston Rings

Depending on the distance between the nominal lines, $h(x)$, three different modes of lubrication are possible:

- a) Pure Hydrodynamic Lubrication
- b) Mixed Lubrication
- c) Pure Boundary Lubrication

In pure hydrodynamic lubrication, a sufficient amount of oil separates the two surfaces such that there is no asperity contact between them. The transition from pure hydrodynamic lubrication to mixed lubrication occurs when the following criteria is met:

$$\frac{h}{\sigma} < 4 \quad (2.1)$$

where $\sigma = \sqrt{\sigma_{ring}^2 + \sigma_{liner}^2}$ is the combined roughness between the ring surface and the liner [11]. In mixed lubrication, there is oil between the two surfaces in contact, but there is also portion of the ring and liner surfaces between which the spacing is sufficiently small that Eq. (2.1) is satisfied, and therefore these parts of the surfaces are also considered to be in boundary contact. The transition between mixed lubrication and pure boundary lubrication occurs when the wetting between the ring and the liner completely disappears, and there is therefore no more oil between the ring and the liner.

The method for the determination of the friction force in each of these lubrication conditions is outlined in the sections that follow.

2.1.1. Pure Hydrodynamic Friction

In this mode of lubrication, the oil supports the load from the ring on the liner, and therefore the amount of friction generated by the ring-liner interaction depends on the properties of the lubricant as well as the film height and width under the ring surface. Determining the friction force thus requires solving coupled equations governing the fluid mechanics of the lubricant and the forces acting on the ring.

The system under consideration is shown in Figure 2-2. In the most general case, the unknowns are the minimum oil film thickness h_0 , the inlet wetting coordinate x_1 and the outlet wetting coordinate x_2 (the profile of the ring surface is assumed to be known, in which case once h_0 is known, $h(x)$ is also known). It should be noted that although there appears to be a transitional region in which oil attaches to the ring and detaches from the ring at x_1 and x_2 , respectively, it was shown in [11] that if viscous diffusion is the method of attachment, this region is of negligible axial width compared to the axial width of the ring, B , and can thus be neglected.

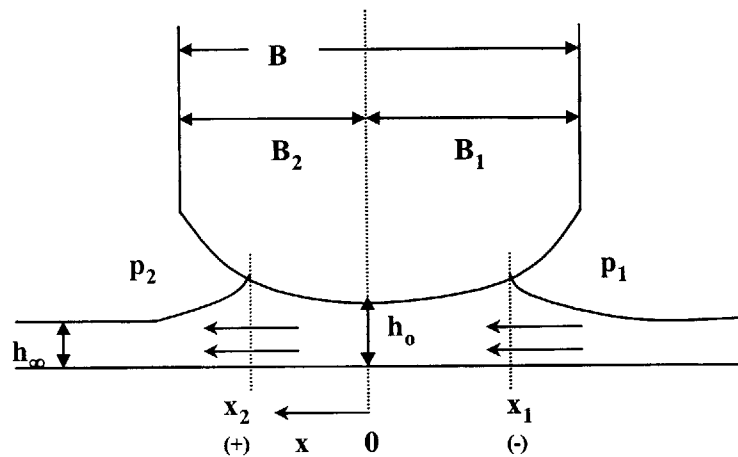


Figure 2-2: Hydrodynamic Lubrication Between the Ring and the Liner

In the most general case, three equations are needed to solve for the unknowns. One equation comes from consideration of conservation of mass and conservation of momentum applied to the oil film under the ring surface. This equation relates the pressure gradient in the oil film to its height and width. A second comes from a radial force balance on the system. A third equation comes from either application of mass conservation on the oil film assuming that the oil supply h_∞ is known, or from an empirical condition for the pressure gradient at the outlet. These governing equations are derived in detail in Section 2.2.

The number of unknowns may be reduced depending on the wetting condition at the leading edge or trailing edge of the ring running surface. The wetting condition describes

the point on the ring running surface at which the oil attaches and detaches. The following possible wetting conditions exist:

- a) Fully-flooded inlet and outlet
- b) Fully-flooded inlet and partially-flooded outlet
- c) Partially-flooded inlet and fully-flooded outlet
- d) Partially-flooded inlet and outlet

Fully-flooded conditions occur when there is an excess of oil available to fit under the ring, as illustrated below in Figure 2-3 (for fully-flooded inlet).

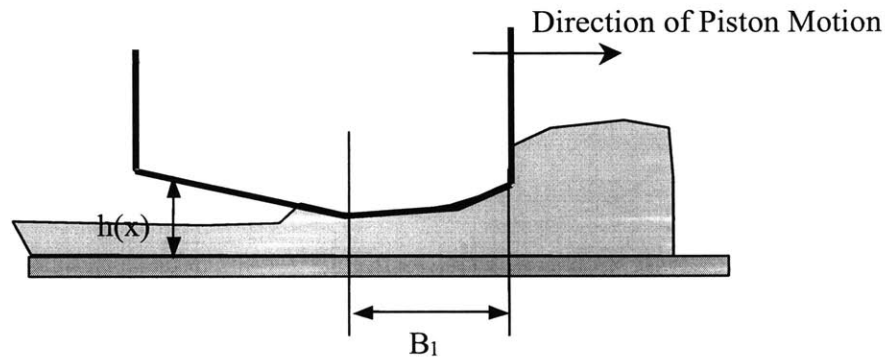


Figure 2-3: Illustration of the Fully-Flooded Inlet Condition

For this condition, $x_1 = -B_1$ and there are thus only two unknowns in the problem (x_2 and h_0). The fully-flooded outlet condition is defined analogously, and also involves only two unknowns as well (x_1 and h_0). In partially-flooded conditions, there is an insufficient amount of oil supply to the ring to completely fill the space between the ring and the liner, and therefore the point of attachment (or detachment) of the oil film is somewhere underneath the ring running surface rather than at its edge.

In the general case where partially-flooded conditions are present at both the leading edge and the trailing edge, the friction between the ring and the liner is determined as follows:

$$F_f = \int_{x_1}^{x_2} \tau dx$$

The shear stress, τ , appearing in the above equation is defined by Eq. (A.5) and is derived in detail in Appendix A. Using Eq. (A.5), the friction force can be expressed as a function of the oil film height and width:

$$F_f = \int_{x_1}^{x_2} \left(\frac{\mu U}{h} - \frac{h}{2} \frac{dp}{dx} \right) dx \quad (2.2)$$

Therefore, once the oil film height and width are determined from the solution of the governing equations, the friction force from hydrodynamic lubrication can be determined.

2.1.2. Pure Boundary Friction

Pure boundary friction occurs when no oil exists between the ring and the liner, and therefore the load from the ring on the liner is completely supported by asperity contact. Since there is no oil between the ring and the liner, $x_1=x_2=0$, and therefore the only unknown in the problem is h_0 , which can be determined using a radial force balance. This will be shown in detail in Section 2.2.

In this case, the friction force is given by the following expression:

$$F_f = \int_{x_{c1}}^{x_{c2}} a_{asp} p_c dx \quad (2.3)$$

where a_{asp} is the friction coefficient governed by the surface properties, x_{c1} and x_{c2} define the boundaries of the portion of the ring-liner surfaces that are in asperity contact according to Eq. (2.1), and p_c is the contact pressure between the two surfaces. The contact pressure is given by the following empirical fit used by Hu [12] based on Greenwood-Tripp's theory [13]:

$$p_c = K_c \left(4 - \frac{h}{\sigma} \right)^z \quad (2.4)$$

where K_c depends on asperity and material properties and z is a correlation constant described in [12].

2.1.3. Mixed Friction

As would be expected, the friction between the ring and the liner in mixed lubrication is the sum of the contributions from pure hydrodynamic and pure boundary friction. Mixed friction is thus calculated as follows:

$$F_f = \int_{x_1}^{x_2} \tau dx + \int_{x_{c1}}^{x_{c2}} a_{asp} p_c dx \quad (2.5)$$

2.2. Governing Equations for Piston Ring Friction and Lubrication

In this section, the governing equations describing piston ring friction and lubrication that were introduced briefly in the previous section will be developed in detail. The method of solution of these equations will then be outlined for the different wetting conditions that can be present throughout the engine cycle. The solution of the governing equations yields the unknowns that are required to determine the friction force between the ring and the liner according to the equations derived in the previous section.

2.2.1. The Reynolds Equation

The Reynolds Equation relates the height, width and shape of the oil film between the ring and the liner with the pressure gradient that is generated therein. A detailed derivation of the 2-D Reynolds Equation for incompressible lubricants can be found in Appendix A. In the present study, a quasi 2-D approach is used in which the parameters defining ring-liner lubrication are determined at specific circumferential locations on the piston, and the Reynolds Equation thus reduces to a 1-D form at each of these locations. Eq. (A.9) thus becomes:

$$\frac{\partial}{\partial x} \left(\frac{h^3}{\mu} \frac{dp}{dx} \right) = 6U \frac{\partial h}{\partial x} + 12 \frac{\partial h}{\partial t} \quad (2.6)$$

To further simplify this equation, the terms in Eq. (2.6) can be scaled as follows:

$$U \frac{\partial h}{\partial x} \sim LN \left(\frac{h}{B} \right)$$

$$\frac{\partial h}{\partial t} \sim hN$$

where N is the engine speed in rev/s, L is the stroke length, h is the oil film thickness under the ring, U is the piston velocity, and B is the axial height of the ring. Comparison of the above terms yields:

$$\frac{\frac{\partial h}{\partial t}}{U \frac{\partial h}{\partial x}} \sim \frac{B}{L} \ll 1$$

Therefore, the unsteady term in the Reynolds Equation can be neglected everywhere in the cycle except near dead centers where the piston velocity U becomes very small. With this simplification, valid in all parts of the cycle other than at end-strokes, Eq. (2.6) reduces to:

$$\frac{\partial}{\partial x} \left(\frac{h^3}{\mu} \frac{dp}{dx} \right) = 6U \frac{\partial h}{\partial x} \quad (2.7)$$

2.2.2. Radial Force Balance

A radial force balance on the ring shown in Figure 2-2 yields:

$$\sum F_r = p_1(B_1 + x_1) + \int_{x_1}^{x_2} p(x) dx + p_2(B_2 - x_2) - p_1(B_1 + B_2) - W = 0 \quad (2.8)$$

Setting Eq. (2.8) to zero assumes that the system is quasi-static in the radial direction, which has been shown to be a reasonable assumption in previous work in this area [11].

It should be noted that within the integral term, the asperity contact pressure p_c given in Eq. (2.4) should be added to $p(x)$ wherever the condition given by Eq. (2.1) is met and boundary lubrication conditions are present.

2.2.3. Conservation of Mass

In partially-flooded conditions, conservation of mass can be applied to the oil at the inlet of the ring surface as depicted in Figure 2-2. The following expression is obtained:

$$Q(x_1) = Uh_\infty \quad (2.9)$$

$Q(x_1)$ is derived in Appendix A and is given by Eq. (A.6). This equation is not valid for the fully-flooded cases because the oil entering or exiting the ring in those cases may be in excess and therefore does not have a uniform velocity at a height of h_∞ as implied in Eq. (2.9).

2.2.4. Boundary Conditions

Values for the pressures at the inlet and outlet of the oil film are assumed to be known:

$$\begin{aligned} p(x_1) &= p_1 \\ p(x_2) &= p_2 \end{aligned} \quad (2.10)$$

If the outlet is partially-flooded, the Reynolds exit condition has been shown to be valid [11]:

$$\frac{dp}{dx}(x_2) = 0 \quad (2.11)$$

This equation does not apply at the end strokes because of the small piston velocity. In these regions of the cycle, another exit condition is needed, which accounts for the unsteadiness of the inlet or exit point of oil attachment. This condition is only applicable a few crank degrees from the end-stroke regions, and is discussed in detail in [11].

2.3. Effect of Dynamic Phenomena in the Piston Ring Pack

As discussed in Section 1.2.3, the dynamics of the piston ring-liner system have a considerable effect on the lubrication conditions between the ring and the liner, and the friction generated by their interaction. Several dynamic phenomena have a significant impact on the relative angle between the ring and the liner, which alters the position of

the point on the ring running surface that is closest to the liner (hereafter referred to as the minimum point). If the position of the minimum point changes, the amount of space available for oil to fit between the ring and the liner will change, and therefore the friction and lubrication conditions will also change.

In general, the ring-liner relative angle is the sum of the contributions due to ring static twist, ring dynamic twist, piston tilt, groove tilt, and bore distortion. These effects vary around the circumference of the ring due to the asymmetry introduced by the presence of the ring gap. All of these effects must be taken into account in order to determine the lubrication and friction between the ring and the liner.

2.4. Model Formulation

2.4.1. Overview of Modeling Tools

The determination of the friction and lubrication conditions between the ring and the liner, taking into account the dynamic effects discussed in the previous section, requires the simultaneous solution of the system of nonlinear equations that were derived in Section 2.2. This calculation cannot be performed analytically. It is further complicated by the roughness of the surfaces of the ring and the liner that must be taken into account through the introduction of flow factors in the governing equations [14]. In addition, the oil supply to a given piston ring depends on the oil film thickness left on the liner by the passage of the previous ring during the engine cycle, and therefore mass conservation must be preserved between the three rings in the piston ring pack to accurately model the system. These requirements necessitated the development of modeling tools in order to predict the performance of the piston ring pack for a given set of design parameters.

Such a set of modeling tools were developed by T. Tian in the Sloan Automotive Lab at MIT over the past decade. Since their initial development, the models have been tested and applied extensively to a wide range of engine types and sizes, from large-bore heavy-

duty diesel engines to Formula one racing engines. This section contains a brief description of the aspects of the models that are most relevant to the present study. A more complete description of these models and their capabilities can be found in [11,15,16].

2.4.2. Solution of Governing Equations

The model solves the governing equations derived in the previous section at each crank angle of the engine cycle, for each of the rings. The link between the equations and unknowns for each combination of inlet and outlet conditions is briefly summarized in this section.

It should be noted that the governing equations derived in Section 2.2 and the equations used to solve for the unknowns in the model are slightly different. In the model, the volumetric flow rate of the oil at the trailing edge of the ring is introduced as an additional unknown. This allows the use of Eq. (A-6) instead of the Reynolds Equation. The two methods are entirely equivalent, and the introduction of the flow rate as an additional unknown replaces the additional integration constant that would need to be determined if the Reynolds Equation were used. This can be seen by the appearance of the derivative of the pressure distribution in the Reynolds Equation, which requires that this equation be integrated once before being combined with any of the other equations to solve for the unknowns. In Eq. (A-6), the pressure distribution does not appear as a derivative, and this equation can therefore be directly combined with the other equations to solve for the unknowns. It should also be noted that the averaged forms of Eq. (A-4) and Eq. (A-6) were used in the model. These averaged forms take into account the roughness of the surfaces using the approach mentioned in Section 2.1 and by the inclusion of flow factors as mentioned in the previous section. Derivations of the averaged forms of these governing equations can be found in [14].

Table 2-1 below contains a description of the method of solution of the governing equations for the different inlet and outlet conditions that are encountered. It should be noted that there is an additional case that is not considered here for simplicity. In the model, the exit condition near the end of the strokes takes into account the unsteadiness of the wetting location, and the unsteady terms cannot be eliminated from the Reynolds Equation as they were in Eq. (2.7). In addition, it should be noted that the model actually uses equations that include flow factors to account for the roughness of the surfaces of the ring and the liner. Finally, the model accounts for the dynamic twist of the piston rings, which alters the ring-groove relative angle and therefore the position of the minimum point on the ring running surface. A more complete description of all of these specific aspects of the model can be found in [11,15,16].

Inlet/Outlet Conditions	Unknown(s)	Method of Solution
Fully-flooded inlet Fully-flooded outlet	h_o	<ul style="list-style-type: none"> Integrate Eq. (2.7) once, yielding an unknown constant Express $p(x)$ in Eq. (2.8) as dp/dx by integrating by parts, then substitute in the result of the integration of Eq. (2.7) Integrate Eq. (2.7) once more, using boundary conditions given by Eq. (2.10), and combine the result with the above equation to solve for the unknown constant and h_o simultaneously
Partially-flooded inlet Fully-flooded outlet	x_1, h_o	<ul style="list-style-type: none"> Apply the approach for the fully-flooded inlet and outlet case The additional equation which is needed to solve for the additional unknown comes from Eq. (2.9) and Eq. (A.6)
Fully-flooded inlet Partially-flooded outlet	x_2, h_o	<ul style="list-style-type: none"> Follow the approach for the fully-flooded inlet and outlet case, but use Eq. (2.11) after the first integration of Eq. (2.7) to solve for the unknown constant
Partially-flooded inlet Partially-flooded outlet	x_1, x_2, h_o	<ul style="list-style-type: none"> Follow the approach for the fully-flooded inlet, partially-flooded outlet case The additional equation which is needed to solve for the additional unknown comes from Eq. (2.9) and Eq. (A.6)

Table 2-1: Summary of Method of Solution of Governing Equations

In two of the cases considered, solving the governing equations requires that the oil film thickness on the liner, $h_{o\infty}$, be known. Mass conservation is thus preserved between the three rings so that the oil left on the liner by the passage of the previous ring is the oil supply to the ring that follows. The calculations must therefore be performed in a specific order in the model. The oil control ring is first considered for an entire engine cycle, assuming that it is fully-flooded on both the upstroke and the downstroke. This is used to establish an initial estimate for the oil film thickness on the liner. There is a region on the liner in which the piston travels, but where the oil control ring cannot reach (between top dead center of the top ring and top dead center of the oil control ring as illustrated in Figure 3-7 in Section 3.2.1). In this region, no oil is initially assumed to be present. Following the initial determination of the liner oil film thickness based on the fully-flooded oil control ring, the calculation subsequently considers each ring in succession, with the order depending on whether or not the piston is traveling in an upstroke or downstroke. On downstrokes, the oil supply to the second ring is what is left on the liner by the oil control ring, and similarly for the top ring. On upstrokes, the oil supply to the top ring is what the top ring leaves behind on the previous downstroke.

2.4.3. Additional Modeling Considerations

There is an uncertainty in the model that significantly affects the calculated friction and lubrication conditions between the ring and the liner. In actual engine operating conditions, the oil supply to the second ring during downstrokes comes from both the oil control ring-liner interface and any oil that might be accumulated on the third land of the piston. Oil transport on the third land on the piston is the subject of considerable research at this time, and as a result, the amount of oil accumulated on the third land at any moment in the engine cycle is not known exactly [17,18]. As a result, the approach taken in this study was to consider two oil supply conditions as upper and lower bounds for the actual oil supply to the second ring during downstrokes, as was done by Tian in [19]. The upper bound case for oil supply, hereafter referred to as OS1, considers the second ring to be fully-flooded during downstrokes, which is the maximum possible oil supply

that could be provided to the second ring. The lower bound case, hereafter referred to as OS2, considers the second ring to be supplied by the oil control ring-liner interface only, and assumes no oil accumulated on the third land of the piston. These two conditions were used in this study when exploring different potential piston ring designs in order to bracket the true oil supply and therefore the true magnitude of the friction force generated between the ring and the liner. The two oil supply sources are illustrated below in Figure 2-4.

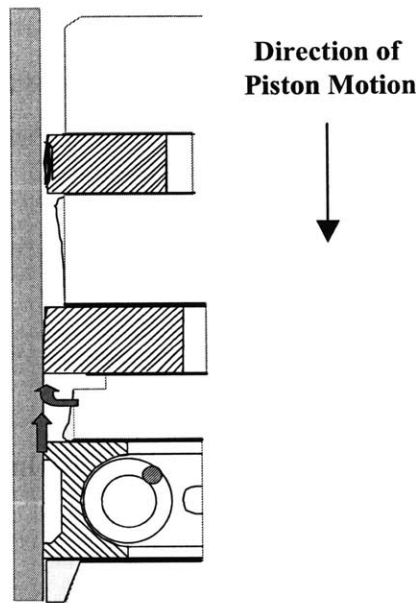


Figure 2-4: Illustration of the Two Sources of Oil Supply to the Second Ring During Downstrokes

The model was used extensively in this study to predict the performance of the piston ring pack in terms of friction and lubrication for different ring designs. This model facilitated the identification of the primary sources of friction in the piston ring pack of modern internal combustion engines, which is the subject of the Chapter 3, as well as the development of reduced friction designs, which is discussed in detail in Chapters 4, 5 and 6.

(This page was intentionally left blank)

3. Primary Sources of Friction in the Piston Ring Pack

In this Chapter, the primary sources of friction in the piston ring pack are identified. Since the results depend on the operating conditions of the engine under consideration, this Chapter begins with an investigation of the effect of engine operating conditions on friction in the piston ring pack. The primary sources of friction are then identified for the different operating conditions, and physical insight is provided to explain why these are the largest sources of friction.

3.1. Effect of Engine Operating Conditions on Sources of Friction

3.1.1. Modern Internal Combustion Engine Operating Conditions

Modern internal combustion engines operate in a variety of speed and load conditions depending on their application. In passenger cars and larger transport trucks, loads and speeds vary considerably due to the variety of driving conditions encountered. Racing engines typically operate at high speeds and high loads. Stationary power generation engines operate in high load, low speed conditions because the high load generates more power and the low speed is needed to interface with the electric generator and the power grid.

Both engine speed and load affect the friction generated between the piston rings and the liner. In addition, oil supply plays a very important role in ring-liner lubrication. In the sections that follow, these effects are analyzed separately and general trends are then developed for the dominant contributors to piston ring friction in the different engine operating conditions.

3.1.2. Effect of Engine Speed

The effect of engine speed on the friction generated between the piston rings and the liner can be seen from the relations developed in Chapter 2 and Appendix A. In Eq. (A.5), the second term involving the pressure gradient integrated over the wetted width typically ends up resulting in a much smaller contribution than the first term. Therefore, friction scales roughly as follows:

$$F_f \sim \frac{\mu U}{h} B \quad (3.1)$$

where h is the oil film thickness and B is the ring axial width. The minimum oil film thickness can be related to the piston velocity through the following scaling relationship derived from Eq. (2.7):

$$h \sim \sqrt{\frac{\mu UB}{p}} \quad (3.2)$$

where p is the pressure in the oil film, which is assumed to be a sole function of x as shown in [11]. Combining Eq. (3.1) and Eq. (3.2), it can be seen that the friction power loss scales with piston speed as follows:

$$P_f \sim \mu^{1/2} U^{3/2} \quad (3.3)$$

The viscosity term is included in this relationship because it depends on the piston speed. The extent of this dependence varies according to the type of oil under consideration. In the case of multigrade oils, which are considered to be shear-thinning fluids, the viscosity is controlled by the shear rate, which depends directly on the piston speed, as explained in Appendix A. As piston speed increases, the viscosity will decrease, and therefore the net effect of these changes on friction power loss is the result of a compromise between them.

For a single grade oil, the viscosity of the oil depends only on its temperature, which is controlled primarily by the temperature distribution along the liner. As piston speed increases, the liner temperature may increase, causing a reduction in lubricant viscosity. Therefore, for the case of single grade oils, friction power losses only increase with

higher engine speeds if the reduction in lubricant viscosity does not offset the increase in piston speed.

It should be noted that Eq. (3.3) is only valid for hydrodynamic or mixed lubrication. The dependence of friction power loss on piston velocity would be linear for pure boundary lubrication conditions.

It should also be noted that for a given set of engine geometric parameters (crank radius, connecting rod length, etc.), the piston speed is directly related to the rotational speed of the crankshaft [20]. Therefore, the piston speed can also be replaced by the rotational speed of the engine crankshaft in Eq. (3.3). This modified form of Eq. (3.3) will be used later in this Chapter.

3.1.3. Effect of Engine Load

The effect of engine load on friction is less straightforward. In order to maintain constant engine speed when the load on the engine increases, the amount of air and fuel brought into the cylinder to be compressed and burned during combustion must be increased. As a result, higher peak pressures are reached in the cylinder.

The friction generated by the piston rings is significantly affected by the pressures attained in the cylinder throughout the engine cycle. The cylinder pressure controls the land pressures, which affect the ring dynamics and therefore the lubrication conditions encountered by the rings throughout the engine cycle. Although in general, the contribution of friction as a percentage of the engine's indicated power output reduces as load increases, major changes in load may result in a change in the type of piston ring-liner friction that dominates in different parts of the cycle. This is best illustrated through the use of an example, which is described in the following section.

3.1.4. Illustration of Effect of Speed and Load on Piston Ring Friction

To illustrate the effect of speed and load on friction, the friction model introduced in Chapter 2 was used to analyze the piston ring friction generated throughout the cycle in a Waukesha natural gas power generation engine for different operating conditions. More detailed specifications for the engine are provided in Chapter 5. Since it used in power generation applications, it is designed for low speed, high load operation (1800 rpm and 200 psi BMEP). The results in this section were all obtained assuming the maximum oil supply condition (OS1).

Figure 3-1 shows the friction power losses of each of the piston rings throughout the engine cycle at the standard low speed, high load operating condition. It can be seen from the figure that the highest contributors to friction in the engine cycle are the top ring around top dead center (TDC) of compression/expansion and the oil control ring throughout the engine cycle.

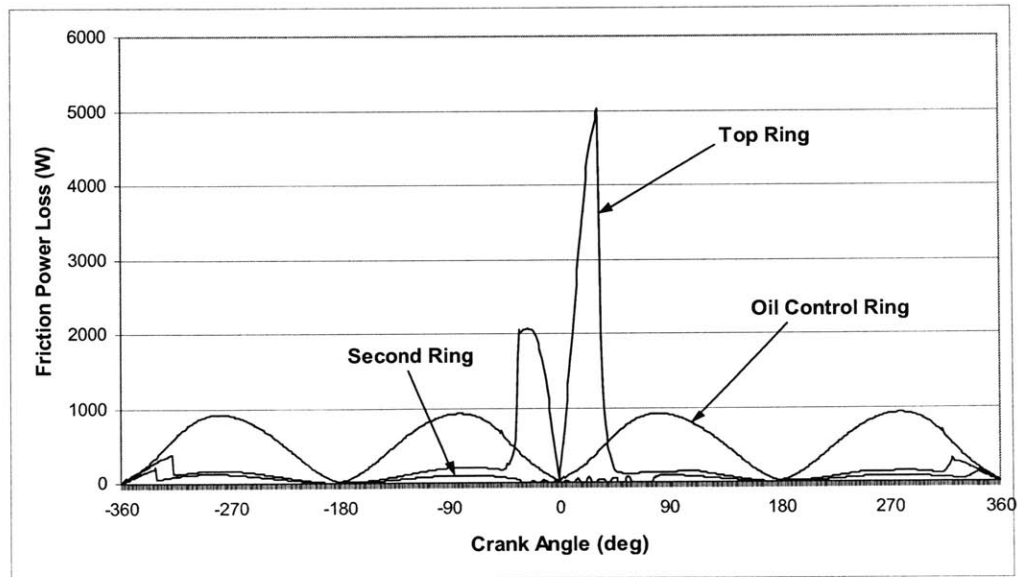


Figure 3-1: Friction Power Loss Contributions in the Piston Ring Pack

This is confirmed in Figure 3-2, which shows the FMEP contributions of each of the piston rings. The determination of FMEP from friction power losses is derived in

Appendix B. This figure also shows the FMEP contributions from each of the rings from boundary lubrication. It is clear that most of the top ring friction comes from boundary lubrication in the part of the cycle around TDC of the compression/expansion strokes.

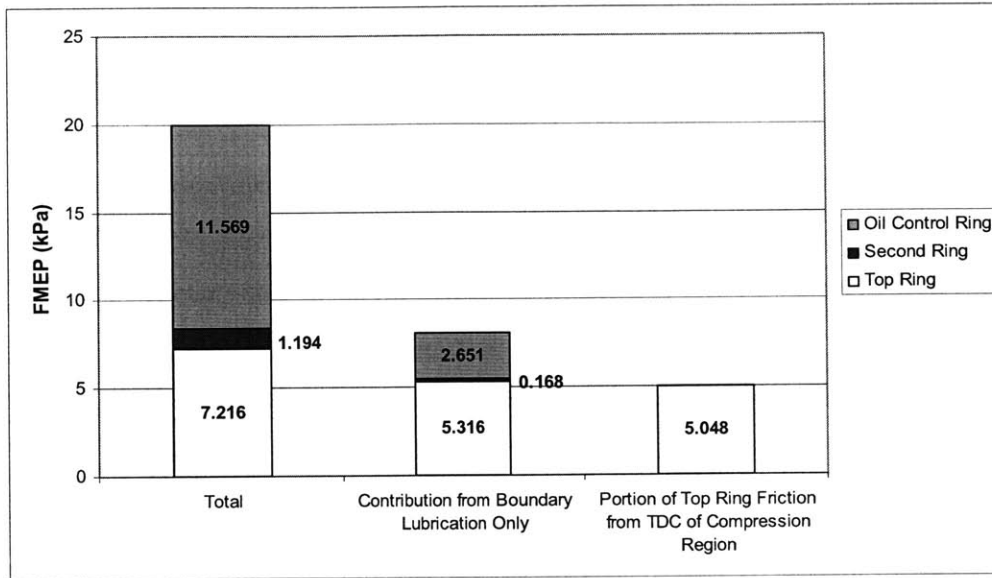


Figure 3-2: FMEP Contributions in the Piston Ring Pack

To demonstrate the effect of varying engine load, a different set of cylinder pressure data was used as an input into the friction model. This pressure data was taken from another engine, but nevertheless it can still be used to illustrate the effect of decreasing engine load on friction. The peak pressure is approximately 20 bars for this case compared to a value of 80 bars at the standard operating condition. Figure 3-3 shows the friction power losses of each of the piston rings throughout the engine cycle, and Figure 3-4 shows the FMEP contributions of each of the rings. By comparing these figures with the earlier results for the higher load conditions, the effect of reducing engine load on friction can immediately be seen. In this case, the contribution of the top ring friction generated near TDC of compression/expansion is reduced and the portion of top ring friction coming from boundary lubrication conditions is lower as well, indicating a higher overall contribution from top ring friction generated at midstroke. The main contributor to friction in the low load case is clearly the oil control ring.

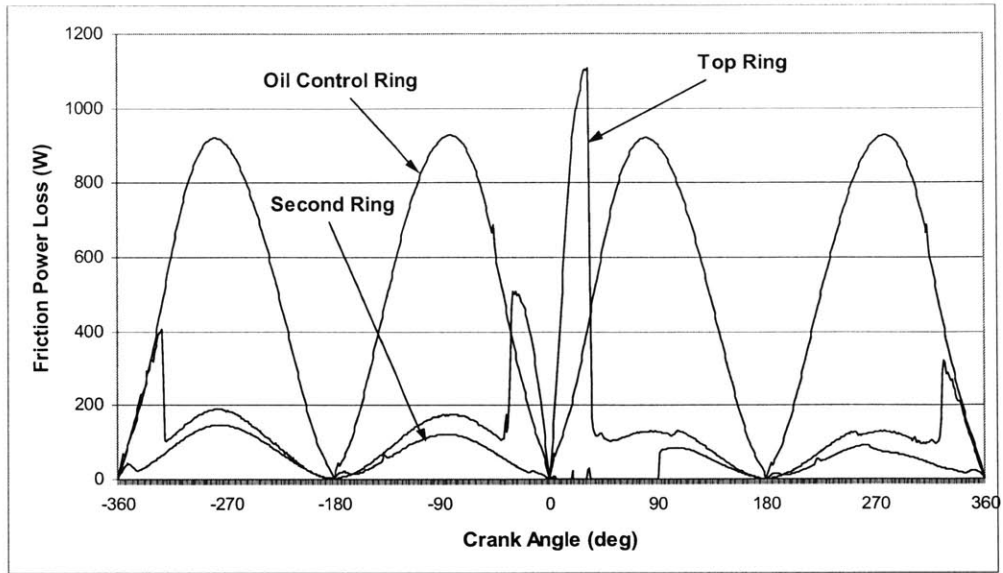


Figure 3-3: Friction Power Loss Contributions of the Ring Pack at Lower Load Condition

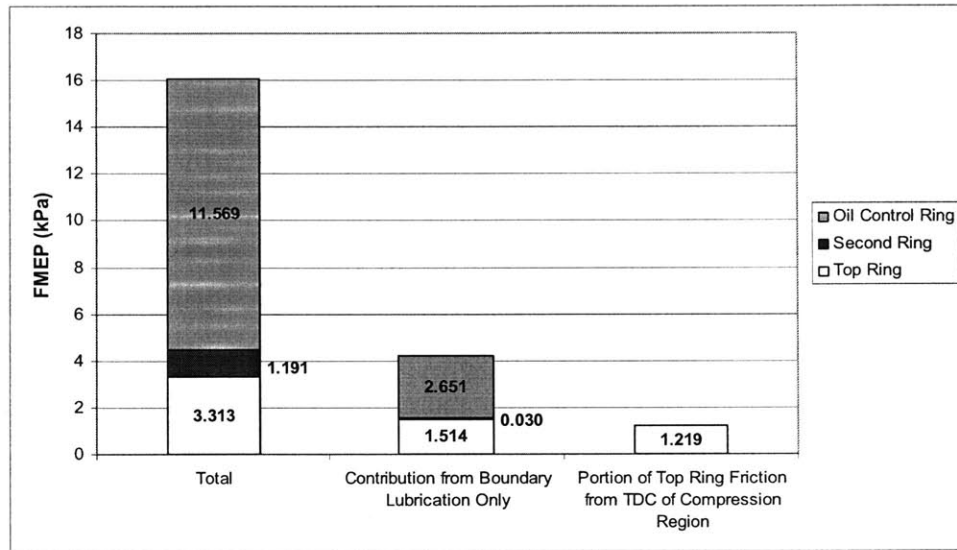


Figure 3-4: FMEP Contributions of the Ring Pack at Lower Load Condition

To illustrate the effect of engine speed, results were obtained for an engine speed of 3000 rpm for the same cylinder pressure data used to generate the low load, low speed case. It should be noted that the increased engine speed may have an effect on the liner temperature distribution and therefore on the lubricant viscosity, as pointed out in Section 3.1.2. Justification for neglecting this effect can be provided using the Waukesha engine

data for this specific case. According to Eq. (3.3), for an increase in engine speed from 1800 to 3000 rpm to be offset by a change in oil viscosity, the viscosity would need to be reduced by a factor of approximately 4.5. According to the Vogel Equation, which is used by the model to determine the viscosity of the oil at a specific temperature along the liner, the change in temperature that would be required to achieve a reduction in viscosity by a factor of 4.5 would be between 50 and 100°C, depending on the point in the engine cycle under consideration [11]. Such a change in liner temperature could not feasibly result from this change in engine speed. Therefore, the effect of the change in viscosity can be neglected in this case. This analysis also shows that in general, for the purpose of comparing the main contributors to friction between a low speed and a high speed case, the effect of the change in viscosity can safely be neglected.

With this in mind, the friction power losses of the piston ring pack and the FMEP contributions are plotted again in Figure 3-5 and Figure 3-6, respectively, for the high speed case.

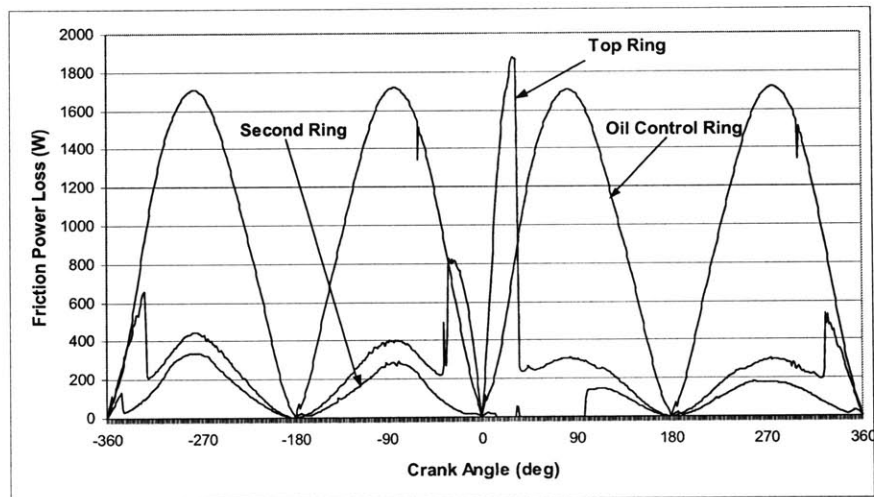


Figure 3-5: Friction Power Losses in the Piston Ring Pack at Low Load, High Speed

In this case, the contribution of the top ring friction from boundary lubrication around TDC of compression/expansion is reduced even more compared to the low load, low speed case, although this difference would be less significant if the higher cylinder

pressure data corresponding to the higher engine speed were used. Still, for this case, the portion of the total top ring friction from hydrodynamic lubrication conditions during the midstroke region of the engine cycle is larger. This result is expected because of the stronger dependence of friction power losses on engine speed in hydrodynamic lubrication conditions compared to boundary lubrication conditions. It can also be seen from these results that friction from the oil control ring is the most significant contributor to piston ring pack friction in the low load case.

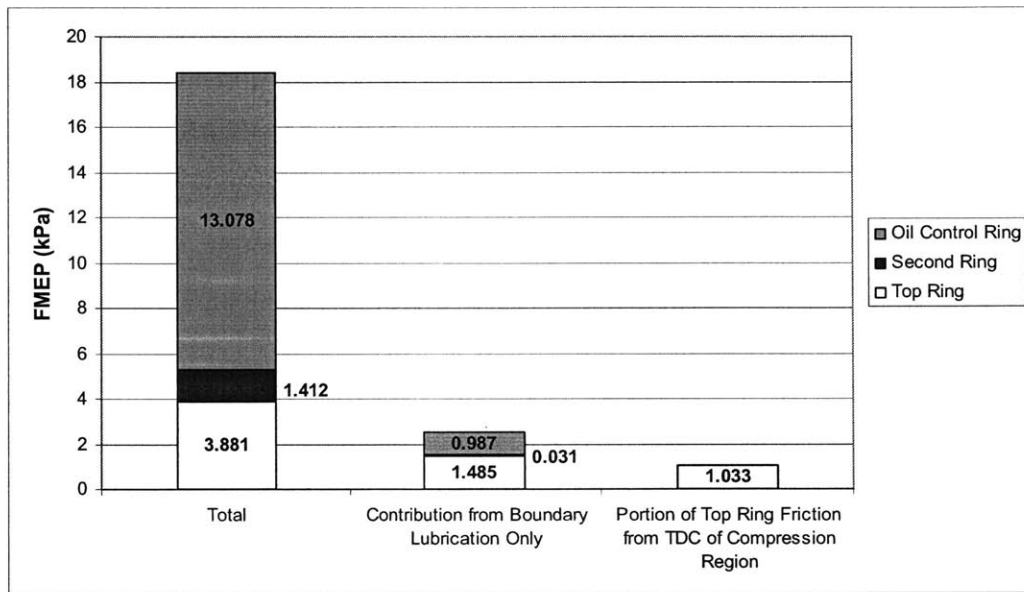


Figure 3-6: FMEP Contributions in the Ring Pack at Low Load, High Speed

The scaling relationship between friction power loss and speed can also be seen from these results. Comparing Figure 3-3 and Figure 3-5, around TDC of compression/expansion, the ratio of top ring friction power loss for the high speed case to the low speed case is about $1900/1100=1.7$, which is roughly the same as the ratio of the engine speed, $3000/1800=1.7$. This was expected for pure boundary lubrication conditions. In the midstroke region, the ratio of peak top ring friction power losses during the intake stroke is roughly $443/200=2.2$, which is approximately equal to the engine speed ratio as defined in Eq. (3.3), namely $(3000/1800)^{3/2}=2.2$.

3.1.5. Effect of Oil Supply on Piston Ring Friction

The amount of oil supplied to the different piston rings throughout the engine cycle has a significant effect on the friction and lubrication conditions between the rings and the liner. In Chapter 2, the approach used to model oil supply in this study was described. This involved evaluating each of the reduced friction designs at both a maximum (OS1) and minimum (OS2) oil supply condition, since the exact oil supply rate is unknown. In the previous section, all of the results were obtained assuming the maximum oil supply condition (OS1). It turns out that for all of the speed and load conditions that were investigated in the previous section, the results are quite similar for the OS2 case. The main difference is that the top ring contributes more significantly to friction in all speed and load conditions because of the reduced oil supply. Previous studies conducted using the friction model have shown that the top ring typically encounters boundary lubrication conditions throughout a considerable portion of the engine cycle for the minimum oil supply condition [19].

It was also briefly noted in Chapter 2 that the amount of oil on the liner in the region above TDC of the oil control ring was set to zero in the first cycle of the calculation. This is because the oil control ring can never travel above its own TDC position, and there is thus no direct oil supply to the upper rings between TDC of the oil control ring and TDC of the top ring. As a result, the only source of oil to this part of the liner is what is brought into this region by the top ring or the second ring in subsequent cycles. There is therefore much less oil supply to this section of the liner, and it is thus hereafter as the ‘dry region.’ The dry region is illustrated in Figure 3-7 below.

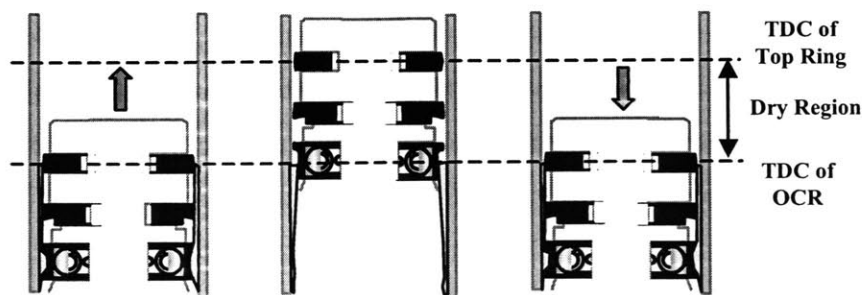


Figure 3-7: Illustration of the Dry Region

It may be possible to bring oil into this region in certain circumstances. The effect of the presence of oil in the dry region during the first engine cycle should be investigated in order to understand the implications of the assumption of zero initial oil film thickness along the liner in this region, since it was used throughout this study. In the remainder of this section, the impact of the initial oil film thickness on the evolution of the lubrication conditions in the dry region will be discussed, and the effect of the oil film thickness in this region on friction will be identified.

Figure 3-8 shows the evolution of the lubrication conditions in the dry region for the case where no oil is initially assumed to be present. Figure 3-8 a), b), and c) show the oil film thickness on the liner before (light black line) and after (dark black line) passage of the top ring during the first, second, and third cycles, respectively. As can be seen from these plots, there is no oil in the dry region, which extends from roughly 40 degrees before to 40 degrees after top dead center (TDC is located at 0 degrees in these plots). However, there is a slight difference between the exact amounts of oil brought into this region by the top ring in the compression stroke and brought out during the expansion stroke. This can be seen by comparing Figure 3-8 a) and Figure 3-8 b). In Figure 3-8 a), the liner oil film thickness before passage of the top ring is slightly smaller than the film thickness left behind by the top ring as the top ring enters the dry region during the compression stroke. Then, on the expansion stroke, the liner oil film thickness is unchanged after the passage of the top ring, and therefore, the additional oil that was brought into the region during the compression stroke remains on the liner for the next cycle. In Figure 3-8 b), during the second cycle, the location of the nonzero oil film thickness is advanced from 33 to 31 degrees before TDC. Similarly, the nonzero oil film thickness location is advanced from 31 to 30 degrees before TDC between the second and the third cycle. After 4 cycles, there is no further advancement of the nonzero oil film thickness, and the dry region is therefore fully evolved. It can be concluded from this analysis that if zero oil film thickness is initially assumed to be present in the dry region, it is unlikely that this region will become wetted during any subsequent engine cycle.

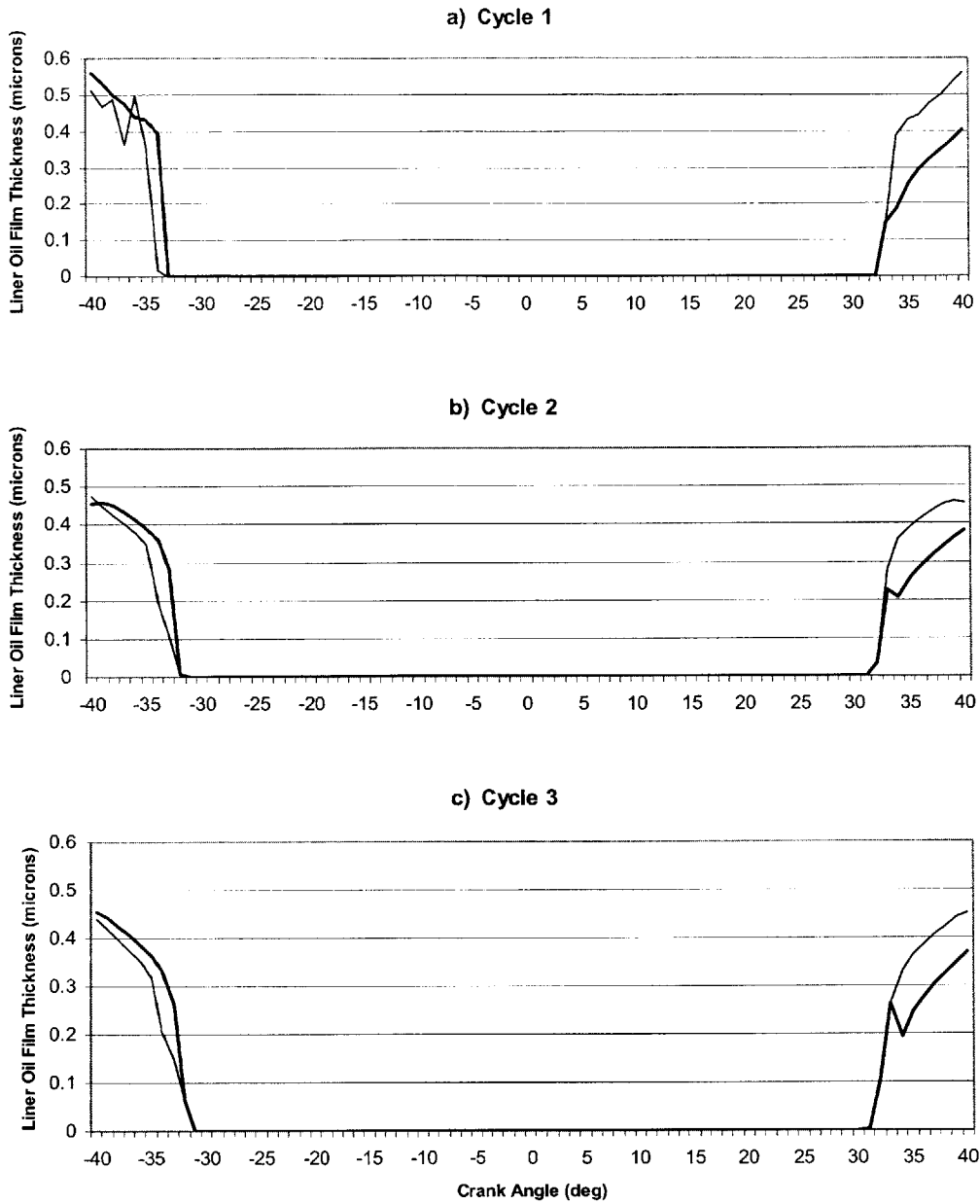


Figure 3-8: Evolution of the Dry Region

For comparison, model predictions were also obtained assuming that the oil film thickness in the dry region was initially 1 micron. Figure 3-9 a), b), and c) show the liner oil film thickness before (light black line) and after (dark black line) passage of the top ring for the third, fourth and fifth cycles, respectively. Figure 3-9 a) shows that in the third cycle, oil is available in the dry region until about 5 degrees before TDC, at which

point oil starts to accumulate under the top ring and no oil is left behind on the liner. Just before this occurs, between 10 and 5 degrees before TDC, a larger oil film thickness is left on the liner after passage of the top ring than before, and the top ring is clearly releasing some of the oil that was accumulated in the earlier part of the stroke. Then, after passing TDC, on the expansion stroke, the liner oil film thickness before and after passage of the top ring is the same, which indicates that the top ring does not carry out the oil that was brought into this region. As a result, in the fourth cycle, as shown in Figure 3-9 b), a much larger oil film thickness is available to the top ring before it reaches TDC compared to the third cycle. The top ring releases some of its accumulated oil just before TDC, but this time, it carries out all of the oil from in this region to the other parts of the cycle, as indicated by the zero oil film thickness after passage of the top ring during the expansion stroke. In the fifth cycle, as shown in Figure 3-9 c), the top ring is able to bring some oil into the dry region, much like the case in the third cycle. In fact, the fifth and third cycles are almost identical. This is also true for all of the subsequent even cycles. It can thus be concluded from this analysis that if nonzero oil film thickness is initially assumed to be present in the dry region, a balance is eventually reached in which the amount of oil brought into the dry region in odd cycles is balanced by the amount of oil brought out during even cycles.

The effect of the oil film thickness in the dry region on friction is the most relevant issue in this study. For the cases in which zero initial oil film thickness was assumed in the dry region, the model predictions indicated that the top ring was in pure boundary lubrication near TDC of the compression/expansion strokes, and that this contributed to high friction power losses. If oil could be brought into the dry region, then the top ring would no longer be in pure boundary lubrication, and the friction generated due to boundary contact would be reduced. Figure 3-10 and Figure 3-11 below show the friction power loss and FMEP contributions, respectively, for the case where initial oil film thickness in the dry region is assumed to be 1 micron. As can be seen from the figures, the main contributors to friction are still the top ring and the oil control ring, but the relative contribution of the oil control ring is larger. The lower FMEP contribution from the top ring around TDC of compression/expansion is a result of the larger portion of the overall

radial load acting on the back of the ring being supported by hydrodynamic pressure. Since hydrodynamic friction is typically much smaller than boundary friction, if a greater portion of the load is sustained by hydrodynamic lubrication, the overall friction losses are reduced.

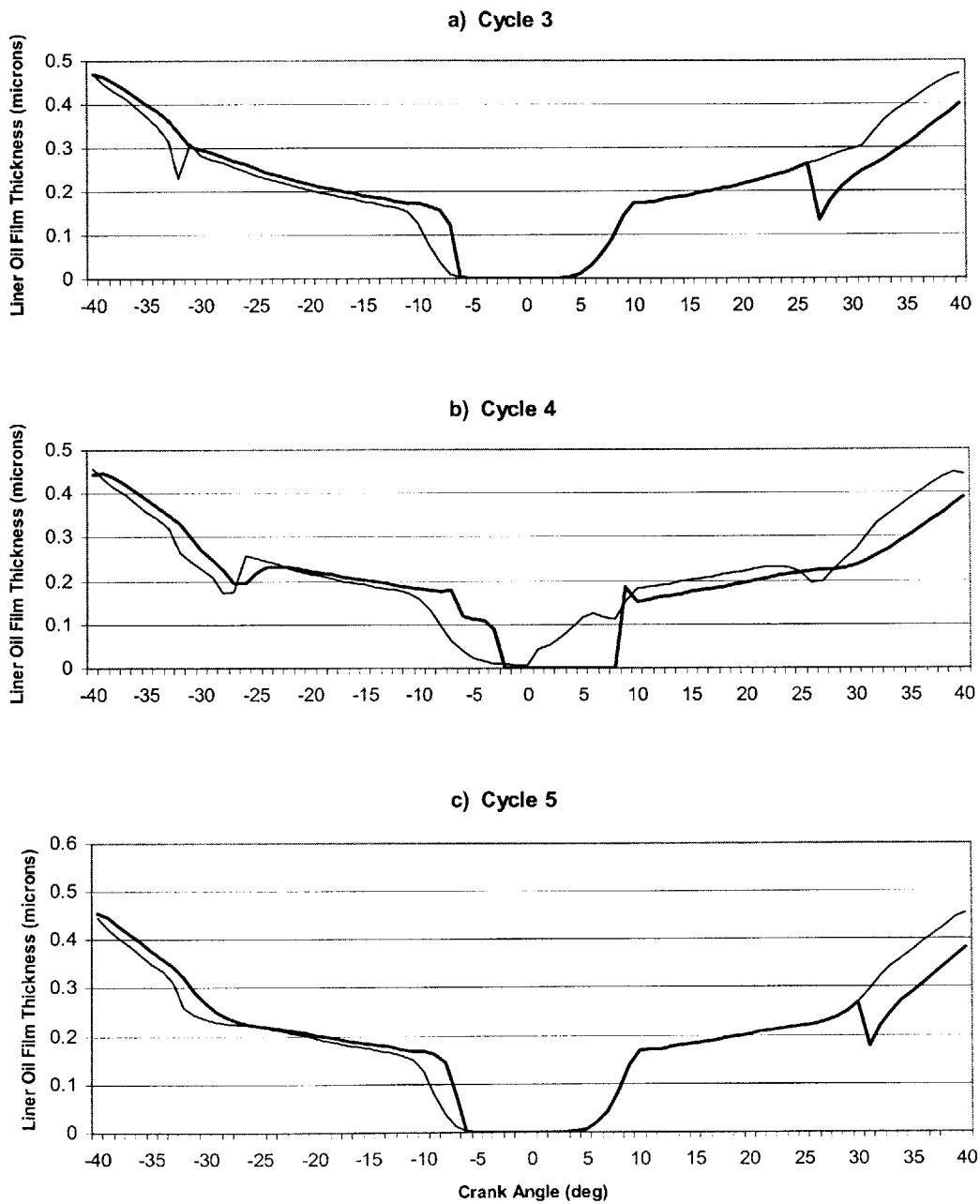


Figure 3-9: Evolution of the Dry Region with Nonzero Initial Oil Film Thickness

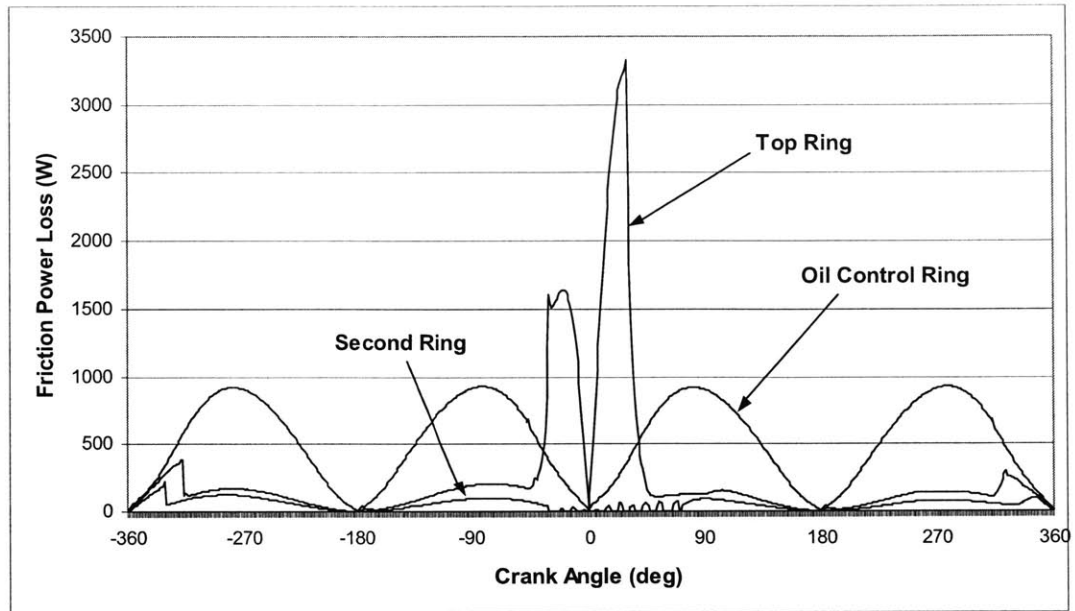


Figure 3-10: Friction Power Losses in Dry Region with Nonzero Initial Oil Film Thickness

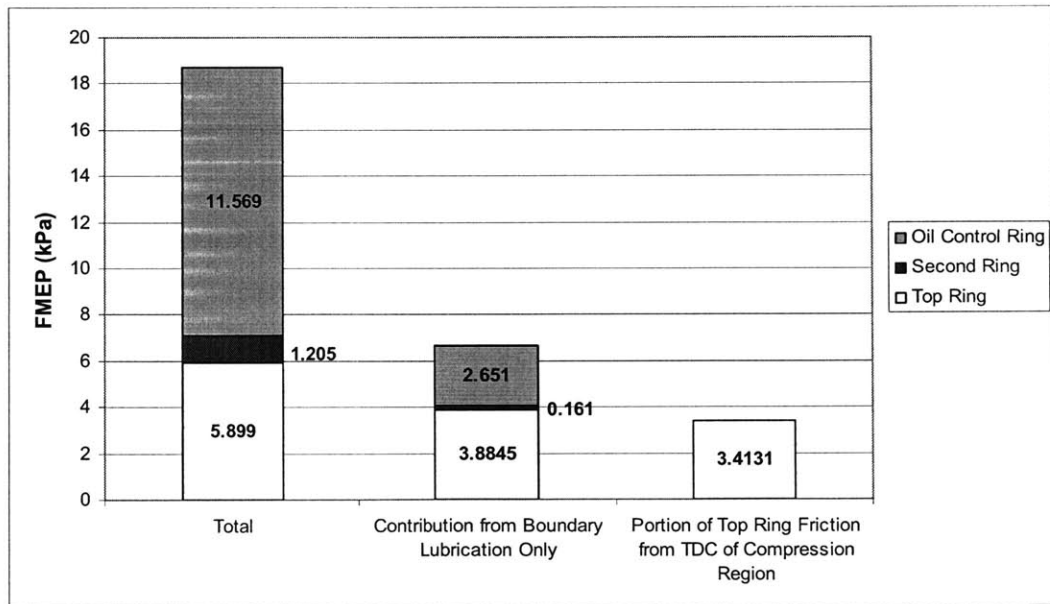


Figure 3-11: FMEP Contributions in Dry Region with Nonzero Initial Oil Film Thickness

More detailed studies conducted by Tian with the friction model in the past have indicated that it is difficult to bring oil into the dry region on the pin side of the piston [19]. It was also shown in these studies that if piston tilt is sufficiently large, the top ring

can bring oil into the dry region on the minor thrust side of the piston, due to the large oil film thickness that is untouched by the rings on the intake stroke which becomes available just before the top ring enters the dry region on the compression stroke. Significant bore distortion, leading to poor conformability of the oil control ring and the second ring, was also identified as a possible method by which oil could become available to be brought into the dry region [19].

It is therefore unlikely that any significant amount of oil exists in the dry region on the pin side of the piston. Therefore, for the remainder of this study, model predictions were obtained assuming that the oil film thickness in the dry region is initially zero. The implications of this assumption will be mentioned where appropriate.

3.1.6. Summary of the Effect of Engine Operating Conditions on Piston Ring Friction

Table 3-1 below identifies the main contributors to friction in different engine operating conditions.

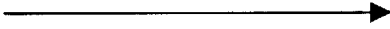


		Increasing contribution from top ring boundary friction around TDC of compression 	
		Low load	High load
Boundary friction power loss increasing as U 	Low speed	-Oil control ring throughout engine cycle	-Oil control ring throughout engine cycle -Top ring around TDC of compression/expansion
Hydrodynamic friction power loss increasing as $\mu^{1/2}U^{3/2}$ 	High speed	-Oil control ring throughout engine cycle	-Oil control ring throughout engine cycle -Top ring around TDC of compression/expansion

Table 3-1: Summary of Main Contributors to Friction for Different Engine Operating Conditions

It should be noted that this table is only valid for engines using single grade oil. As was pointed out in Section 3.1.2, for multigrade oil, the engine speed has a strong dependence on the viscosity of the lubricant, and therefore it is difficult to draw conclusions about the main contributors to friction in this case.

The remainder of this study is focused on developing friction reduction strategies for high load, low speed engines using single grade oil because in this case, high pressures are generated and severe lubrication conditions are present due to the effect of engine speed on oil film thickness. It was therefore the most interesting case to consider in order to study friction and oil transport. In addition, since both the top ring near TDC of compression and the oil control ring throughout the engine cycle contribute most significantly to friction power losses at this speed and load, the same strategies developed to reduce friction in this case could be applied to reduce oil control ring friction in the lower load condition. Because of the greater importance of top ring friction from hydrodynamic lubrication around the midstroke region in lower load conditions, a short theoretical analysis was also performed in this study to develop an approach that could be used to develop some secondary friction reduction strategies for the top ring in the midstroke region. The results from this study are presented in Section 6.3.

For high load, low speed operating conditions, the largest contributors to friction were identified as the top ring around TDC of compression and the oil control ring throughout the engine cycle. In the sections that follow, physical explanations for each of these high contributions are provided.

3.2. Physical Insight into Primary Sources of Friction in High Load, Low Speed Engines

3.2.1. Top Ring around TDC of Compression

The high friction generated by the top ring in the region around TDC of compression is a result of the combination of poor oil supply to the top ring in the dry region, and high pressure generated in the cylinder by compression and combustion. In high load operating conditions, high peak pressures are generated in the cylinder by compression and combustion. As the pressure in the cylinder rises during the compression stroke, the top ring gradually conforms to the lower groove flank, as shown in Figure 3-12 below. No oil is depicted between the top ring and the liner in this figure in order to reflect the poor oil supply to this region, which was discussed in Section 3.1.5.

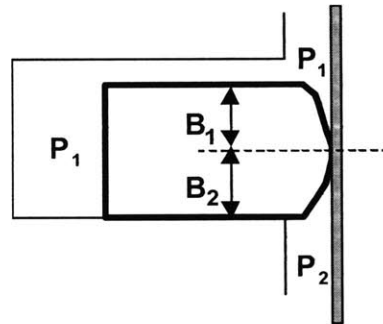


Figure 3-12: Illustration of the Top Ring near TDC of Compression

If no oil is assumed to exist between the ring and the liner in this region around TDC of compression/expansion, and the top ring is assumed to conform well to the lower groove flank, the friction force acting on the top ring is from pure boundary lubrication conditions and can thus be estimated as the product of the radial load acting on the back of the ring and the coefficient of friction:

$$F_f = a_{asp}[(p_1 - p_2)B_2 + W] \quad (3.4)$$

where a_{asp} is the coefficient of friction between the ring and the liner, and W is the ring load due to tension.

The power loss due to friction is the product of the friction force in Eq. (3.4) and the piston speed at that instant. Although the piston speed is small near TDC, the friction force is very high and therefore the product of friction and piston speed is large, as was shown in Figure 3-1 for the Waukesha natural gas engine. Significant top ring friction power losses occur in this region of the engine cycle as a result. This effect would be even more significant in larger Diesel engines, where the peak cylinder pressure can reach 200 bars.

3.2.2. Oil Control Ring Throughout Engine Cycle

The high friction generated by the oil control ring throughout the engine cycle is a result of its high tension. Here, the tension is generated by the ring's own elasticity, and is thus equivalent to the amount of force required to close the ring gap in order to fit the ring inside the cylinder bore. As explained in Chapter 1, the principal function of the oil control ring is to regulate the amount of oil that reaches the upper rings. As a result, the high tension is necessary in order to promote conformability of the oil control ring to the bore. Good conformability is difficult to achieve in practice because of the nonuniform distortion of the cylinder bore due to mechanical deformation and thermal gradients. As a result, the best way in which to ensure adequate conformability of the oil control ring to the bore is by designing the oil control ring with a high tension.

The high tension force acting on the small lands of the oil control ring results in a high unit pressure exerted on the oil film under the lands. This idea is illustrated in below in Figure 3-13.

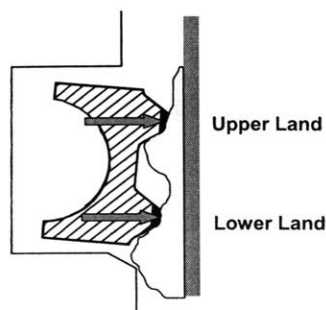


Figure 3-13: Illustration of Effect of Oil Control Ring Tension on Oil Film Thickness

As a result, the oil film thickness that passes under the oil control ring is reduced and adequate oil control is achieved in this way. This can be seen by consideration of the radial force balance in Eq. (2.8). Assuming that the land pressures around the oil control ring are equal and close to atmospheric pressure, they can be neglected in this analysis. Therefore, the force due to ring tension is balanced by the pressure generated in the oil film:

$$W = \int_0^B p dx$$

Here, for simplicity, the oil control ring is assumed to be fully-flooded with oil, and therefore the pressure developed in the oil film is related to the load due to tension through the following scaling relationship:

$$p \sim \frac{W}{B} \quad (3.5)$$

Now, scaling the Reynolds' Equation (Eq. (2.7)) yields the relationship between the pressure developed in the oil film and the film height:

$$h \sim \sqrt{\frac{\mu UB}{p}} \quad (3.6)$$

Eq. (3.5) shows that a high ring load due to tension results in higher pressure developing in the oil film, which reduces the film thickness according to Eq. (3.6). The reduced film thickness leads to higher friction between the ring and the liner according to Eq. (3.1).

If no oil were to exist between the oil control ring and the liner, the high tension force would result in more severe asperity contact pressure according to Eq. (2.4), which would result in higher friction according to Eq. (2.3).

Therefore, regardless of the amount of lubrication under the oil control ring, the high tension generates high friction between this ring and the liner. In the Chapter that follows, several design strategies will be developed to reduce the friction generated by both the oil control ring and the top ring along the liner.

(This page was intentionally left blank)

4. Friction Reduction Strategies

The following chapter contains a description of recommended strategies to reduce the friction generated by the main contributors identified in Chapter 3. The relative friction reduction potential of each design strategy is investigated using the modeling tools described in Chapter 2. Adverse effects that may result from implementation of the designs are discussed, and additional designs to minimize these adverse effects are developed and recommended.

4.1. Top Ring

An equation describing the friction generated by the top ring along the liner in the region near TDC of compression was given in the previous Chapter (Eq. (3.4)). Due to the high pressures generated near TDC of compression, the pressure term typically exceeds the ring load due to tension by at least an order of magnitude. Therefore, designs to reduce friction should be focused on reducing the contribution from the pressure difference acting on the lower part of the top ring. Since the pressure difference is controlled by the compression and combustion process, which will not be changed in this study, the most effective way to reduce top ring friction in this region is by reducing the area exposed to the high pressure difference (B_2 in Figure 3-12).

At this point, it should be noted that this design strategy was developed assuming that there is no oil in the dry region. Pure boundary lubrication conditions were indeed predicted to be present in the dry region by the model, as was discussed in Section 3.1.5. However, it was also pointed out in this section that in certain circumstances, oil can be brought into the dry region and mixed lubrication may be achieved. If this were the case, the suggested design strategy of reducing B_2 would still reduce friction, but it would be slightly less effective because in mixed lubrication conditions, the portion of the net radial load supported by the oil film is much greater than the portion supported by asperity contact. The reduction in B_2 would still reduce boundary friction by reducing

the net radial load, but since the part of the load supported by hydrodynamic pressure is generally larger than that supported by asperity contact, the strategy would be less effective at reducing friction overall if oil were present in the dry region.

There are several practical ways in which the reduction of B_2 can be accomplished, and they are described in the sections that follow.

4.1.1. Skewed Barrel Profile

The top ring can be manufactured such that the physical length of the region below the minimum point is reduced. This is generally referred to as a skewed barrel profile design. Such a design clearly reduces the area over which the high pressure difference acts, which reduces the friction generated between the top ring and the liner in this region. This design was investigated in some of the previous studies described in Chapter 1, and a reduction in friction was observed by its implementation [1,6]. The design is illustrated below in Figure 4-1, where it is compared to a symmetric barrel profile.

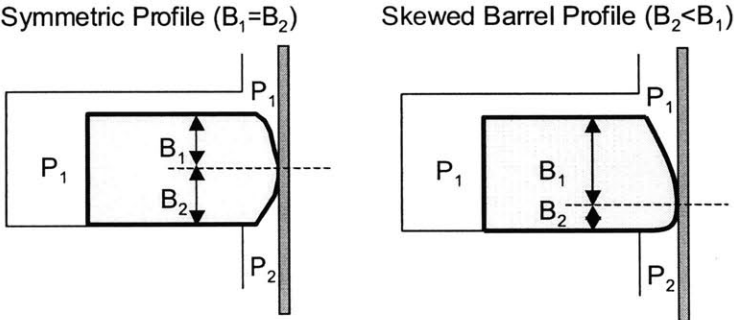


Figure 4-1: Illustration of Skewed Barrel Profile Design

4.1.2. Top Ring Groove Upward Tilt

The high pressures generated in the cylinder due to compression and combustion force the top ring to conform well to the lower groove flank around TDC of compression. As a

result, if an upward groove tilt angle were introduced in the top ring groove, the point on the ring that is closest to the liner (the minimum point) would move down along the profile if the top ring were to conform to the upward tilted groove around TDC of compression. This idea is illustrated below in Figure 4-2. As would be the case for the skewed barrel profile design, this design would result in a reduction of area over which the high radial pressure difference acts, and would therefore reduce friction.

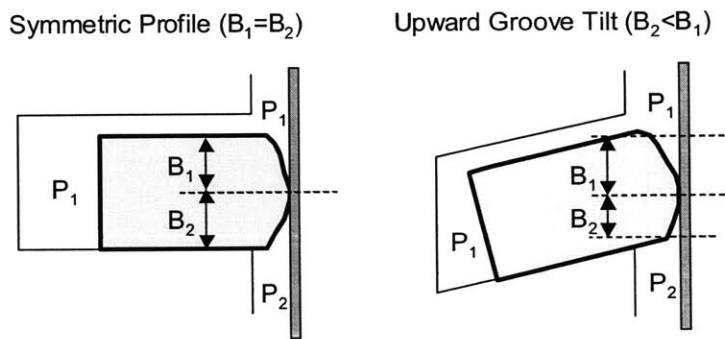


Figure 4-2: Illustration of Top Ring Upward Groove Tilt Design

4.1.3. Reduced Top Ring Axial Height

One other method by which to reduce the area over which the high radial pressure difference acts around TDC of compression would be to reduce the overall axial height of the top ring. This would reduce both B_1 and B_2 , and since the high pressure difference acts over B_2 , friction could be reduced using this design. This idea is illustrated below in Figure 4-3.

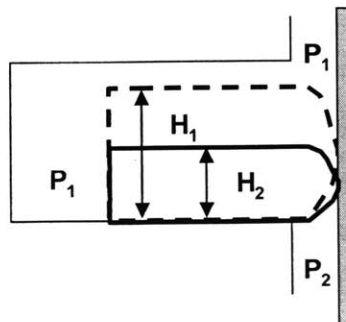


Figure 4-3: Illustration of Reduced Axial Height Design

4.2. Oil Control Ring

4.2.1. Reduced Tension Oil Control Ring

Since the friction generated by the oil control ring is a result of its high tension, the best way in which to reduce oil control ring friction would be to reduce the ring tension. This would almost certainly be accompanied by an increase in oil consumption due to poorer conformability. This will be discussed in more detail in the following section, and designs will be recommended to compensate for this adverse effect.

4.3. Adverse Effects of Reduced Friction Designs

4.3.1. Reduced Ring Life

Reduced ring life was reported in previous studies that were conducted on reduced axial height rings. In particular, Hill and Newman identified reduced axial height as causing reductions in axial stiffness [4]. Based on their experimental results, they concluded that compression rings should be at least 1.5 mm in axial height. Failures were observed and the tests had to be terminated after 50 hours when rings whose axial heights were below this value were used in their study.

4.3.2. Increased Top Ring Groove Wear

One of the adverse effects of the upward top ring groove tilt design discussed in Section 4.2.2 is that it can result in increased top ring groove wear. When the cylinder pressure rises sufficiently to push the top ring downward to conform to the groove, concentrated contact is first made at the outer diameter (OD) corner of the lower groove flank because of the upward tilt angle. This effect is illustrated in Figure 4-4 below, in which the contact pressure distribution between the ring and the lower groove flank is compared

between the baseline design with no upward groove tilt and the upward groove tilt design. The graph shows the contact pressure distribution between 100 degrees before TDC and 100 degrees after TDC since this is the region of interest in the engine cycle. As can be seen in the graph, fairly uniform contact pressure distribution is achieved from ID to OD in the baseline design, although there is a slight increase in the contact pressure at the OD corner for this design. This is because the high pressure above the top ring in the area between the groove edge and the liner can cause the ring to rotate around the OD corner by a small amount close to TDC of compression. The upward groove tilt design therefore results in a large concentrated contact pressure at the OD corner of the groove.

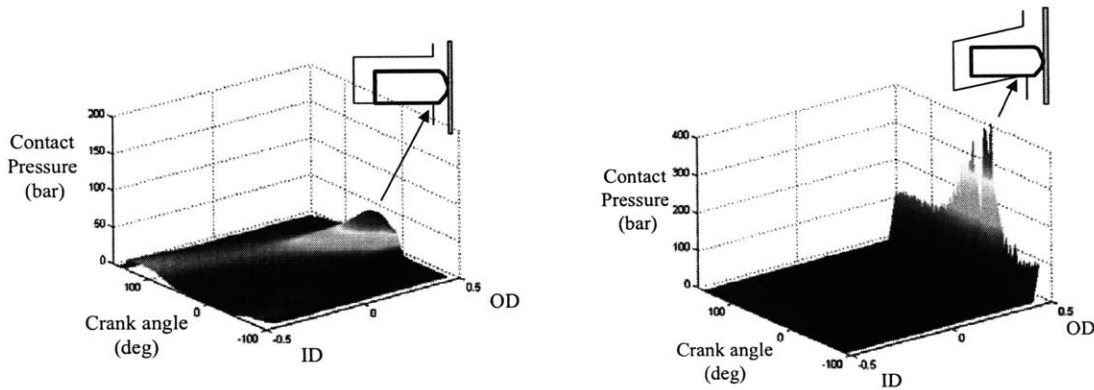


Figure 4-4: Effect of Upward Top Ring Groove Tilt

Because of the highly concentrated contact pressure at the OD corner of the upward tilted top ring groove, this corner will be subjected to significant wear and will likely flatten out over time. As a result, the upward groove tilt angle will gradually decrease until the design is effectively undone and the groove is no longer tilted. Clearly, a design to compensate for this effect is needed if this upward groove tilt design is to be useful for practical purposes. Such a design will be recommended in Section 4.4.1.

4.3.3. Increased Oil Consumption

In Section 4.2.1, it was noted that reducing oil control ring tension will compromise the ring's conformability to the liner, which will likely result in increased engine oil

consumption. In reality, this depends on whether or not the oil that passes the oil control ring-liner interface is able to reach the combustion chamber. It also depends on the extent of the bore distortion in the engine, which is not known exactly. Nevertheless, it is likely that if a significant amount of excess oil passes the oil control ring-liner interface, at least part of this oil will reach the crown land and will be consumed. Therefore, the reduced tension oil control ring design should be implemented with another design to compensate for the likely increase in oil consumption. Two designs that could potentially achieve this purpose will be described in Sections 4.4.2 and 4.4.3

4.4. Designs to Compensate for Adverse Effects

4.4.1. Effect of Top Ring Static Twist on Top Ring Groove Wear

As discussed in Section 4.3.2, the upward top ring groove tilt design results in a large concentrated contact pressure at the OD corner of the groove, which can quickly wear the OD corner and render the design ineffective. One way in which to compensate for this effect is by introducing a positive static twist in the top ring. This can be accomplished by adding a small groove in the in the upper ID corner of the top ring.

If there is no groove in the upper ID corner of the ring, the cross-section is approximately symmetric. As a result, when the ring is installed in the cylinder bore and the radial load due to tension is applied, pure bending occurs about the axis that is normal to the plane of the ring as the ring gap is closed. If a small section of material is removed from the upper ID corner of the ring, the cross-section becomes asymmetric, and the location of the centroid and the angle of the principal axes of the cross-section will change. As a result, when the ring is installed in the cylinder bore and the uniform radial load due to tension force is applied, the cross-section will be subjected to a twisting moment as well as a bending moment.

If a certain amount of material is removed from the upper ID corner of the ring such that the positive twist introduced by this change is larger than the upward groove tilt angle, the ring will settle down on the lower groove flank much more gradually as the cylinder pressure rises during the compression stroke. As a result, a more uniform contact pressure distribution between the ring and the lower groove flank will be achieved with such a design, as illustrated in Figure 4-5 below. This will prevent the upward groove tilt design from becoming worn. The contact pressure distribution in the case of the upward groove tilt combined with the positive top ring static twist yields roughly the same uniformity in the contact pressure distribution as the baseline design with no upward groove tilt. It is therefore reasonable to expect that this design would wear no less than the baseline design. The combination of the upward groove tilt with the positive top ring static twist thus reduces friction without introducing any adverse effects.

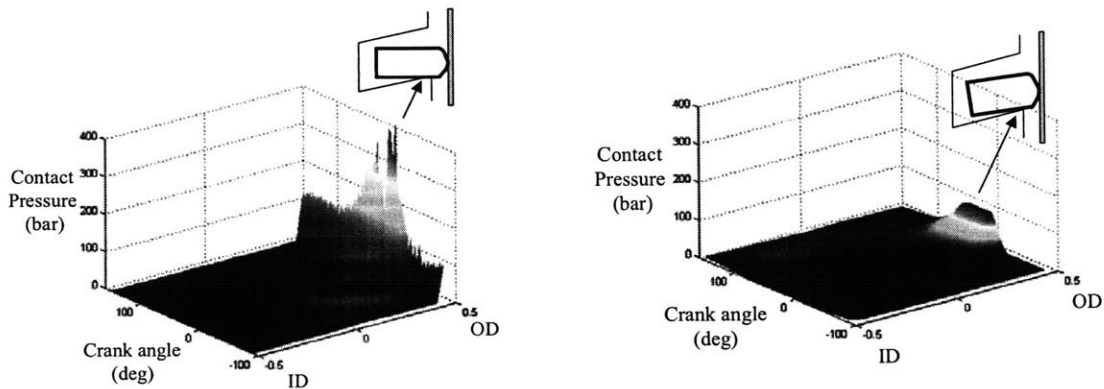


Figure 4-5: Effect of Top Ring Static Twist

4.4.2. Effect of Second Ring Design on Oil Consumption

The second ring is typically designed with either a positive static twist or a negative static twist. With a positive static twist, the ring is more stable and therefore no ring flutter occurs near TDC of compression. A complete description of the flutter phenomenon as well as a more thorough discussion of the link between static twist and ring stability can be found in [21]. It is commonly believed that second ring flutter near TDC of compression results in oil transport to the crown land and eventually to oil consumption.

As a result, the second ring is often designed with a positive static twist so that no flutter occurs around TDC of compression.

One of the consequences that can occur as a result of the use of such a design is that the second ring can remain fixed on the lower groove flank for most of the cycle. This is because a second ring with positive static twist can seal the path where gas would normally flow to the lower lands, as shown below in Figure 4-6. As a result, there is a significant pressure rise in the second land and this pressure cannot be relieved to the lower lands through the blocked path. Because of the inability of the gas to flow from the second land to the lower lands, pressure in the second land builds, and can exceed the cylinder pressure near the end of the expansion stroke. At the beginning of the exhaust stroke, this pressure difference tends to force the top ring to lift, whereas the downward pointing inertia force pushes the top ring down, resulting in a phenomenon called top ring reverse flutter. Previous studies have shown that top ring reverse flutter may be an important source of oil consumption [18,21,22].

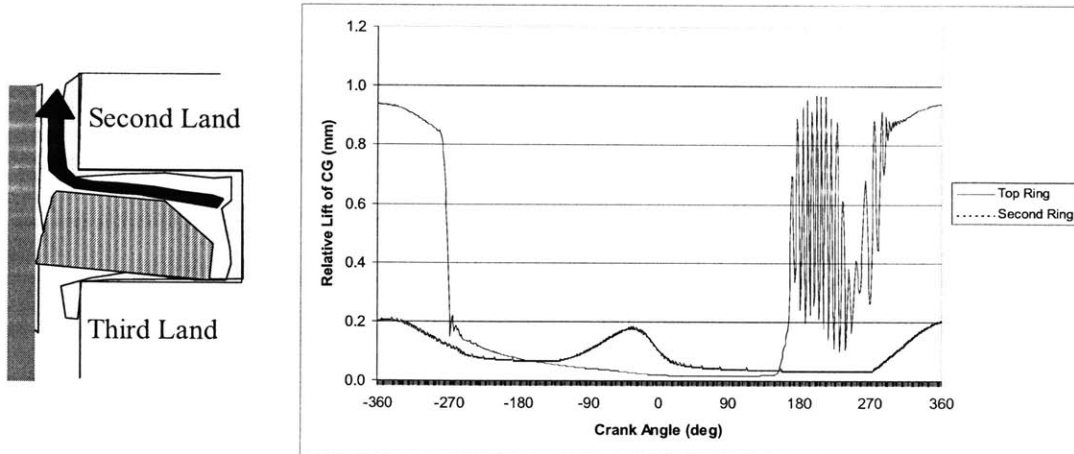


Figure 4-6: Top Ring Reverse Flutter

There is another potential adverse consequence that can result from the use of a second ring with positive static twist. With a larger second ring static twist, a more significant portion of the taper face becomes exposed to the higher second land gas pressure. Due to the sealing created between the second ring and the top OD corner of the second ring

groove, the high gas pressure can push the ring inward to allow the gas flow to pass through the ring-liner interface. This is a phenomenon called second ring collapse, and it is illustrated in Figure 4-7 below. Operating conditions and designs to avoid second ring collapse are discussed in [21]. Second ring collapse is undesirable for oil consumption because it allows a significant amount of gas to flow past the ring-liner interface and to reach the third land, where pressure builds up and gas flow can subsequently carry oil into the second ring groove and upwards towards the combustion chamber.

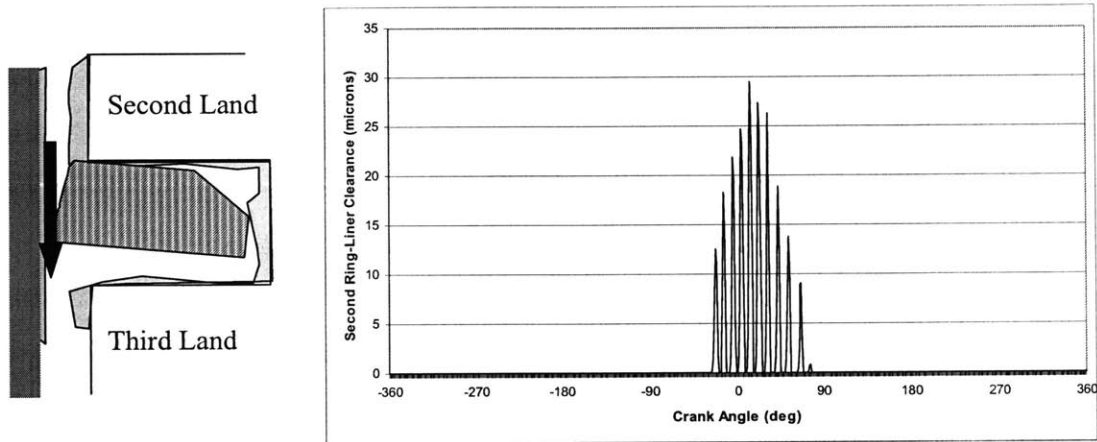


Figure 4-7: Second Ring Collapse

A second ring with a negative static twist allows the gas flow to penetrate to the lower lands from the second land, and therefore eliminates top ring reverse flutter, and the potential second ring collapse. This result is illustrated in Figure 4-8.

The elimination of top ring reverse flutter through the use of the negative static twist second ring design has the potential to reduce oil consumption in the engine. It is therefore recommended that this design be used with the reduced tension oil control ring so that the reduction in tension does not significantly increase oil consumption overall.

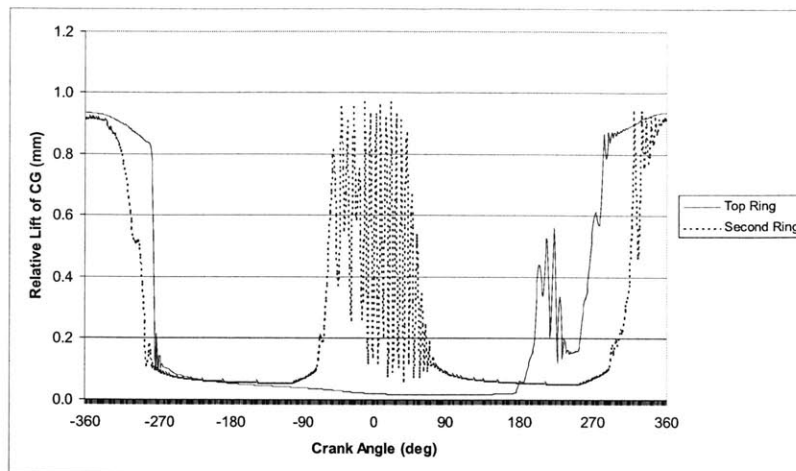
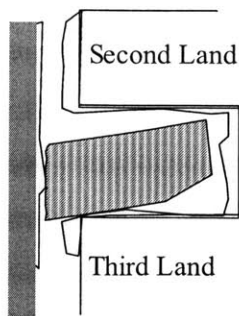


Figure 4-8: Second Ring with Negative Static Twist

4.4.3. Effect of Oil Control Ring Conformability on Oil Consumption

Another design strategy that could be used in combination with the reduced tension oil control ring to compensate for the increased oil consumption is the reduction of the radial thickness of the cross-section of the oil control ring. If the cross-sectional area is reduced, the moment of inertia is also reduced. This is because the moment of inertia is determined by the sum of the squares of the radial distances between the centroid of the cross-section and the origin at each element of area of the ring. Therefore, if the overall area is reduced, there are fewer contributions to the overall area, and the moment of inertia is thus reduced. If this is the case, bending is promoted about the axis perpendicular to the plane of the ring, leading to improved conformability.

However, designing the oil control ring with a smaller area results in a reduction in the structural strength of the ring, which may compromise ring life. A stiffer material could be used to compensate for this effect, but this would result in a decrease in conformability overall, since the stiffness of the material has a more significant effect on conformability than the cross-sectional area of the ring. Therefore, the improvement in conformability that can be achieved by a reduction in the cross-sectional area of the ring is limited by structural considerations, and may not be the most effective design strategy.

4.5. Additional Design Limitations

4.5.1. Manufacturing Limitations

Typical axial heights of piston rings range from 1 mm to 4 mm. As a result, machining the rings to precisely match the design specifications is difficult, and tolerances are often on the order of the design values themselves. Care thus needs to be taken when developing designs to ensure that allowances are made for such tolerances.

Certain designs are limited by these tolerances. In particular, the top ring profile can only be machined within certain tolerances, and as a result, there are limitations on the design values that can be specified.

In this study, the effect of producing designs at the limits of the various tolerances was evaluated using the modeling tools. In other words, the friction reduction potential of each of the designs was assessed for each case with an upper and a lower limit representing the extreme cases for machining the rings at the edge of the tolerance ranges. This facilitated the optimization of the final designs to ensure that a reduction in friction was predicted by the modeling tools.

4.5.2. Transition to Boundary Lubrication at Midstroke

In several of the designs presented in the previous sections, the physical length between the top ring's minimum point and its lower edge in the untwisted state (B_2 in Figure 3-12) was reduced. If this length is reduced significantly, it can result in the onset of boundary lubrication conditions throughout the entire engine cycle.

For most of the engine cycle, the top ring is typically designed to be in hydrodynamic lubrication, except near dead centers when piston speed is reduced significantly and hydrodynamic lubrication cannot be sustained. If B_2 is reduced beyond a certain extent,

the top ring will become fully-flooded at the leading edge on downstrokes. This is because the oil supply is fixed, but the amount of space available under the ring is decreasing as B_2 is reduced. Once the top ring becomes fully-flooded on downstrokes, because of the fixed oil supply, less oil can fit under the ring as B_2 is reduced further. Therefore, further reduction in B_2 results in a reduction in oil film thickness, h_o , and eventually, the condition defined in Eq. (2.1) is met and boundary lubrication conditions are present even in the midstroke regions of the engine cycle. As was pointed out throughout this study, boundary friction losses are much higher than friction losses from hydrodynamic lubrication, and therefore the onset of this condition throughout the cycle causes a significant increase in the friction generated by the top ring along the liner. This condition thus sets an upper limit on the potential reduction of B_2 through a reduction in axial height or through the use of a skewed barrel profile.

In general, as long as boundary lubrication conditions are not present in the midstroke regions of the engine cycle, the top ring friction generated in the midstroke region is a negligible part of the total friction generated by the top ring for high load, low speed operating conditions. However, as pointed out in Chapter 3, for low load, high speed conditions, midstroke friction generated by the top ring becomes significant. Although the present study focuses on high load, low speed engines, an approach to identify strategies for the reduction of top ring midstroke friction was also suggested. This was included because once the contribution of the top ring friction generated around TDC of compression/expansion is reduced through various design changes, the top ring friction at midstroke is the next area which can be targeted for further friction reduction. This approach for the future development of design strategies to reduce top ring friction at midstroke is described in Section 6.3.

5. Application of Reduced Friction Design Strategies to a Natural Gas Power Generation Engine

In the following chapter, the reduced friction strategies developed in Chapter 4 are applied to re-design the piston rings of a natural gas power generation engine with the goal of reducing friction to improve the engine's efficiency. Model predictions are first obtained to compare the effectiveness of each of the low-friction design strategies in the Waukesha engine. Based on the results of this comparison, several low-friction designs were selected for experimental investigation. The logic behind this selection process is briefly described. The experimental procedure used to evaluate the designs is then described in detail, and the results are presented and compared with the corresponding model results for those specific changes.

5.1. Description of Engine and Relevant Specifications

The engine selected for this study was a Waukesha spark-ignited natural gas power generation engine. Relevant specifications for this engine are shown in below in Table 5-1. The operating condition selected for this study was based on a typical operating condition that is ideal for interfacing with power generation equipment. It should be noted that all of the model predictions that will be presented in the sections that follow are based on normalized design values so that the current design values remain confidential.

Engine Configuration	6 Cylinders, Inline
Displacement	18 L
Bore, Stroke	152 mm, 165 mm
Speed	1800 rpm
Load Condition	1360 kPa BMEP

Table 5-1: Waukesha Engine Specifications

5.2. Reduced Friction Designs and Model Predictions

In the section that follows, model predictions are presented to illustrate the effect of implementing the different design strategies investigated in this study on friction in the Waukesha engine. The results are presented in terms of FMEP, which is the integrated effect of the friction power losses over the engine cycle, normalized by the engine's displaced volume. Details on the determination of FMEP from friction power losses throughout the engine cycle are given in Appendix B. In this study, model predictions were obtained for both oil supply conditions, OS1 and OS2, to bracket the actual FMEP between the upper and lower limits.

5.2.1. Reduced Tension OCR

Model predictions for the effect of reducing oil control ring tension on friction in the Waukesha engine are presented in the figures below. Figure 5-1 and Figure 5-2 show the effect of reducing oil control ring tension on oil control ring FMEP and total ring pack FMEP, respectively.

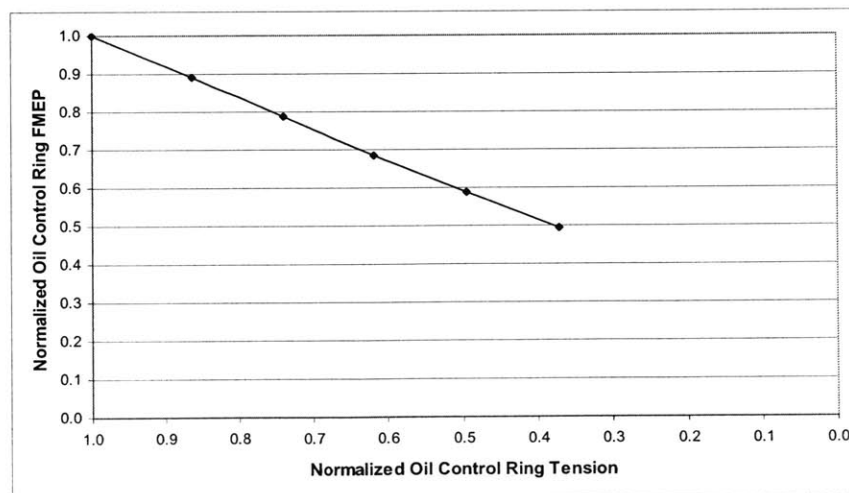


Figure 5-1: Effect of Oil Control Ring Tension on Oil Control Ring FMEP

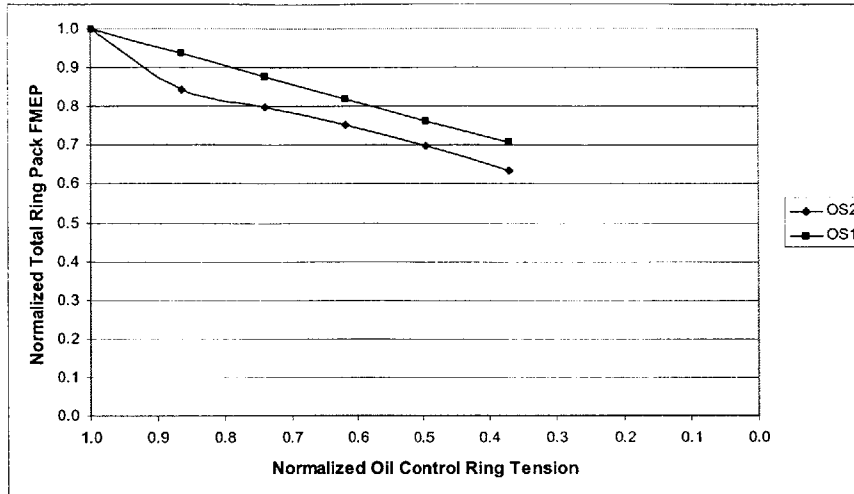


Figure 5-2: Effect of Oil Control Ring Tension on Total Ring Pack FMEP

It should be noted that in Figure 5-2, there is no distinction between OS1 and OS2 as the oil supply conditions do not affect the oil control ring, which is assumed to be fully-flooded on both upstrokes and downstrokes in the model as discussed in Chapter 2. It can be seen in the above figures that if oil control ring tension were reduced by half of its total value, oil control ring FMEP would be reduced by 40% and total ring pack FMEP would be reduced by 30-35%.

The sharp decrease in total ring pack FMEP in the case of OS2 for a reduction in oil control ring tension from a normalized value of 1.000 to 0.864 can be attributed to the top ring gaining hydrodynamic lubrication on the expansion stroke for the cases where the tension is below the normalized value of 0.864. If the tension is larger than this value, the oil control ring leaves an insufficient amount of oil on the liner and the top ring is in pure boundary lubrication conditions throughout the engine cycle.

5.2.2. Skewed Barrel Top Ring

Model predictions for the effect of a skewed barrel top ring profile on top ring friction in the Waukesha engine are presented in the figures below. In Section 4.1.1, the effect of

decreasing B_2 on friction was discussed. Figure 5-3 and Figure 5-4 show the effect of the reduction of B_2 on top ring FMEP and total ring pack FMEP, respectively.

As can be seen from the figures, the introduction of a skewed barrel profile can reduce top ring FMEP by up to 45% irrespective of the oil supply condition, and total ring pack FMEP by 15-25%. The reduction in total ring pack FMEP is larger for the case of OS2 because the top ring contributes much more significantly to the total ring pack FMEP due to the poorer oil supply assumed in this case.

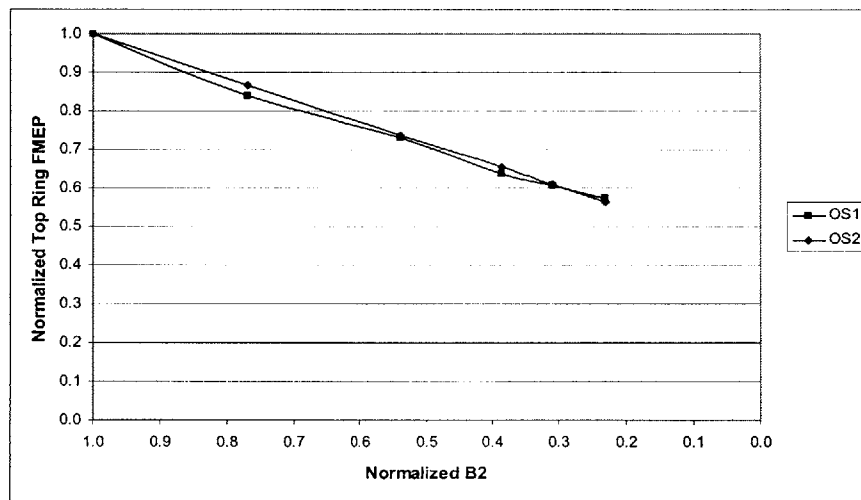


Figure 5-3: Effect of Skewed Barrel Profile on Top Ring FMEP

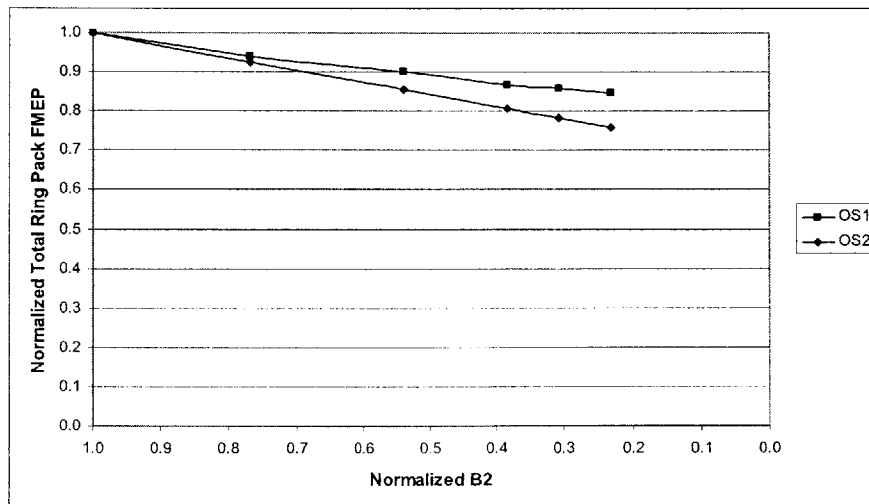


Figure 5-4: Effect of Skewed Barrel Profile on Total Ring Pack FMEP

5.2.3. Reduced Axial Height Top Ring

Model predictions for the effect of reducing the axial height of the top ring on friction in the Waukesha engine are presented in the figures below. Figure 5-5 and Figure 5-6 show the effect of the reduction of axial height on top ring FMEP and total ring pack FMEP, respectively.

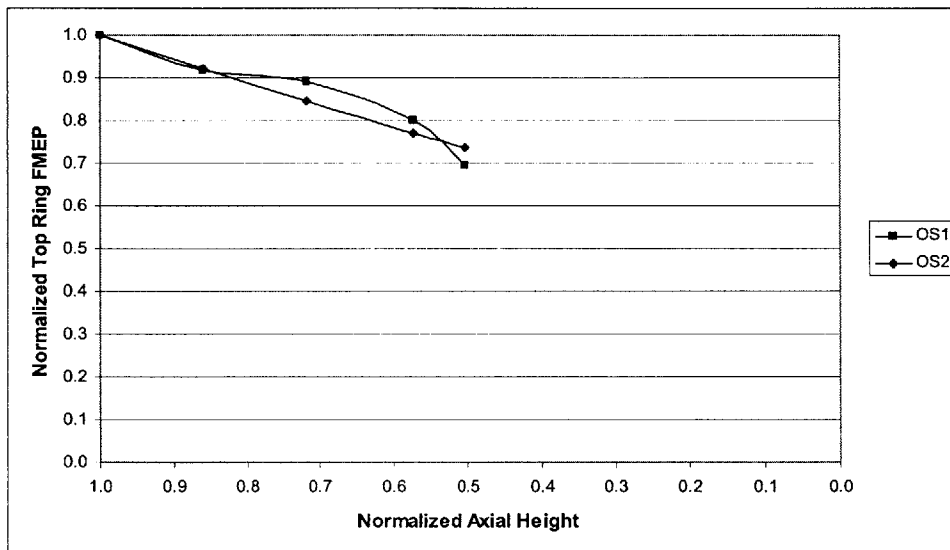


Figure 5-5: Effect of Top Ring Axial Height on Top Ring FMEP

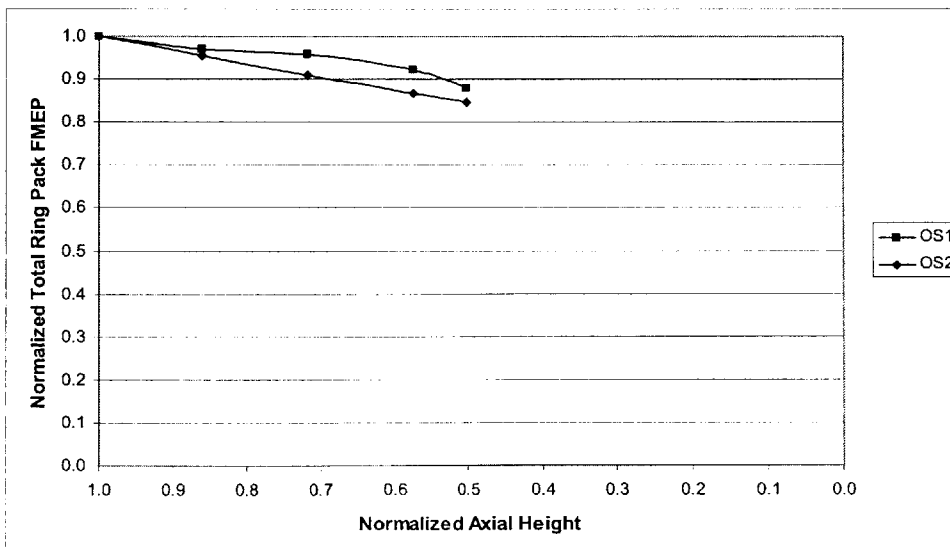


Figure 5-6: Effect of Top Ring Axial Height on Total Ring Pack FMEP

As can be seen in the figures, a reduction in the axial height of the top ring can result in a reduction in top ring FMEP of up to 25%, regardless of the oil supply condition. For the case of the total ring pack, FMEP can be reduced by 10-15% by a reduction in top ring axial height. Again, as in the case of the skewed barrel profile, the reduction of total ring pack FMEP is higher for the case of OS2 because of the larger contribution of the top ring to total ring pack friction in that case.

It should be noted that since the focus of this study is on the reduction of top ring boundary friction around TDC of compression, the objective is to reduce B_2 and therefore either the skewed barrel profile or the axial height reduction should yield similar results. However, the reduced axial height rings have been shown to have lower structural strength, leading to earlier failure, as discussed in Section 4.3.1. Therefore, the skewed barrel profile design is more advantageous from the standpoint of ring life and reduced friction.

5.2.4. Upward Top Ring Groove Tilt

Model predictions for the effect of increasing the top ring groove tilt on friction in the Waukesha engine are presented in the figures below. Figure 5-7 and Figure 5-8 show the effect a top ring groove with an upward tilt on top ring FMEP and total ring pack FMEP, respectively.

As can be seen in the figures, the upward top ring groove tilt can result in a reduction in top ring FMEP of up to 25%, regardless of the oil supply condition. For the case of the total ring pack, FMEP can be reduced by 10%.

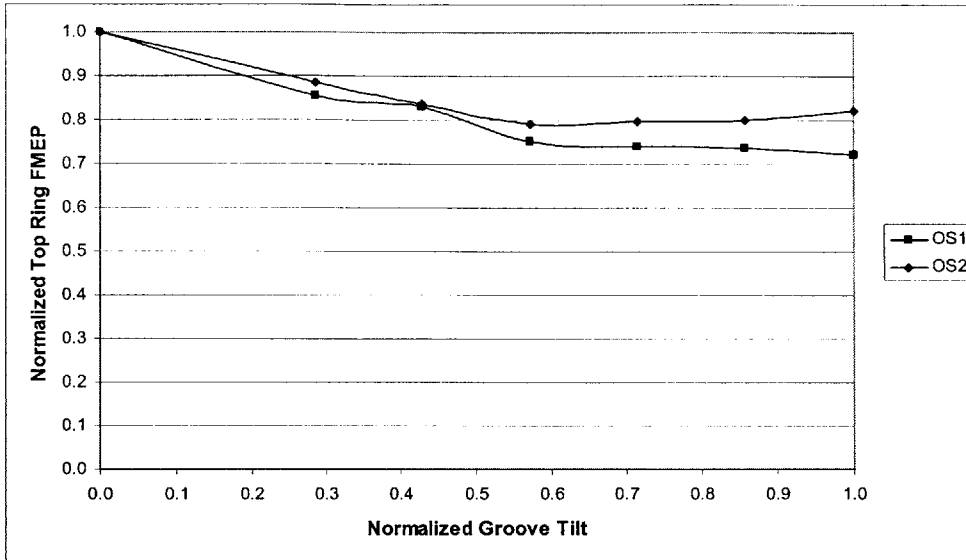


Figure 5-7: Effect of Top Ring Groove Upward Tilt on Top Ring FMEP

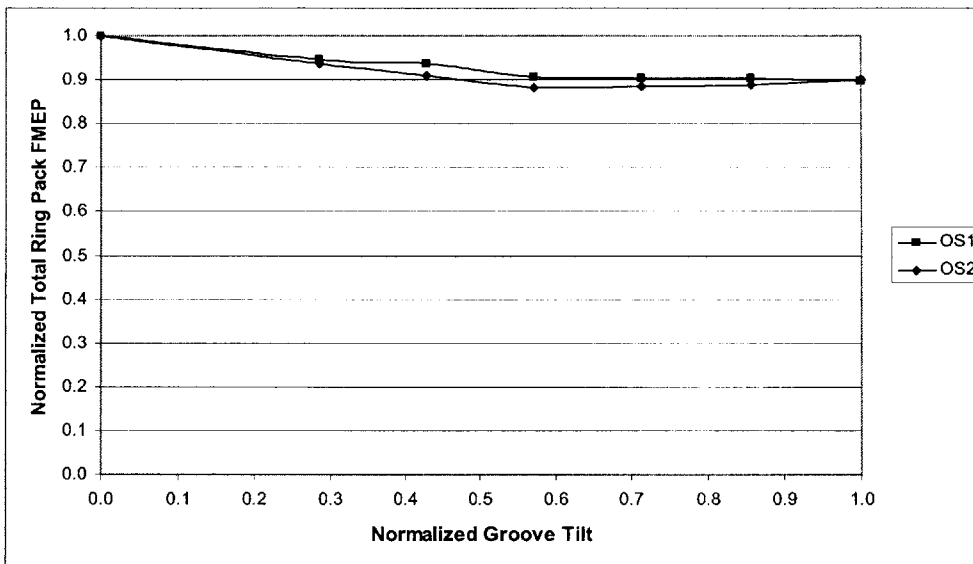


Figure 5-8: Effect of Upward Top Ring Groove Tilt on Top Ring FMEP

There are several trends that can be observed from these figures that require more detailed explanation. Firstly, for the case of both OS1 and OS2, for an increase in groove tilt beyond a normalized value of 0.571, the FMEP remains fairly constant. This can be explained by considering the dynamics of the top ring as it travels in the dry region. The development of this upward groove tilt strategy assumed that the top ring would conform fairly well to the lower groove flank and that as a result, the position of the minimum

point on the top ring would be lower on the profile when the groove tilt was increased. However, the top ring does not actually conform very well to the lower groove flank during this part of the engine cycle. This is confirmed by the model predictions, and is illustrated by a plot of the top ring twist as shown below in Figure 5-9 for the case of three upward groove tilts with normalized values of 0.429, 0.857 and 1. It should be noted that the small fluctuations in the ring twist Figure 5-9 are a result of the instability of the ring in this configuration due to the concentrated outer diameter contact on the lower groove flank. As can be seen from this figure, the top ring twist increases between groove tilts of 0.429 and 0.857, but between 0.857 and 1, there is no significant increase. As a result, the minimum point position does not change and there is no reason to expect a reduction in FMEP.

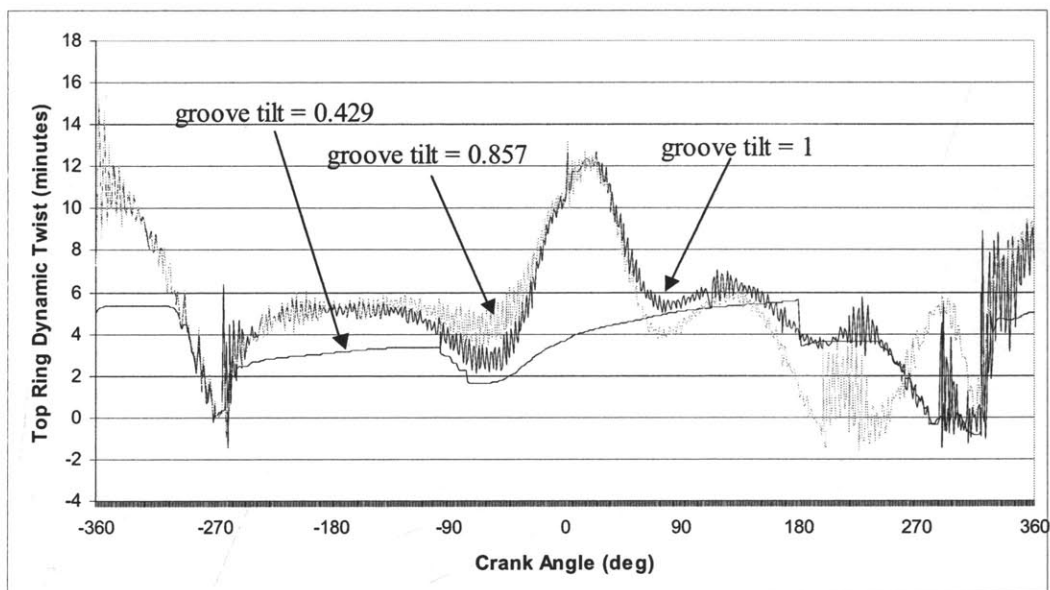


Figure 5-9: Effect of Groove Tilt on Top Ring Dynamic Twist

Before providing insight into this apparent limit in top ring twist that is reached after a certain groove tilt is exceeded, the governing forces and moments acting on the top ring to create the positive twist around TDC of compression must first be described. The positive top ring twist around TDC of compression is a result of the counterclockwise net moment acting on the top ring during this period. In Figure 5-10, the integrated moments

acting on the top ring around TDC of compression are plotted, along with the resulting top ring dynamic twist. The convention adopted in this figure is that a positive moment results in a positive or counterclockwise twist. It can be seen from Figure 5-10 that there is a clockwise moment exerted by the high gas pressure acting on the part of the top ring surface that is exposed to the clearance between the groove and the liner. Moments due to gas pressures acting on the rest of the top and bottom ring surfaces are balanced, because of the ability of the high-pressure gas to penetrate to the region below the ring due to the ring-groove configuration, as can be seen in the illustration of the top ring-groove configuration in Figure 5-11. The net moment due to the high gas pressure acting on the ring in the clearance between the groove and the liner is roughly balanced by the counterclockwise moment from asperity contact between the bottom face of the ring and the lower groove flank. The unbalanced positive moment acting on the top ring that results in the positive twist around TDC of compression comes from the force due ring-liner interaction.

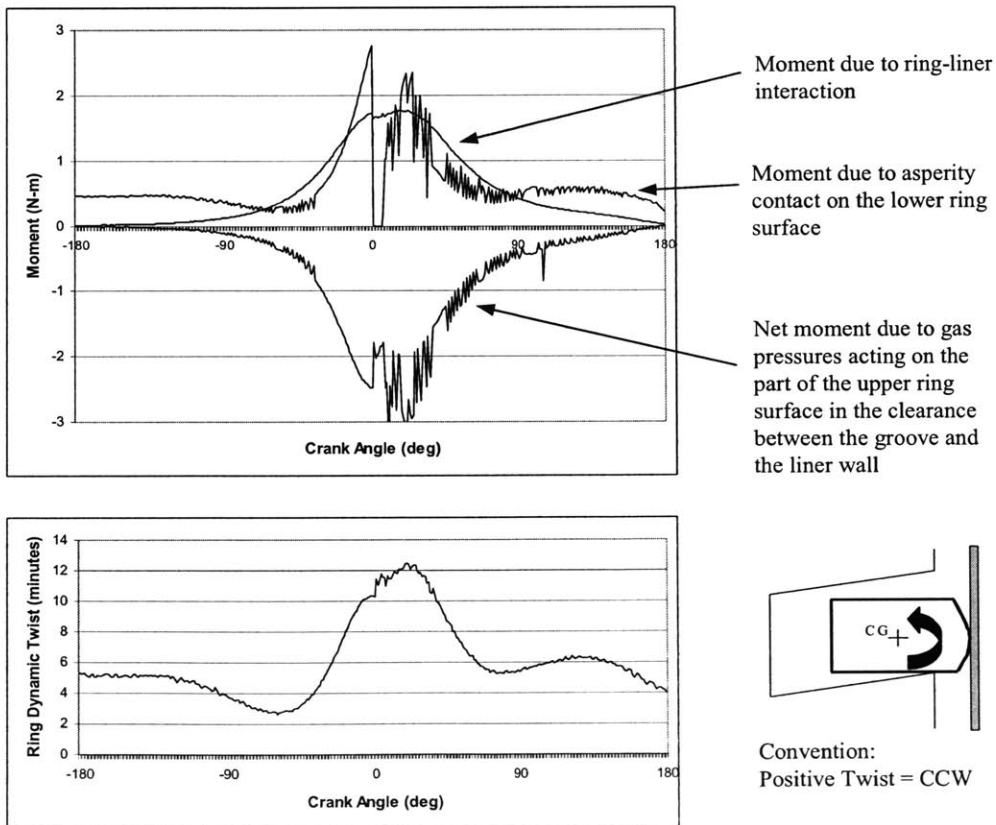


Figure 5-10: Top Ring Moments and Twist

To better explain the source of this moment, a simple diagram illustrating the forces and acting on the top ring around TDC of compression is shown in Figure 5-11. For illustrative purposes, without loss of generality, the second land pressure is assumed to be zero. The net force exerted by the ring on the liner due to the radial pressure difference is balanced by a reaction force of equal magnitude from the liner on the ring, which is concentrated around the minimum point. For simplicity, this force is assumed to act through the minimum point. There is thus a net positive moment acting on the ring because the line of action of the resultant of the pressure force acting on the inside surface of the ring is below the line of action of the resultant force acting at the minimum point.

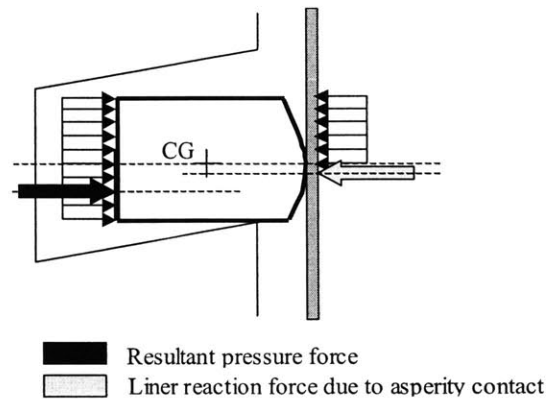


Figure 5-11: Illustration of Moments due to Ring-Liner Interaction

Now that the governing forces that lead to the top ring twist around TDC of compression have been described, insight can be given to explain the effect of increasing groove tilt on top ring twist. The difference in the top ring dynamic twist observed when top ring upward groove tilt is increased is actually a result of the change in the moment acting on the lower face of the top ring due to oil and gas pressure. When the upward groove tilt is small, there is less space between the lower ring surface and the groove and therefore more of the force acting on the lower ring surface comes from oil squeezing from the oil layer between the lower ring flank and the lower groove flank. As groove tilt is increased, more space exists between the ID of the lower surface of the top ring and the lower groove flank, and therefore there is less contact with oil. As a result, less negative moment is generated by oil squeezing and therefore the ring tends to twist more

positively. This is shown below in Figure 5-12, which shows the integrated moment due to oil squeezing acting on the lower flank of the top ring for normalized groove tilts of 0.571 and 0.714, respectively. As can be seen in this figure, for a normalized groove tilt of 0.571, the integrated moment due to oil squeezing acts to create a positive twist at first, but then as the ring twists, the direction of this moment reverses due to the increasing contact area with the oil towards the ID of the top ring and the net oil squeezing moment becomes negative. For the case of a normalized groove tilt of 0.714, the oil squeezing moment is always positive because the larger groove tilt creates more space between the top ring and the lower groove flank towards the ID corner of the ring and therefore there is no contact with the oil to create a negative moment.

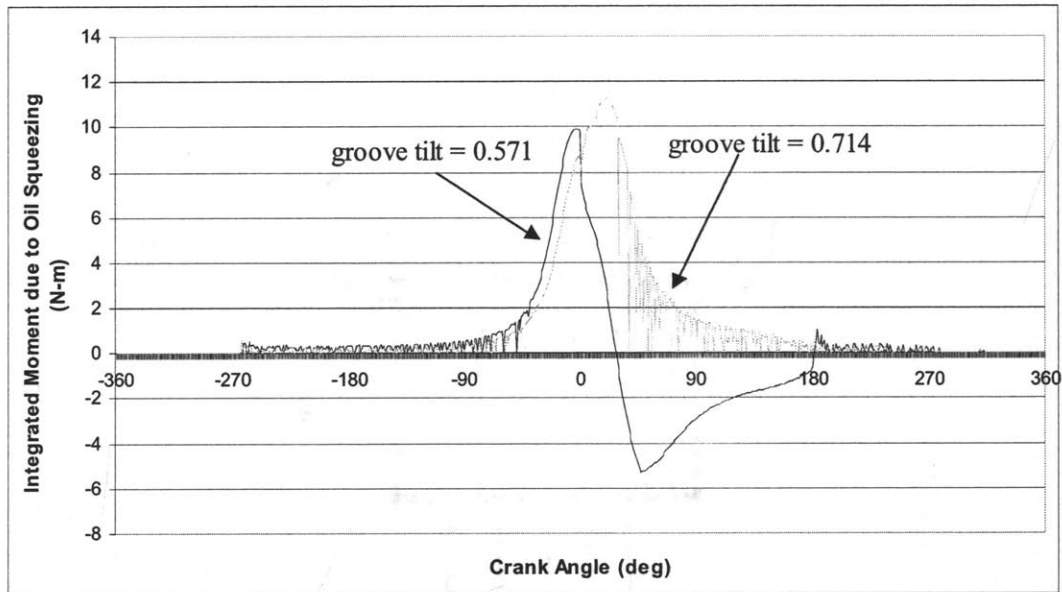


Figure 5-12: Effect of Groove Tilt on Oil Squeezing

Beyond a certain increase in groove tilt, there is no noticeable difference in the ring twist because no contact is made with the oil film between the lower ring surface and the groove and therefore further increase in groove tilt angle has no effect on top ring dynamics.

In summary, the net positive top ring twist that occurs around TDC of compression comes from the unbalanced moment due to ring-liner interaction. As groove tilt is increased, the contribution of the negative moment from oil squeezing between the lower ring surface and the lower groove flank decreases because less contact is made with the oil film. This occurs until a certain groove tilt is exceeded, at which point no further contact is made with the oil film. Therefore, there is no further increase in top ring positive twist beyond that groove tilt.

5.3. Experimental Validation

In order to validate the model predictions that were described in the previous sections, several reduced friction ring designs were procured and tested on the engine described in Section 5.1. All of the experimental work in this study was conducted at Colorado State University by students and faculty in the Engines and Energy Conversion Lab. Based on the model predictions obtained in the previous sections and the methods developed to minimize the adverse effects of the reduced friction designs, certain combinations of designs were selected for testing in this study. These are presented in the test matrix contained in Table 5-2 below.

Design Name	Top Ring	Second Ring	OCR	Piston
Baseline	Stock	Stock	Stock	Stock
Low-Tension OCR	Stock	Stock	Reduced Tension	Stock
Skewed Barrel Top Ring	Skewed Barrel	Stock	Stock	Stock
Low-Tension OCR, Reduced Oil Consumption	Stock	Negative Static Twist	Reduced Tension	Stock
Upward Top Ring Groove Tilt	High Static Twist	Stock	Stock	Upward Top Ring Groove Tilt
Optimized System	Skewed Barrel	Negative Static Twist	Reduced Tension	Stock

Table 5-2: Test Matrix

It should be noted that the reduced axial height top rings were not procured and tested in the experimental evaluation because the reduction in friction expected from this design is less than the reduction in friction expected from implementation of the other low-friction top ring designs. In addition, the smaller axial height is expected to reduce ring life. Therefore, this design was not investigated in the experimental portion of this study. In addition, although they were originally intended to be included in the experimental portion of this study, time constraints prevented the experimental investigation of the top ring groove upward tilt design and the second ring with negative twist.

5.3.1. General Description of Experimental Setup

The Waukesha VGF18GL engine described in Section 5.1 was installed and instrumented in the Engines and Energy Conversion Lab at Colorado State University. The experiments were conducted with the primary goal of assessing the friction reduction achieved by the implementation of the reduced friction designs contained in Table 5-2. However, since the goal of this study was also to evaluate potential adverse effects that may occur as a result of implementation of the reduced friction designs, oil consumption and blowby were measured as well. Interring pressures were also measured to assess the level of agreement between the model and the experiment. Since the model provides information about the land pressures throughout the engine cycle, for certain portions of the cycle, data from the transducers can be compared with the model predictions. Pressure transducer data is both accurate and reliable and therefore this is an effective way to compare the results of the model with those obtained experimentally.

The engine was instrumented with the equipment shown in Figure 5-13 below.

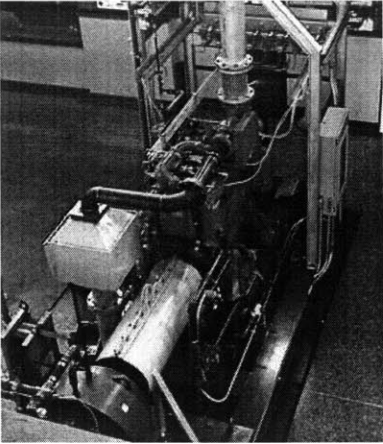
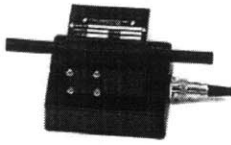
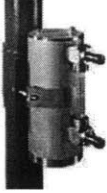


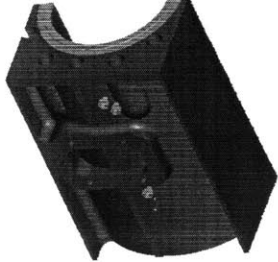
Dynamometer	Blowby Flowmeter	Oil Consumption Meter
		
	Cylinder Pressure Transducers (6)	Interring Pressure Transducers (3)
		

Figure 5-13: Experimental Setup

5.3.2. Description of Instrumentation

The interring pressure transducers were located at three specific positions along the liner in cylinder #5. Transducer 1 was located in between the TDC position of the top ring and the TDC position of the second ring. Transducer 2 was located between the TDC position of the second ring and the TDC position of the oil control ring. Transducer 3 was located between the BDC position of the top ring and the BDC position of the second ring. These locations were chosen so as to provide pressure data in the most interesting parts of the engine cycle for this study. As mentioned previously, the accuracy of pressure measurements obtained from pressure transducers makes this an effective method by which to check the consistency between the model and the experiment.

A J-Tec Associates inline blowby flowmeter was used to measure the flow rate of the blowby gases in this study. This meter uses the principle of vortex shedding to measure the flow rate of the blowby gases. A small strut inside the flow tube creates Karman vortices, and the frequency of the vortices is measured by an ultrasonic beam. Since the

Strouhal number, $St = fL/v$, is constant over a wide range of Reynolds numbers, the flow velocity is directly proportional to the vortex shedding frequency. The volumetric flow rate is determined from the flow velocity.

Oil consumption was measured using an AVL 403S Oil Consumption Meter. This device uses a sensor to measure the change in oil level in the sump. The sensor is a cylindrical container of oil filled to the same level as the sump, mounted at the same height above the ground. To measure oil consumption, a refill method is used in which a predetermined mass of oil to be used to refill the system is set as an input into the control unit. The engine is then run over a certain measurement time, and the number of times required to refill the system in order to keep the oil level in the sensor constant is recorded. Since the mass of oil used to refill the system is a predetermined input, knowing the number of times required to refill the system, the total amount of oil consumed over the measurement period can be determined. This information can then be used to calculate the oil consumption rate. Obtaining accurate results with this method requires that no changes in speed and load of the engine be made during the measurement time. In addition, the engine must be at a thermally stable at the desired operating condition when the test begins.

5.3.3. Experimental Procedure

The following procedure was used to obtain the required data from the experiment for each set of piston rings as described in the test matrix in Table 5-2.

For each test that was conducted, the engine was run for 30-45 minutes to allow it to reach thermal stability. Thermal stability was achieved when the cooling water reached 180°C and the oil temperature reached 175°C. After these temperatures were reached, they were held at that level by a closed-loop control system. The operating conditions for each of the tests were fixed at 200 psi BMEP and 1800 rpm. Once thermal stability was

achieved, 1000 cycles of cylinder pressure data were recorded over all 6 cylinders. In addition, 1000 cycles of interring pressure data were recorded in cylinder #5.

The torque and blowby flow rate, along with other slow-speed measurement data such as temperatures and pressures taken in various parts of the engine were then taken using a 5 minute running average with a 1 Hz sampling frequency during that time. It should be noted that the load cell used to measure torque was calibrated to an accuracy of +/-10 Nm.

Oil consumption data was averaged over three hours and measurements were taken on an hourly basis following the 30-45 minute warm-up period to thermally stabilize the engine, and the 5 minute running average tests. Oil consumption was measured for each of the different designs, but could not be compared to any specific model prediction, as the model is not currently capable of predicting overall oil consumption quantitatively.

Friction reduction was quantified by measuring the change in FMEP from the baseline design for each of the reduced friction designs. The method used for this calculation is described in detail in Appendix B. It was not possible to measure the specific FMEP contribution from the piston ring pack in this study, because this would require knowing the exact contribution of the ring pack to overall friction in the engine. Although this information was available from motoring friction data obtained from a teardown test, motoring friction data does not reflect the effect of high pressures in the cylinder, which has a very important effect on friction [1]. Therefore, the only way in which the designs could be evaluated was by measuring the change in FMEP for each of the designs compared to the baseline case. With this method, it is not necessary to know the specific contribution of the ring pack friction to overall FMEP, as the change in FMEP should reflect only the effect of changing the piston rings, provided everything else is held relatively constant.

Before any of the reduced friction designs were investigated, test results were first obtained from running the engine with the stock piston ring pack. This was done for several purposes:

- To investigate and evaluate the variability and repeatability of the pressure measurements obtained by CSU
- To compare the land pressure measurements with the model predictions in order to assess the level of agreement between the model predictions and experimental results
- To obtain baseline values for FMEP, blowby and oil consumption to assess both the level of agreement between the model and the experiment, and the change in these measured values resulting from implementation of the reduced friction designs

Results from the baseline test in terms of each of the above criteria are presented in the sections that follow.

5.3.4. Variability and Repeatability of Measured Data

One of the most major concerns in this study in the comparison between the model predictions and experimental results was the potential variation in the ambient conditions and engine operation that might lead to appreciable variations in the IMEP data obtained and lack of repeatability in the measurements. If the variability in the IMEP data were on the order of the expected friction reduction, the experimental component of this study would be inconclusive. This was less likely to be the case with a larger data set, and therefore three test runs were conducted at the operating condition being tested. An average was taken over the three tests in order to try to minimize the potential errors introduced by these factors.

In order to evaluate the variability and repeatability of the pressure measurements, IMEP data was calculated from the cylinder pressure data for each of the 1000 cycles over all six cylinders, and is plotted in a histogram in Figure 5-14. For ease of comparison, a normal distribution is plotted above the IMEP data. It should be noted that insufficient

data was available to account for the variation in the crank angle at which peak pressure is achieved, and therefore only the mean value of this crank angle was used in the determination of the IMEP data shown in the figure. This would affect the calculated IMEP's slightly, but more significantly, would lead to an overestimate of the standard deviation of the data. Nevertheless, even with these considerations in mind, the measurements still form a normal distribution, and data from other tests is expected to take on a similar form. It should also be noted that the data in Figure 5-14 below was only taken over one test run. In the tests that were conducted for the purposes of evaluating friction reduction in this study, the data was taken over three test runs and averaged, which should reduce the standard deviation and make the actual distribution even closer to normal.

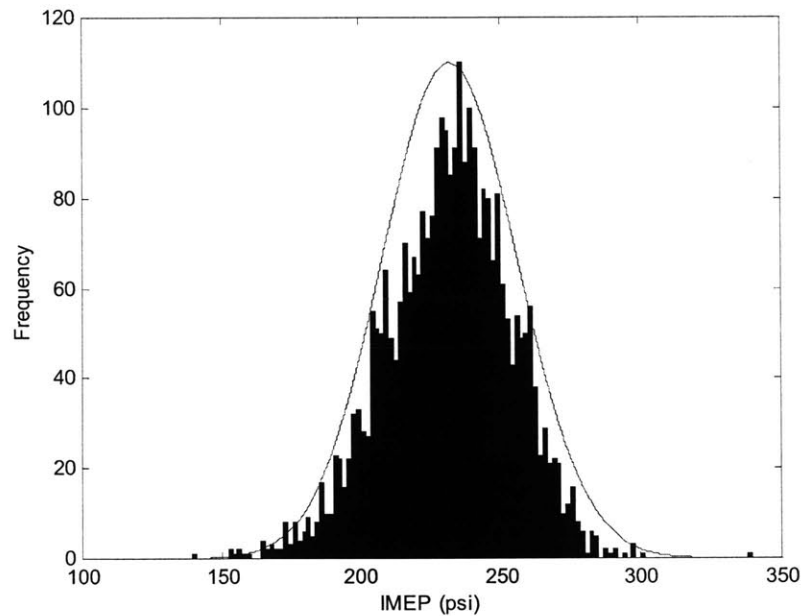


Figure 5-14: Distribution of IMEP Measurements

Since the data follows a normal distribution, if a reduction in friction is observed on average between the different designs that are to be investigated in this study, it is much more credible than if the data were scattered in a more random pattern. Since the reduction in friction is expected to be small compared to the values being measured, the credibility of any conclusions that are drawn depends on the spread of the data obtained.

A normal distribution indicates that a sufficient number of data points have been taken to ensure that a credible average value is obtained, and this lends belief to conclusions that were drawn in this study.

To further reinforce the quality of the conclusions drawn from this study, a statistical analysis was conducted on all of the data obtained from each of the tests in order to determine whether or not a change has occurred between designs. Hypothesis testing was conducted on the difference in the mean values using a confidence interval of 95%. The details of this calculation are described in Appendix B.

5.2.5. Comparison of Pressure Data

To assess the level of agreement between the model and the experiment, the interring pressure data obtained from the transducers in cylinder #5 was compared to the land pressures predicted by the model. In order to carry out this comparison, a representative cycle was taken out of the 1000 cycles of pressure data recorded. A representative cycle was used rather than averaged data so that no physically significant fluctuations in the pressure were damped out by the averaging process. The experimentally obtained pressure data is shown in Figure 5-15 below, along with a diagram illustrating the locations of the pressure transducers along the liner in cylinder #5.

The cylinder pressure data from the representative cycle mentioned above was used as input into the model and interring pressure predictions were obtained. In order to more carefully consider the qualitative agreement between the experiment and the model, certain parts of the engine cycle were compared more closely. It should be noted that data for the entire engine cycle could not be compared because the pressure transducers only measure interring pressures in certain parts of the cycle, whereas the model predicts land pressure data throughout the cycle. The region of most significance for comparison is the region around TDC of compression, as this is where two of the transducers are

located. For clarity, the pressure predictions obtained experimentally are magnified below in Figure 5-16 to show the region of interest.

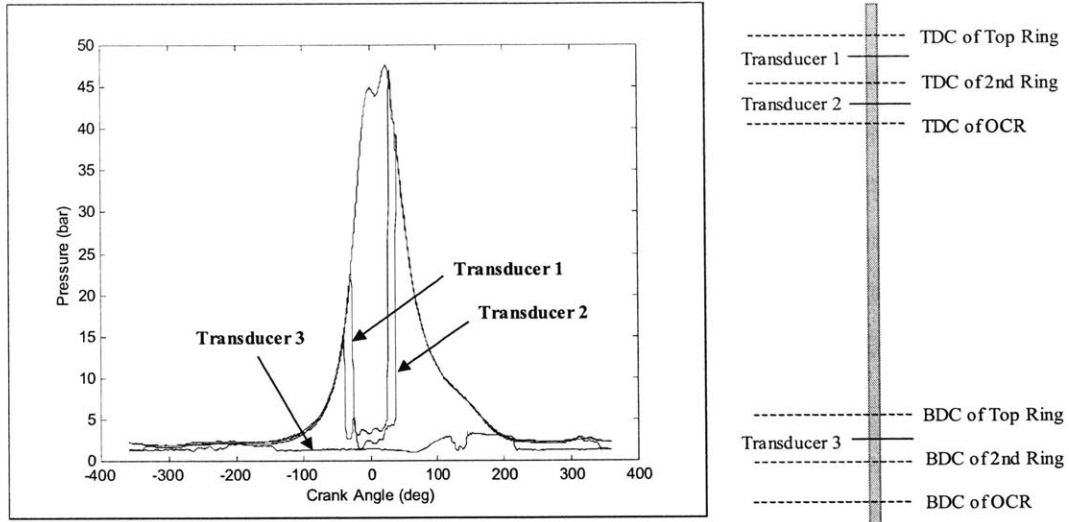


Figure 5-15: Experimental Pressure Data

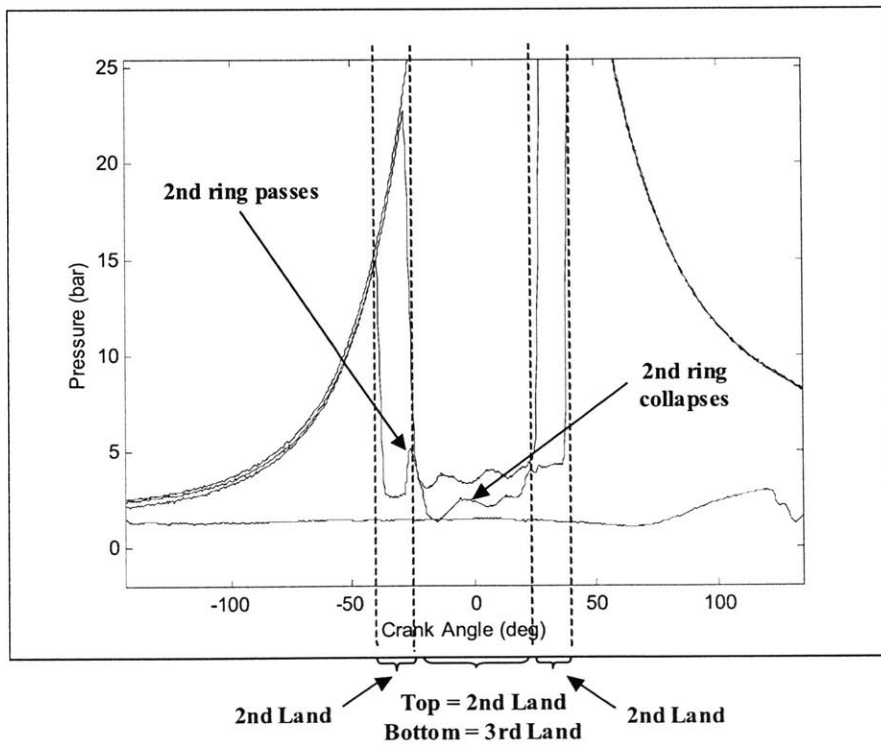


Figure 5-16: Magnified View of Pressure Data around TDC of Compression

The fluctuations that can be seen in the land pressure data are likely to be a result of a phenomenon called second ring collapse, which was briefly mentioned in Section 4.4.2. The physics of second ring collapse is discussed in detail in [21]. Ring collapse occurs when the upper ID corner of the ring is sealed against the top of the groove, and therefore the pressure acting downward on the ring face is able to push the ring inward before it can push it downward, as was depicted in Figure 4-7. This results in a large flow rate of gases from the cylinder passing through the ring-liner interface until the tension of the ring pushes it back against the liner and the process repeats again. This phenomenon happens more readily to the second ring as a result of its tendency to seal the upper OD corner of the groove and block the path for gas flow into the second ring groove. The spike that is present in the data from Transducer 2 in Figure 5-16 occurs when the second ring passes the transducer. When this happens, the volume of the region exposed to the transducer hole is significantly reduced and therefore the pressure increases, resulting in the spike. It is interesting to note that the same spike is not observed when the second ring passes at the beginning of the expansion stroke. If the second ring were collapsing during that period, there would be a significantly larger separation between the ring and the liner and this would explain the missing pressure spike.

To evaluate the agreement between the model and experiment, both model predictions and experimental pressure data are plotted in the region of interest around TDC of compression in Figure 5-17 below. In this figure, the dot-dashed lines indicate the pressure transducer data that was shown in Figure 5-16, and the solid lines represent data obtained by the model as indicated in the figure.

Overall, there is very good qualitative and quantitative agreement between the experimental and the model. In accordance with experimental findings, the model predicts second ring collapse in the region around TDC of compression as shown by the pressure fluctuations in the second and third land that are similar in magnitude to the experimental predictions. Good agreement is obtained in terms of the magnitude of the pressure data over most of the region under consideration.

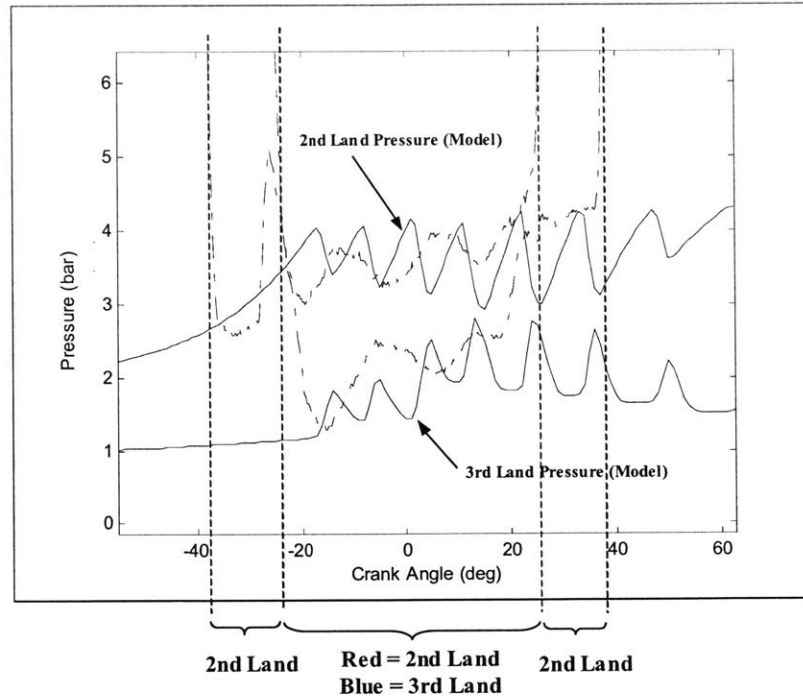


Figure 5-17: Comparison of Pressure Data between Model and Experiment

This comparison between the pressure data was carried out for each of the ring designs that were investigated in this study. For brevity, data is not shown for each case, as there was generally good agreement observed.

Having established good agreement in the pressure data between the model and the experiment, the designs were then evaluated and compared to assess friction reduction, as well as any potential changes in oil consumption or blowby. These results are included in the sections that follow, beginning with the baseline test results, which were used as a basis for comparison for each of the reduced friction designs.

5.3.6. Baseline Test Results

The baseline test results are summarized in Table 5-3 below. As discussed previously, the FMEP value obtained experimentally represents friction power losses in the entire engine, whereas the model predicted value represents the FMEP contribution from the

piston ring pack alone. As a result, the FMEP contribution from the piston rings based on the experimental data that is given in the table is estimated assuming that the rings account for 20% of the total engine friction losses. This is the best estimate that can be made using the available data.

	Model Prediction		Experimental Data
	OS1	OS2	
FMEP (kPa)	18.97	33.29	28.25
Blowby (L/min)	69.4	69.4	72.35 ± 2.39
Oil Consumption (g/hr)	N/A	N/A	48.30 ± 0.34

Table 5-3: Results for the Baseline Case

It can be seen from the table that the estimated FMEP obtained experimentally lies in between the values corresponding to the minimum and maximum oil supply conditions obtained using the model. The fact that it is closer to the value obtained from the model for the minimum oil supply condition indicates that there may in fact be very little oil supply to the dry region. However, this cannot be established conclusively here, as this value was obtained based on an estimate for the contribution of the piston rings to overall engine friction. Blowby data also shows good agreement between the model and the experiment. A specific value for oil consumption could not be predicted by the model, and therefore a comparison could not be made with the experimentally obtained value.

5.3.7. Results for Reduced Tension Oil Control Ring

The stock oil control ring was modified to reduce tension by 50% for this test. This was accomplished by cutting the spring in half, as the length of the spring is directly proportional to the ring tension. The springs were cut by the ring manufacturer, and the tension of each of the rings was subsequently measured to ensure that no significant variation existed between the rings to be used in the different cylinders. The model predictions for the low-tension oil control ring design were obtained using the average ring tension between all of the rings as input. The results for this test are shown below in

Table 5-4. It should be noted that FMEP reduction is the first category in this table, as opposed to the table in the previous section, which listed the overall FMEP in the engine. This is the metric that is used to compare the model and the experiment in this study, and since the contribution of the piston rings to the overall friction is not known exactly, this is the most effective way to quantify the results.

	Model Prediction		Experimental Data
	OS1	OS2	
FMEP Reduction from Baseline (kPa)	4.71	9.15	11.17 ± 1.54
Blowby (L/min)	83.9	83.9	75.43 ± 3.40
Oil Consumption (g/hr)	N/A	N/A	105.73 ± 1.50

Table 5-4: Results for Reduced Tension Oil Control Ring

FMEP was reduced by between 5 and 10 kPa using this design according to the model predictions for both OS1 and OS2, and by 11.17 kPa according to the experimental data within a 95% confidence interval. Oil consumption increased by a factor of roughly 2 as a result of this change, as was expected because of the reduced ability of the oil control ring to conform to the liner due to its reduced tension.

5.3.8. Results for Skewed Barrel Top Ring

The stock top ring was modified by introducing a skewed barrel profile as described in Section 4.1.1. The extent of skewness was such that the location of the minimum point was 15% of the total axial height from the bottom surface of the ring in the untwisted state.

A skewed barrel top ring design actually has a similar effect on groove wear as the upward tilted groove design discussed in Section 4.3.2. As the top ring is pushed down to conform to the lower groove flank around TDC of compression/expansion, there is an unbalanced pressure force acting on the upper ring face in the clearance between the groove and the liner which causes the top ring to rotate around the lower OD corner of

the groove. There is therefore more concentrated contact at the OD corner of the groove, which tends to wear down the groove and may result in the minimum point moving up along the profile if the ring stays conformed to the groove, which would result in higher friction.

As a result, a slight positive static twist was introduced in the top ring in order to prevent this concentrated OD contact. The exact dimensions of the groove required to achieve a certain static twist were determined using a set of models developed by L. Liu. A more detailed description of these models can be found in [23].

The results for the top ring with a skewed barrel profile are shown below in Table 5-5. It was mentioned previously that it is difficult to manufacture a skewed barrel profile to the exact desired dimensions. As a result, there was some variation in the exact location of the minimum point on the profile between the different rings. To facilitate the modeling process, the ring manufacturer measured the final dimensions of each of the rings at different circumferential locations. To account for this in the model predictions, a minimum and maximum case was obtained for each oil supply condition for the range of values that were measured on the different rings after the machining process. Extreme cases represented the mean value for all of the rings plus or minus one standard deviation.

	Model Prediction		Experimental Data
	OS1	OS2	
FMEP Reduction from Baseline (kPa)	1.19-1.47	5.59-6.14	N/A
Blowby (L/min)	84.9	83.8	66.07 ± 1.03
Oil Consumption (g/hr)	N/A	N/A	38.58 ± 0.39

Table 5-5: Results for Skewed Barrel Profile Top Ring

No experimental result for FMEP reduction was available for comparison in this case. This is because the combustion conditions varied significantly between this test and the baseline test. This is a direct result of the variation in the composition of the natural gas that was obtained from the pipeline at the different times of year at which the tests were

conducted. The low-tension oil control ring test was conducted only several weeks after the baseline test, and therefore the fuel composition did not vary significantly over this period of time. However, much more time elapsed between the low-tension oil control ring test and the skewed barrel top ring test. The amount of variation in the fuel composition was so significant that the air-fuel ratio had to be varied in an attempt to achieve similar stability in the combustion conditions. Unfortunately, this introduced significant error in the experimental data and as a result, no useful friction data can be reported for this case. The model shows promising results, with values for friction reduction from the baseline case between 1 and 6 kPa, depending on the oil supply condition assumed.

Oil consumption data is exactly what was expected for this case. Oil consumption reduced by 20% compared to the baseline case for the skewed barrel top ring, which is due to the reduced force from radial pressure acting on the top ring near TDC of compression/expansion. Because of the reduced net radial load on the top ring in this part of the engine cycle, the ring does not conform as well to the liner, and this allows more downward gas flow to escape through the ring-liner interface, which can carry oil towards the combustion chamber.

Blowby actually reduced for this case, but this may have been affected by the variation in the engine operating conditions. Blowby typically scales roughly with peak cylinder pressure, which is greatly affected by the combustion conditions. Since the combustion conditions varied significantly in this test compared to the baseline test, the blowby data obtained for this case may not be reliable. The blowby predicted by the model is almost identical for the case of the skewed barrel top ring compared to the baseline case.

5.3.9. Results for Combined System

The original intention of this study was to test an optimized system that combines all of the individual benefits of each of the designs discussed in the previous sections. Such a

system would consist of the best low-friction top ring design, the second ring design with negative twist, and the reduced tension oil control ring. Model predictions indicated that the top ring design that resulted in the largest friction reduction was the skewed barrel top ring. This design also contributes to a reduction in oil consumption, which was shown experimentally. Therefore, according to the model predictions, the optimized system should consist of a skewed barrel top ring, a negative twist second ring, and a reduced tension oil control ring.

The model predictions for this optimized system are presented in Table 5-6 below. Due to the sensitivity of these predictions to the exact shape of the skewed barrel top ring, the approach used and described in Section 5.3.8 was used to account for the tolerances involved in the top ring profile. As a result, a range of values was obtained for friction reduction for each oil supply condition according to the model predictions.

	Model Prediction		Experimental Data
	OS1	OS2	
FMEP Reduction from Baseline (kPa)	13.44-13.71	15.32-20.96	N/A
Blowby (L/min)	91.8	91.8	N/A
Oil Consumption (g/hr)	N/A	N/A	N/A

Table 5-6: Results for Combined System

As can be seen from this table of results, FMEP can be reduced by as much as 21 kPa according to the model predictions. In addition, there was no significantly adverse effect on blowby introduced by these design changes. Unfortunately, no oil consumption data was available for this test, but the result is expected to be close to the baseline value, because the increase in oil consumption due to the reduced oil control ring tension is expected to be offset by the reduction in oil consumption due to the second ring negative twist and the skewed barrel top ring.

Overall, according to the model predictions, a reduction in friction of 35% is possible by implementing the skewed barrel top ring, the second ring with negative twist, and the

low-tension oil control ring. This optimized system thus has the potential to improve efficiency and reduce emissions in high load, low speed engines. Quantitative estimates for these improvements are provided in Chapter 7.

6. Further Opportunities for Friction Reduction

In the sections that follow, several additional opportunities for friction reduction are discussed. These strategies were not explored in full detail in this study, and are therefore only mentioned as important areas for future consideration.

6.1. Liner Roughness

The liner roughness affects both the friction generated from hydrodynamic lubrication as well as the amount of friction generated in mixed lubrication conditions. In the case of pure hydrodynamic friction, the liner roughness will affect the flow factors introduced in the governing equations that were mentioned in Section 2.4. Although the liner roughness does not affect the amount of boundary friction generated, Eq. (1) shows that the criteria for transition to boundary lubrication will be affected by the combined roughness between the ring and the liner, and therefore changes in the liner roughness may result in a larger portion of the engine cycle in mixed lubrication.

Model predictions indicate that significant friction reduction can be achieved by reducing liner roughness. These predictions are shown for the Waukesha engine in Figure 6-1 below. As can be seen from the figure, liner roughness has the potential to reduce total ring pack FMEP by 10-15%.

The actual liner roughness that can be achieved in practice is limited by manufacturing processes. It is also believed that some liner roughness is advantageous as it improves oil transport by introducing grooves in which oil can be stored and made available in different parts of the engine cycle. However, model predictions for this case indicate that reductions in liner roughness beyond 50% of the current value yield only small reductions in friction. As a result, improvements in oil transport and a significant friction reduction can be achieved by reducing liner roughness by 50% in the Waukesha engine.

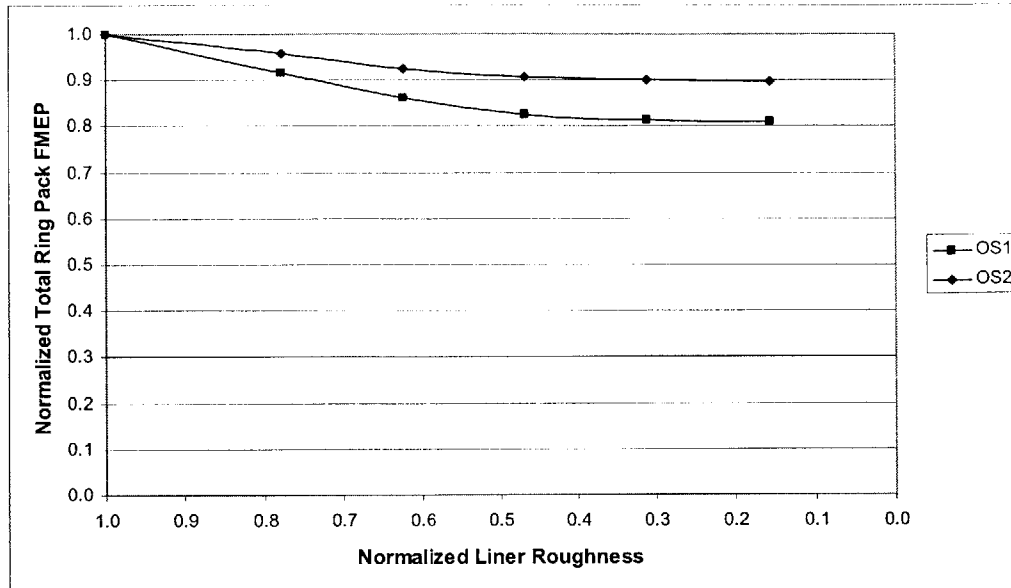


Figure 6-1: Effect of Liner Roughness on Total Ring Pack FMEP

As a result of the above considerations, there may be an optimal liner roughness in order to maximize oil transport and minimize friction in different types of engines. This could be investigated in more detail in future studies. In addition, it should be noted that the model currently uses a Gaussian distribution to model surface roughness. Studies could also be conducted with the goal of incorporating more realistic methods to describe roughness statistically. For example, levels of skewness and kurtosis could be incorporated into the description of the roughness of a surface and this may help to provide insight into the optimal liner design to achieve minimum friction and maximum oil transport.

6.2. Piston Land Height Reduction

Another way in which top ring friction can be reduced in the region around TDC of compression is to reduce the physical length of the dry region identified in Section 3.1.5. Reducing the length of this region can be achieved by reducing the second and third land heights on the piston, as shown in Figure 3-7.

Model predictions for the reduction in total ring pack FMEP in the Waukesha engine from a reduction in second and third land heights is shown below in Figure 6-2. As can be seen from this figure, these changes have the potential to reduce friction by 5%.

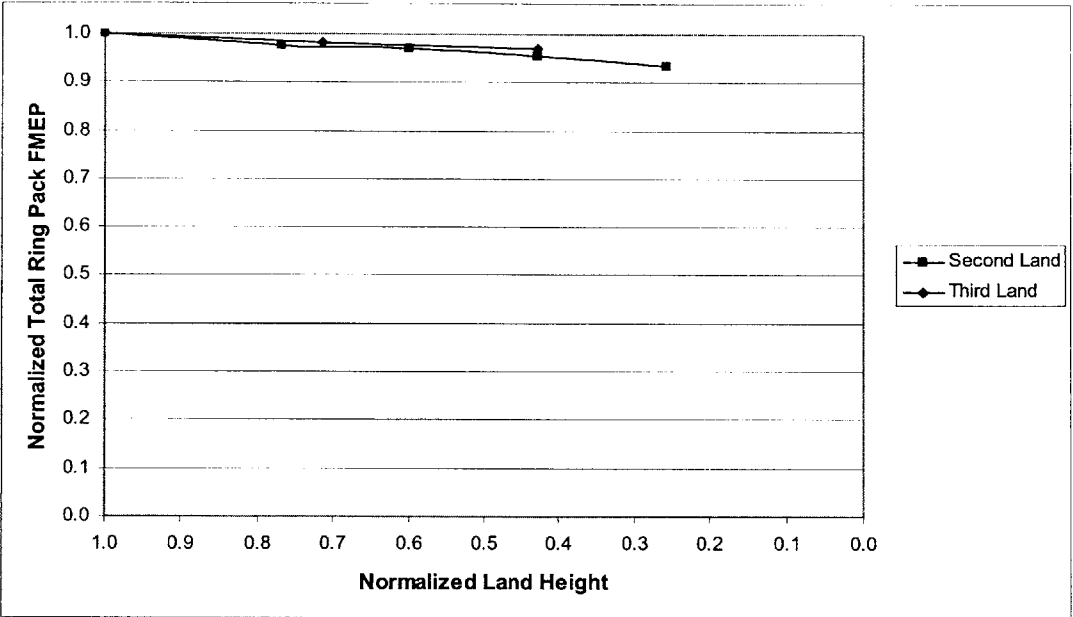


Figure 6-2: Effect of Land Heights on Total Ring Pack FMEP

It should be noted that only results for OS1 are presented in the above figure. This is because reducing the length of the dry region would have no effect if OS2 were the actual oil supply condition, since in this case the top ring was predicted to be in boundary lubrication throughout the engine cycle and therefore there is no real distinction between the dry region and the rest of the liner for this condition.

Reducing the land heights may have other adverse effects, such as significantly reducing the structural strength of the piston. More analysis would therefore be needed to ensure that this is not the case. Depending on the extent to which land heights are to be reduced, a full Finite Element Analysis may be required. As a result, due to the time involved in this study, investigation of this type of design is left for potential future consideration.

6.3. Further Insights into Potential Designs for Reduced Top Ring Friction at Midstroke from Nondimensionalization of Governing Equations

In Chapter 2, the equations governing piston ring friction and lubrication were derived and the method of solution was outlined. The use of the friction and lubrication model was necessary in order to solve the governing equations, as they could not be solved analytically. There is, however, another method that can be used to study the relationship between the parameters governing friction and lubrication in the piston ring pack without solving the equations exactly. If the governing equations are written in nondimensional form and combined, relationships between nondimensional parameters can be established and potential friction reduction strategies can be extracted. This would be a faster, more general method that could be used to conduct parametric studies to identify design strategies, without obtaining specific model predictions for those strategies. It would also be advantageous because the results would not be specific to a particular engine, and therefore general trends could potentially be extracted.

In Chapter 3, justification was given for the emphasis of this study on the top ring friction near TDC of compression and the oil control ring friction generated throughout the engine cycle. It was briefly noted that top ring friction around the midstroke region can become on the same order of magnitude as the friction around TDC of compression in higher speed, lower load engines. In this section, the governing equations from Chapter 2 are nondimensionalized for the top ring in the midstroke region to lay the foundation for future work in the development of general reduced friction strategies for these operating conditions.

In this investigation, the inlet and outlet wetting coordinates, x_1 and x_2 , respectively, are treated as unknowns and the minimum oil film thickness, h_o , is considered to be a known value that can be determined from application of conservation of mass and the Reynolds' Equation, provided the oil supply, h_{∞} , is known. Although the minimum oil film thickness is not an explicitly known value, it must be treated as such in order to

nondimensionalize the equations in a physically meaningful way. The two unknowns (x_1 and x_2) will be determined in the analysis that follows.

As shown in the previous section, during the midstroke region of the cycle, the Reynolds' Equation reduces to:

$$\frac{\partial}{\partial x} \left(\frac{h^3}{\mu} \frac{dp}{dx} \right) = 6U \frac{\partial h}{\partial x} \quad (2.7)$$

Assuming negligible viscosity changes in the flow direction, Eq. (2.7) can be integrated as follows:

$$h^3 \frac{dp}{dx} = 6\mu U h + C_1 \quad (6.1)$$

For partially-flooded outlet conditions, which is typically applicable to the top ring at midstroke, the Reynolds exit condition applies:

$$\frac{dp_2}{dx} = 0$$

Applying this boundary condition to Eq. (6.1) yields:

$$\frac{dp}{dx} = 6\mu U \left(\frac{h - h_2}{h^3} \right) \quad (6.2)$$

Integrating a second time yields:

$$\int_{x_1}^{x_2} \left(\frac{h - h_2}{h^3} \right) dx = \frac{p_1 - p_2}{6\mu U} \quad (6.3)$$

From Chapter 2, since the system is assumed to be quasi-steady in the radial direction, application of a radial force balance yields:

$$\sum F_r = p_1(B_1 + x_1) + \int_{x_1}^{x_2} p(x) dx + p_2(B_2 - x_2) - p_1(B_1 + B_2) - W = 0 \quad (2.8)$$

The pressure term can be integrated by parts, which yields the following result:

$$\int_{x_1}^{x_2} p(x) dx = p \Big|_{x_1}^{x_2} - \int_{x_1}^{x_2} x \frac{dp}{dx} dx$$

Upon substituting this result into Eq. (2.8), after some simplification and rearrangement, the following result is obtained:

$$\int_{x_1}^{x_2} x \left(\frac{h-h_2}{h^3} \right) dx = -\frac{1}{6\mu U} [W + (p_1 - p_2)B_2] \quad (6.4)$$

The following parabolic profile is assumed for the top ring:

$$h(x) = h_o + \frac{x^2}{2a} \quad (6.5)$$

The following nondimensionalization is consistent with Eq. (6.5):

$$x^* = \frac{x}{\sqrt{2ah_o}}$$

$$h^* = \frac{h}{h_o}$$

It should be noted that it would not be as physically meaningful to nondimensionalize x by the ring width, B , for example. This is because x does not depend on the ring width for partially-flooded conditions. If the ring width is increased, there is no reason to expect the wetting locations to change. However, for partially-flooded conditions, x does depend on the minimum oil film thickness and therefore it is used as a variable for nondimensionalization. Substituting these nondimensional parameters into the governing equations Eq. (6.3) and Eq. (6.4) yields:

$$\int_{x_1^*}^{x_2^*} \frac{h^* - h_2^*}{h^{*3}} dx^* = \sqrt{\frac{h_o}{2a}} \left(\frac{(p_1 - p_2)h_o}{6\mu U} \right) \quad (6.6)$$

$$\int_{x_1^*}^{x_2^*} x^* \frac{h^* - h_2^*}{h^{*3}} dx^* = -\frac{1}{6\mu U} \left(\frac{h_o}{2a} \right) [W + (p_1 - p_2)B_2] \quad (6.7)$$

For brevity, the following nondimensional parameters are introduced:

$$N_1 = \sqrt{\frac{h_o}{2a}} \left(\frac{(p_1 - p_2)h_o}{6\mu U} \right)$$

$$N_2 = \frac{W}{6\mu U} \left(\frac{h_o}{2a} \right)$$

$$N_3 = \frac{(p_1 - p_2)B_2}{6\mu U} \left(\frac{h_o}{2a} \right)$$

In terms of the above parameters, Eq. (6.6) and Eq. (6.7) are of the form:

$$\int_{x_1^*}^{x_2^*} \frac{h^* - h_2^*}{h^{*3}} dx^* = N_1$$

$$\int_{x_1^*}^{x_2^*} x^* \frac{h^* - h_2^*}{h^{*3}} dx^* = -(N_2 + N_3)$$

These are implicit equations of the form:

$$f_1(x_1^*, x_2^*, N_1, N_2, N_3) = 0$$

$$f_2(x_1^*, x_2^*, N_1, N_2, N_3) = 0$$

Therefore, solutions are of the form:

$$x_1^* = X_1(N_1, N_2, N_3)$$

$$x_2^* = X_2(N_1, N_2, N_3)$$

These solutions can be equivalently expressed as functions of combinations of the nondimensional parameters, omitting constants. Following this approach, more physically-based parameters are used in place of N_1 and N_3 and are defined as follows:

$$N_4 = \frac{N_1}{N_3} = \frac{\sqrt{2a} h_o}{\sqrt{h_o} B_2} = \frac{\sqrt{2ah_o}}{B_2}$$

$$N_5 = \frac{N_2}{N_3} = \frac{W}{\Delta p B_2}$$

The solutions are thus equivalently given by:

$$x_1^* = X_1(N_2, N_4, N_5)$$

$$x_2^* = X_2(N_2, N_4, N_5) \tag{6.8}$$

Now, substituting Eq. (6.2) into the expression for shear stress derived in Appendix A (Eq. (A.5)), shear stress can be expressed as follows:

$$\tau(x) = \frac{\mu U}{h^2} (2h - 3h_2) \tag{6.9}$$

Hydrodynamic friction force per unit circumferential length is given by:

$$F_f = \int_{x_1}^{x_2} \tau(x) dx$$

Using Eq. (A.5):

$$F_f = \int_{x_1}^{x_2} \mu U \left(\frac{2h - 3h_2}{h^2} \right) dx$$

Nondimensionalization yields:

$$\frac{F_f}{\mu U} \sqrt{\frac{h_o}{2a}} = \int_{x_1^*}^{x_2^*} \left(\frac{2h^* - 3h_2^*}{h^{*2}} \right) dx^*$$

The result of the integral will be a function of only x_1^* and x_2^* and therefore will be given by the functional form given in Eq. (6.8). The nondimensional friction force per unit circumferential length is thus given by the following functional form:

$$F_f^* = \frac{F_f}{\mu U} \sqrt{\frac{h_o}{2a}} = F \left[\frac{W}{\mu U} \left(\frac{h_o}{2a} \right), \frac{W}{\Delta p B_2}, \frac{\sqrt{2ah_o}}{B_2} \right] \quad (6.10)$$

This functional relationship can be illustrated graphically to gain a better understanding of the parameters on which top ring hydrodynamic friction at midstroke depends most critically. A short program was developed for this purpose, which solves the governing equations numerically at a specific crank angle during the compression stroke. This program uses subroutines from the friction and lubrication model that was discussed previously in Chapter 2. The advantage of the program is that it considers only one crank angle in the cycle, which reduces run-time considerably. The disadvantage is that without consideration of the behavior of the piston ring-pack during the rest of the cycle, the oil film thickness on the liner is unknown, and the results from the subroutine are very sensitive to the initial guess for this value. One method by which to circumvent this issue would be to hold the oil film thickness along the liner constant, which can be physically interpreted as fixing the oil supply to the top ring.

To illustrate the nondimensional relationship using the program, a test matrix was constructed with the different values of the nondimensional parameters. Establishing the test matrix was done by first determining the limiting values of the parameters, using data from the Waukesha engine. The program was run with a coarse range of values between the limits to determine any ranges that yielded boundary lubrication conditions or top ring radial collapse, which were dismissed so as to provide information about strictly

pure hydrodynamic friction. A smaller, more refined grid was then established and the program was executed at these points.

The results are plotted in Figure 6-3 below. The x- and y- axes are the parameters N_2 and N_4 in Eq. (6.9), and the nondimensional friction is plotted on the z-axis. The different surfaces represent different values of the N_5 parameter. This plot represents the entire hydrodynamic friction map for the Waukesha engine at the specific crank angle being studied.

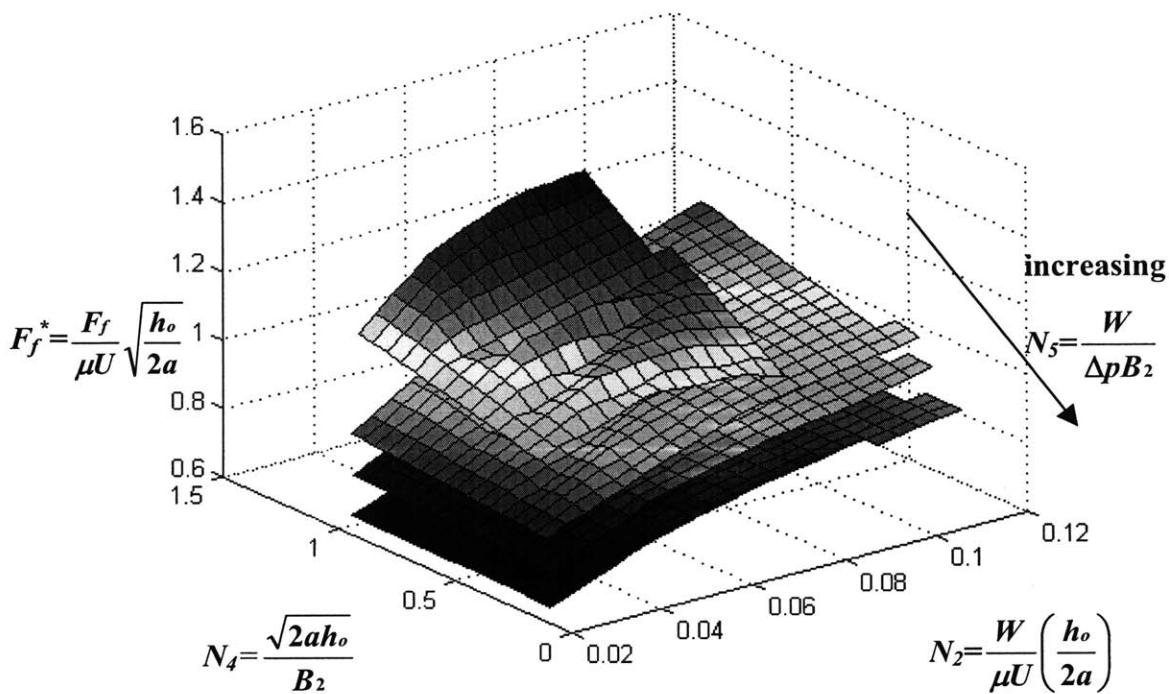


Figure 6-3: Top Ring Hydrodynamic Friction Map

The above figure shows the dependence of the nondimensional friction on the nondimensional parameters in Eq. (6.10) at a specific crank angle in the compression stroke. Using the same approach, similar graphs could be constructed for different regions of the engine cycle and interpreted to develop reduced friction design strategies for the top ring at midstroke. Due to the amount of detailed analysis required, this is left for potential investigation in future studies.

(This page was intentionally left blank)

7. Summary and Recommendations

The piston ring pack is the largest single contributor to friction power losses in modern internal combustion engines. In this study, reduced friction piston ring designs were developed with the help of modeling tools and tested on a full-scale engine. Additional designs were also developed to eliminate adverse effects such as increased oil consumption, blowby or wear that might accompany changes in ring designs to reduce friction.

A historical perspective was first presented to provide insight into the origin and evolution of piston ring designs since the Industrial Revolution. The impact of today's widely different internal combustion engine operating conditions on the main contributors to piston ring friction were identified, and the focus of this study was placed on engines operating in high load, low speed conditions.

For these operating conditions, the primary sources of friction in the piston ring pack were identified as the top ring around TDC of compression/expansion and the oil control ring throughout the engine cycle. The top ring's high contribution to friction near TDC of compression/expansion was a result of the lack of oil supply to this region, in combination with the high gas pressure acting on the back of the ring during this part of the engine cycle. The oil control ring's high contribution was a result of the high tension force acting on the small lands of the ring rails, which resulted in low oil film thickness and therefore a larger part of the engine cycle spent in mixed or boundary lubrication conditions.

Friction reduction strategies were developed in order to reduce the contribution of these primary sources of piston ring friction. For the top ring, the designs that were investigated included a skewed barrel profile, a reduced axial height and an upward tilted top ring groove in the piston. For the oil control ring, the use of rings with lower tension was recommended to achieve a reduction in friction.

Adverse effects that could occur as a result of the implementation of these designs were subsequently identified. The extent of the skewness of the barrel profile on the top ring was limited by manufacturing considerations as well as the potential onset of boundary lubrication conditions throughout the engine cycle. The reduced axial height compromised the structural strength of the top ring, resulting in earlier failure according to previous studies. The upward tilted piston groove was shown to be worn significantly by the top ring, resulting in the elimination of the upward tilt and therefore a shorter-lasting design. The reduced tension oil control ring design caused oil consumption to increase significantly.

Several additional design modifications were proposed to eliminate these adverse effects. The top ring to be used with the upward tilted piston groove was designed to have a positive static twist in order to prevent increased groove wear. A second ring with negative static twist was implemented with the reduced tension oil control ring in order to reduce oil consumption. The skewed barrel top ring was also found to reduce oil consumption.

To investigate the practical potential of these design strategies, prototypes for the reduced friction ring designs were procured and tested on a full-scale Waukesha natural gas power generation engine. First, model predictions were obtained to assess the friction reduction potential of each of the designs. These results were then compared with experimental results obtained from running the full-scale engine with the reduced friction ring designs. The experimental results were obtained by Colorado State University.

The model indicated that the implementation of the combination of all of the low-friction ring designs could reduce friction in the Waukesha engine by 35%. Due to time constraints and difficulties in achieving consistent combustion conditions in this study, the only experimental data that was obtained at this time was for the low-tension oil control ring test. Generally good agreement was found between the model predictions and the experimental results for this case.

Several other potential friction reduction opportunities were also identified in this study and left open as potential areas for further investigation. Reduced liner roughness and smaller piston land heights on friction were found to have potential to reduce friction, but were limited by practical considerations such as manufacturability and structural considerations. Another potential area for future investigation was identified as top ring friction at midstroke, which can become significant in high speed, low load operating conditions. An approach was provided that could be used in future studies to develop reduced friction design strategies for these operating conditions.

The combination of the skewed barrel top ring, the second ring with negative twist, and the low-tension oil control ring resulted in an optimized system with which engine friction was reduced by 35%, without any adverse effects on oil consumption, blowby or wear. In addition, it should be emphasized that no additional cost would result from the implementation of such designs, and no complex modifications would be needed on existing engine components. The combined system would result in an improvement in brake thermal efficiency of 0.5-1%. The improvement in efficiency would translate to a reduction in natural gas consumption of 330,723 ft³ in the Waukesha engine each year. If the engine were operating at 80% capacity in a given year, this would translate to a reduction in fuel cost of \$2,800 per year. More detail on the determination of these estimates is provided in Appendix C.

The design strategies developed in this study thus have promising potential for application in all modern internal combustion engines as they represent simple, low-cost methods to extract significant fuel savings and to reduce harmful environmental damage, without compromising engine performance.

(This page was intentionally left blank)

References

1. Richardson, D.E., "Review of Power Cylinder Friction for Diesel Engines", Internal Report, Cummins Engine Company
2. Nakada, M., "Piston and Piston Ring Tribology and Fuel Economy", Proceedings of International Tribology Conference, Yokohama, 1995
3. Ting, L.L., "A Review of Present Information on Piston Ring Tribology", SAE Paper 852355, 1985
4. Hill, S.B. and Newman, B.A., "Piston Ring Designs for Reduced Friction", SAE Paper 841222, 1984
5. McGeehan, J.A., "A Literature Review of the Effects of Piston and Ring Friction and Lubricating Oil Viscosity on Fuel Economy", SAE Paper 780673, 1978
6. Cullen, Joao A. and Frodsham, Gary M., "Reduced Cross Section Compression Rings for Diesel Engines", SAE Paper 971146, 1997
7. Economou, P.N., Dowson, D. and Baker, A.J.S., "Piston Ring Lubrication – Part I. The Historical Development of Piston Ring Technology", Energy Conservation Through Fluid Film Lubrication Technology: Frontiers in Research and Design, presented at the winter annual meeting of the ASME, New York, Dec. 2-7, 1979, Pg. 1-22
8. Rohde, S.M., Whitaker, K.W. and McAllister, G.T., "A Study of the Effects of Piston Ring and Engine Design Variables on Piston Ring Friction", Energy Conservation through Fluid Film Lubrication Technology: Frontiers in Research and Design, presented at the winter annual meeting of the ASME, New York, Dec. 2-7, 1979, Pg. 117-134
9. Jeng, Y., "Friction and Lubrication Analysis of a Piston Ring Pack", SAE Paper 920492, 1992
10. Tomanik, E., Nigro, E., Zabeu, C.B. and Peixoto, V.J.M., "Reduced Friction Power Cell Components", SAE Paper 2000-01-3321, 2000
11. Tian, T., "Modeling the Performance of the Piston Ring Pack in Internal Combustion Engines", PhD Thesis, Department of Mechanical Engineering, Massachusetts Institute of Technology, June 1997
12. Hu, Y., Cheng, S., Takayuki, A., Kobayashi, Y., Aoyama, S., "Numerical Simulation of Piston Ring in Mixed Lubrication - A Nonaxisymmetrical

- Analysis”, Transactions of the ASME, Journal of Tribology, Vol. 116, July 1994, Pg. 470-478
13. Greenwood, J.A., Tripp, J.H., “The Contact of Two Nominally Flat Rough Surfaces”, Proc. Inst. Mech. Engrs., Vol. 185, Pg. 625-633
 14. Patir, N., Cheng, H.S., “Application of Average Flow Model to Lubrication Between Rough Sliding Surfaces”, Transaction of the ASME, Journal of Lubrication Technology, Vol. 101, April 1979, Pg. 220-229
 15. Tian, T., Wong, V.W. and Heywood, J.B., “A Piston Ring Pack Film Thickness and Friction Model for Multigrade Oils and Rough Surfaces”, SAE Paper 962032, 1996; Also in SAE Trans., J. Fuels Lubricants, 1996, 105(4), Pg. 1783-1795
 16. Tian, T., Noordzij, L.B., Wong, V.W. and Heywood, J.B., “Modeling Piston-Ring Dynamics, Blowby, and Ring-Twist Effects”, ICE - Vol. 27-2, 1996 ASME Fall Technical Conference, Vol. 2, P.g 67-80, Fairborn, Ohio, Oct. 1996
 17. Vokac, A., “An Experimental Study of the Oil Evolution in Critical Piston Ring Pack Regions and the Effect of Piston and Ring Designs in an Internal Combustion Engine Utilizing Two-Dimensional Laser Induced Fluorescence and the Impact on Maritime Economics”, MS Thesis, Department of Mechanical Engineering, Massachusetts Institute of Technology, June 2004
 18. Thirouard, B., “Characterization and Modeling of the Fundamental Aspects of Oil Transport in the Piston Ring Pack of Internal Combustion Engines”, PhD Thesis, Department of Mechanical Engineering, Massachusetts Institute of Technology, June 2001
 19. Tian, T., “Dynamic Behaviors of Piston Rings and their Practical Impact. Part 2: Oil Transport, Friction and Wear of Ring/Liner Interface and the Effects of Piston and Ring Dynamics”, ImechE 2002, Pg. 229-247
 20. Heywood, J.B., “Internal Combustion Engine Fundamentals”, McGraw-Hill Inc., © 1988
 21. Tian, T., “Dynamic Behaviors of Piston Rings and their Practical Impact. Part 1: Ring Flutter and Ring Collapse and their Effects on Gas Flow and Oil Transport”, ImechE 2002, Pg. 209-227
 22. Yilmaz, E., Thirouard, B., Tian, T., Wong, V., Heywood, J.B. and Lee, N., “Analysis of Oil Consumption Behavior During Ramp Transients in a Production SI Engine”, SAE Paper 2001-01-3544, presented at the 2001 SAE Fall Fuel and Lubricant Meeting and Exposition, San Antonio, TX, Sept. 2001

23. Liu, L., Tian, T. and Rabute, R., “Development and Applications of an Analytical Tool for Ring Design”, SAE Paper 2003-01-3112, 2003
24. Montgomery, Douglas C., Runger, George C., Hubele, Norma F., “Engineering Statistics”, Second Edition, John Wiley & Sons, Inc., © 2001
25. Energy Information Administration, “US Total Natural Gas Prices”, 5/6/2004, http://tonto.eia.doe.gov/dnav/ng/ng_pri_sum_nus_m_d.htm
26. Pinkus, Oscar and Sternlicht, Beno, “Theory of Hydrodynamic Lubrication”, McGraw-Hill, 1961
27. Frene, J., Nicolas, D., Degueurce, B., Berthe, D., Godet, M., Hydrodynamic Lubrication: Tribology Series (Vol. 33), Elsevier, 1997
28. Class Notes from Measurement Lab, Department of Mechanical Engineering, McGill University, Montreal, 1998 Edition

(This page was intentionally left blank)

Appendix A: Derivation of Fundamental Equations

A.1. Shear Stress Between the Ring and the Liner and Volumetric Flow Rate of Oil

The shear stress generated between the ring and the liner and the volumetric flow rate of oil can be determined by applying conservation of mass and momentum to a fluid element under the ring surface as follows.

Conservation of Mass [26,27]:

$$\frac{d\rho}{dt} + \frac{\partial}{\partial x}(\rho u) + \frac{\partial}{\partial y}(\rho v) + \frac{\partial}{\partial z}(\rho w) = 0 \quad (\text{A.1})$$

Conservation of Momentum (Navier-Stokes Equations) [26,27]:

x-direction:

$$\rho \left(\frac{\partial u}{\partial t} + u \frac{\partial u}{\partial x} + v \frac{\partial u}{\partial y} + w \frac{\partial u}{\partial z} \right) = -\frac{\partial p}{\partial x} + \mu \left(\frac{\partial^2 u}{\partial x^2} + \frac{\partial^2 u}{\partial y^2} + \frac{\partial^2 u}{\partial z^2} \right) + \rho X$$

y-direction:

$$\rho \left(\frac{\partial v}{\partial t} + u \frac{\partial v}{\partial x} + v \frac{\partial v}{\partial y} + w \frac{\partial v}{\partial z} \right) = -\frac{\partial p}{\partial y} + \mu \left(\frac{\partial^2 v}{\partial x^2} + \frac{\partial^2 v}{\partial y^2} + \frac{\partial^2 v}{\partial z^2} \right) + \rho Y \quad (\text{A.2})$$

z-direction:

$$\rho \left(\frac{\partial w}{\partial t} + u \frac{\partial w}{\partial x} + v \frac{\partial w}{\partial y} + w \frac{\partial w}{\partial z} \right) = -\frac{\partial p}{\partial z} + \mu \left(\frac{\partial^2 w}{\partial x^2} + \frac{\partial^2 w}{\partial y^2} + \frac{\partial^2 w}{\partial z^2} \right) + \rho Z$$

For this particular case and in most bearing lubrication applications, the following assumptions are valid [26,27]:

1. Height of fluid film $y \ll x, z$ (film curvature can be ignored)
2. Negligible pressure variation across fluid film $\Rightarrow \frac{\partial p}{\partial y} = 0$
3. Laminar flow
4. No external forces act on fluid film $\Rightarrow X = Y = Z = 0$

5. Fluid inertia is small compared to viscous shear \Rightarrow LHS terms in Eq. (A.2) neglected
6. All velocity gradients are negligible compared to $\frac{\partial u}{\partial y}$, $\frac{\partial w}{\partial y}$.

With the above assumptions, Eq. (A.2) reduces to:

$$\begin{aligned}\frac{1}{\mu} \frac{\partial p}{\partial x} &= \frac{\partial^2 u}{\partial y^2} \\ \frac{1}{\mu} \frac{\partial p}{\partial z} &= \frac{\partial^2 w}{\partial y^2}\end{aligned}\tag{A.3}$$

An expression for shear stress can be obtained as follows. The following boundary conditions are needed:

$$\begin{aligned}u(y = 0) &= 0 \\ u(y = h) &= U\end{aligned}$$

Integrating the x-direction component of Eq. (A.3) with respect to y and applying the above boundary conditions, an expression for u(y) can be obtained:

$$u(y) = \frac{1}{2\mu} \frac{dp}{dx} (y^2 - hy) + \frac{Uy}{h}\tag{A.4}$$

It should be noted that performing the integration in this way assumes that the viscosity is not a function of the distance from the liner in the cross-flow direction. However, for a shear-thinning fluid, the viscosity is a function of the local shear rate, which is given by the rate of change of the velocity in the cross-flow direction. Although many oils are shear-thinning fluids, it has been shown in [11] that accurate results can be obtained for these oils by approximating the viscosity as the piston speed divided by the average distance between the nominal lines defining the ring and liner surfaces. Therefore, the above integration is still valid even in these cases.

Shear stress is given by:

$$\tau(x) = \mu \left. \frac{\partial u}{\partial y} \right|_{y=0}$$

Using Eq. (A.4):

$$\tau(x) = \frac{\mu U}{h} - \frac{h}{2} \frac{dp}{dx} \quad (\text{A.5})$$

The volumetric flow rate can also be derived using the above results:

$$Q(x) = \int_0^h u(y) dy$$

Using Eq. (A.4):

$$Q(x) = -\frac{h^3}{12\mu} \frac{dp}{dx} + \frac{Uh}{2} \quad (\text{A.6})$$

A.2. Derivation of the Reynolds Equation

A relationship between the film height and width and the pressure distribution under the ring surface can be derived by applying conservation of mass and conservation of momentum to a fluid element under the ring surface.

Starting again with Eq. (A.3), the following boundary conditions can be applied, which assume that the motion of the ring surface occurs only in the x-direction:

$$\begin{aligned} u(y=0) &= 0 \\ u(y=h) &= U \\ w(y=0) &= 0 \\ w(y=h) &= 0 \end{aligned}$$

Integration of Eq. (A.3) and application of the above boundary conditions yields the following result:

$$\begin{aligned} u &= \frac{1}{2\mu} \frac{\partial p}{\partial x} y(y-h) + \frac{h-y}{h} U \\ w &= \frac{1}{2\mu} \frac{\partial p}{\partial z} y(y-h) \end{aligned} \quad (\text{A.7})$$

Substitution of Eq. (A.7) into the expression for conservation of mass given by Eq. (A.1) yields:

$$\frac{\partial}{\partial y}(\rho v) = -\frac{\partial}{\partial x}(\rho u) - \frac{\partial}{\partial z}(\rho w) \quad (\text{A.8})$$

The following boundary conditions will be applied [26,27]:

$$v(y = 0) = \frac{\partial h}{\partial t}$$

$$v(y = h) = 0$$

Now, integrating Eq. (A.8) with respect to y and applying the boundary conditions, assuming an incompressible lubricant, yields [26,27]:

$$\frac{\partial}{\partial x} \left(\frac{h^3}{\mu} \frac{\partial p}{\partial x} \right) + \frac{\partial}{\partial z} \left(\frac{h^3}{\mu} \frac{\partial p}{\partial z} \right) = 6U \frac{\partial h}{\partial x} + 12 \frac{\partial h}{\partial t} \quad (\text{A.9})$$

This is the two-dimensional Reynolds Equation for incompressible lubricants. This equation relates the pressure distribution in the oil film with the film height and width between the ring and the liner.

Appendix B: Metrics for Evaluating Friction Reduction

B.1. Determination of FMEP in the Friction Model

FMEP is a measure of the work done by friction normalized by the engine's displaced volume. It is thus a useful metric with which to compare the performance of different engines in a way that removes the effect of engine or component size. In this study, it is useful in that it provides a simple metric to use in order to evaluate and compare the performance of different piston ring designs.

The determination of the friction force was derived in Chapter 2 for pure hydrodynamic, mixed and pure boundary lubrication conditions. Friction power losses can be obtained from friction force by the following relationship:

$$P_f = UF_f \quad (\text{B.1})$$

In other words, the friction power loss at a given crank angle in the engine cycle can be determined by the product of the friction force and the piston velocity. FMEP is defined as follows:

$$FMEP = \frac{W_f}{V_d} \quad (\text{B.2})$$

To obtain the work done by friction from friction power losses, the following relationship is needed:

$$P_f = \frac{dW_f}{dt} \quad (\text{B.3})$$

This can be rearranged to yield:

$$W_f = \int P_f dt \quad (\text{B.4})$$

Substituting into Eq. (B.2) yields:

$$FMEP = \frac{\int P_f dt}{V_d} \quad (\text{B.5})$$

The friction model discussed in Section 2.4 provides the friction power loss of the different piston rings at each crank angle throughout the engine cycle as output. To convert from time to crank angle, the following relation is needed:

$$\omega = \frac{d\theta}{dt} \quad (\text{B.6})$$

where θ is the crank angle, and ω is the angular velocity of the crankshaft in radians per second. Rearranging and substituting this relationship into Eq. (B.5) yields:

$$FMEP = \frac{\int P_f d\theta}{\omega V_d} \quad (\text{B.7})$$

This integration is carried out numerically in the friction model described in Section 2.4, since friction power loss can be determined at every crank angle from Eq. (B.1).

B.2. Determination of FMEP from the Experimental Results

Before the determination of the FMEP for a given ring design can be described, some introductory comments are required. In particular, the exact definitions of gross IMEP, net IMEP and their relationship to BMEP and FMEP must be clarified.

IMEP defines the work that is delivered to the piston by the cylinder gases. In this study, IMEP was determined from the cylinder pressure data as follows:

$$IMEP = \frac{\int p dV}{V_d} \quad (\text{B.8})$$

The distance between the crank axis and the piston axis at any crank angle is given in [20]:

$$s = a \cos \theta + (l^2 - a^2 \sin^2 \theta)^{1/2} \quad (\text{B.9})$$

where a is the crank radius and l is the connecting rod length. The volume change at any crank angle can be expressed as:

$$dV = -\frac{\pi B^2}{4} \frac{ds}{d\theta} d\theta$$

where B is the bore diameter of the engine, and the negative sign is added to reflect the positive volume change induced by a reduction of the distance between the crank axis and the piston axis. Differentiating Eq. (B.9) and substituting it into the above expression yields:

$$dV = \frac{\pi B^2}{4} \left\{ a \sin \theta \left[1 + \frac{\cos \theta}{[l^2 - a^2 \sin^2 \theta]^{1/2}} \right] \right\} d\theta \quad (\text{B.10})$$

The displaced volume can be expressed as:

$$V_d = \frac{\pi B^2}{4} L \quad (\text{B.11})$$

where L is the stroke length of the engine. Substituting Eq. (B.10) and Eq. (B.11) into Eq. (B.8) yields the desired expression for IMEP:

$$IMEP = \frac{1}{L} \int p(\theta) \left\{ a \sin \theta \left[1 + \frac{\cos \theta}{[l^2 - a^2 \sin^2 \theta]^{1/2}} \right] \right\} d\theta \quad (\text{B.12})$$

The bounds of integration in Eq. (B.12) depend on whether or not the work done to flush out exhaust gases and bring in fresh charge, also called pumping work or PMEP, is to be included in the IMEP. If Eq. (B.12) is integrated over the compression and expansion strokes only, the result is referred to as gross IMEP, or $IMEP_g$. If Eq. (B.12) is integrated over the intake and exhaust strokes only, and the result is subtracted from the gross IMEP, this yields the net IMEP. In other words, gross and net IMEP are related as follows [20]:

$$IMEP_n = IMEP_g - PMEP \quad (\text{B.13})$$

BMEP defines the work that is available at the engine's crankshaft. Therefore, the relationship between gross IMEP, net IMEP, BMEP and FMPEP can be summarized as follows [20]:

$$\begin{aligned} IMEP_g &= BMEP + FMPEP + PMEP \\ IMEP_n &= BMEP + FMPEP \end{aligned} \quad (\text{B.14})$$

In principle, if the BMEP could be held exactly constant, the difference in FMPEP between two designs could be determined by comparing the net IMEP of each of the designs. In reality, there is some variation in the BMEP as the load cannot be perfectly controlled by the dynamometer.

As a result, the following process was used to determine the FMEP of a given design. First, the gross IMEP was determined by integrating the expression in Eq. (B.12) using cylinder pressure data taken over 1000 engine cycles from each of the cylinders over three test runs. The integration was carried out over the compression and expansion strokes for each of the 1000 cycles, six cylinders and three test runs, and the mean value from this data set is the desired gross IMEP. This process was repeated over the entire cycle to determine the net IMEP. The average BMEP was obtained from a set of torque values that were measured from the dynamometer at a rate of 1 Hz for a 5 minute sampling period (or 1 measurement per second). BMEP was determined from torque by dividing by the engine's displaced volume. FMEP was then determined as the difference between the net IMEP and the BMEP. The change in FMEP between designs was evaluated by finding the difference between the FMEP for each of the individual designs. There was therefore a significant amount of error introduced while finding this value, since it is the result of two subtractions and two averaging processes. This error is discussed in detail and quantified in the section that follows.

B.3. Error Analysis of the Experimental Results

For each of the rings that were tested, a statistical analysis was conducted to determine whether or not a reduction in the mean FMEP was achieved. This section begins with a detailed description of this calculation, followed by a short description of the determination of the error in the experimentally measured oil consumption and blowby values.

BMEP data was first obtained for each of the three test runs. Since the data was taken at a rate of 1 sample per second, and this test was conducted over a period of 5 minutes, 300 values were obtained in total for each test. The mean and standard deviation of this data set was taken for each ring design that was tested.

Gross IMEP data was then obtained from the cylinder pressure data as described in the previous section. 1000 cycles of data were taken in each of the six cylinders for the three test runs, yielding a sample size of 18,000 of gross IMEP values. The mean and standard deviation for this data set was determined. A similar approach was also to determine the mean and standard deviation for the PMEP.

The procedure described in the previous section was then used to determine the change in FMEP between two designs once gross IMEP, PMEP and BMEP were determined. As mentioned previously, since each of these values has an average and a standard deviation, a significant amount of error was introduced in manipulating these values.

The following general equation was used to determine the error as a result of a calculation. For a function of two variables, $f(x_1, x_2)$, if the errors in the independent variables were Δx_1 and Δx_2 , the error as a result of an operation is determined by [28]:

$$\Delta f(x_1, x_2) = \sqrt{\left(\frac{\partial f}{\partial x_1} \Delta x_1\right)^2 + \left(\frac{\partial f}{\partial x_2} \Delta x_2\right)^2} \quad (\text{B.15})$$

For example, since net IMEP is determined by the difference between the gross IMEP and PMEP, the associated error was determined as:

$$\Delta IMEP_n = \sqrt{(\Delta IMEP_g)^2 + (\Delta PMEP)^2}$$

This error propagation was carried out for each of the subtractions involved in the determination of the difference in the FMEP between two designs. However, using this method, the error in the result always ended up being larger than the value itself. As a result, a statistical approach was required to assess whether or not there was a difference in the mean FMEP values between different designs.

For this purpose, a hypothesis test was conducted [24]. In this approach, a hypothesis is made about a quantity of interest, in this case, the difference in the FMEP values between two different ring designs. The initial hypothesis is that the difference between the FMEP values between two designs is actually zero. The idea is to use statistical evidence to reject this hypothesis within a certain level of confidence.

Specifically, the hypothesis that the difference in the mean FMEP values between two tests is zero can be rejected provided that:

$$z_0 = \frac{\bar{x}_1 - \bar{x}_2 - \Delta_0}{\sqrt{\frac{\sigma_1^2}{n_1} + \frac{\sigma_2^2}{n_2}}} > z_\alpha \quad (\text{B.16})$$

where \bar{x}_1 and \bar{x}_2 are the mean FMEP values for the ring designs being compared, Δ_0 is the hypothesized value of the difference in the mean values (zero in this case), σ_1 and σ_2 are the standard deviations associated with the mean FMEP values, and n_1 and n_2 are the associated sample sizes. z_α is a value obtained from the standard normal distribution for a given α , which is a measure of the confidence with which the conclusion can be reached. In this study, a 95% confidence interval was used, which corresponds to $\alpha=0.05$.

An example is used to illustrate this approach as well as the process used to conduct the error analysis in this study. For this purpose, the low-tension oil control ring results will be used. The mean values and associated standard deviations from data obtained from the baseline test and the low-tension OCR test are summarized in Table B-1 below.

	Baseline	Low-Tension OCR
BMEP (psi)	200.848 ± 0.152	200.998 ± 0.141
IMEP _n (psi)	221.610 ± 13.094	220.118 ± 8.251
FMEP (psi)	20.762 ± 13.095	19.120 ± 8.252

Table B-1: Data Summary

To determine the associated error in the FMEP, the statistical analysis described above was used with the following values:

$$\bar{x}_1 = 20.762$$

$$\bar{x}_2 = 19.120$$

$$n_1 = n_2 = 18,000$$

$$\sigma_1 = 13.095$$

$$\sigma_2 = 8.252$$

$$\alpha=0.05$$

With these values, the hypothesis that the mean FMEP was the same for the low-tension OCR design as for the baseline design could be rejected because the criteria defined in Eq. (B.16) was met. Specifically, by substituting the above values into Eq. (B.16), the following result is obtained: $14.237 > 1.645$.

The error on the difference in FMEP within 95% confidence can be determined as follows:

$$Error = z_{\alpha/2} \sqrt{\frac{\sigma_1^2}{n_1} + \frac{\sigma_2^2}{n_2}} \quad (B.17)$$

With $z_{\alpha/2} = 1.96$, the error on the FMEP within 95% confidence is 0.226 psi. In kPa, the mean value and error associated with the difference in FMEP for the case of the low-tension oil control ring is 11.17 ± 1.54 . This is the result that appears in Table 5-4.

The error in the blowby data was determined by calculating the standard deviation based on the sample of 300 data points obtained from the blowby flow meter over the five minute averaging period for the three test runs that were considered. To determine the error in oil consumption measured experimentally, it was assumed to be possible to read the refill meter within an accuracy of 1%. Since this value was measured several times and averaged, the overall error was determined by applying the method in Eq. (B.15).

Oil consumption was not determined using the model and therefore no comparison could be made between the model and the experiment. Blowby was measured experimentally and was determined by the model, and a comparison could be therefore be made directly. The change in FMEP between designs was also compared directly. Some explanation should be given to justify this comparison. This is provided in the following section.

B.4. Comparison of FMEP between Model and Experiment

The model and the experiment use slightly different approaches to determine FMEP. In the model, the same cylinder pressure (and therefore IMEP) is used as input and the ring design parameters are varied. The FMEP contribution from the ring pack is provided as output from the model. In the experiment, the FMEP is determined by fixing the BMEP, and by measuring the change in cylinder pressure (and therefore IMEP) resulting from a change in the ring design. These two methods are entirely equivalent. The model's approach assumes that the changes in the ring design affect BMEP, whereas the experimental approach allows the changes in the ring design to affect IMEP. To ensure a consistent comparison between the experimental data and the results from the model, the experimentally measured cylinder pressure data from the baseline case was used as input into the model for all of the different cases considered. This is equivalent to fixing the IMEP. In the experimental approach, BMEP is fixed and the variation in net IMEP between the cases considered reflects the change in the FMEP of the ring pack.

Appendix C: Metrics for Assessment of Results

C.1. Brake Thermal Efficiency

Brake thermal efficiency is given by the following expression [20]:

$$\eta = \frac{P_b}{m_f \dot{Q}_{LHV}} \quad (C.1)$$

The following data was reported by Waukesha for the engine under consideration in this study:

$$\eta_{old} = 0.37$$

$P_{b,old} = 495$ hp (brake power before improvement through friction reduction)

$P_{f,old} = 83$ hp (friction power loss before improvement through ring design changes)

To estimate the improvement in brake thermal efficiency resulting from the reduction in piston ring friction, the following two assumptions will be made:

- The rings are assumed to account for 20% of the total engine friction
- The increase in available energy resulting from the reduction in friction power losses is assumed to translate directly into higher brake power for a given fuel input

Therefore,

$$m_f \dot{Q}_{LHV} = const.$$

The improved efficiency resulting from the reduction in friction power losses is given by:

$$\eta_{improved} = \left(\frac{P_{b,old} + \Delta P_f}{P_{b,old}} \right) \eta_{old} \quad (C.2)$$

A friction reduction of 35% from the baseline value corresponds to the following change:

$$\Delta P_f = (0.35)(0.2)(83 \text{ hp}) = 5.8 \text{ hp}$$

Therefore, the improved brake thermal efficiency is:

$$\eta_{improved} = \left(\frac{495 + 5.8}{495} \right) (0.37) = 0.375$$

Therefore, an improvement in brake thermal efficiency of 0.5% is expected from a reduction in friction of 35%. It should be noted that this result is based on a conservative estimate of the contribution of the piston rings to the total engine friction. If the contribution of the rings to overall engine friction were doubled, for example, the improvement in brake thermal efficiency would be closer to 1%.

C.2. Fuel Cost

If the engine is operated at a constant brake power output for a specific application, the reduction in friction will result in lower fuel consumption. The reduction in fuel consumption and reduction in fuel cost can be estimated for this case.

The following data was reported by Waukesha for the engine under consideration in this study. The exception is the lower heating value and density of natural gas, which was obtained from [20].

$$\eta_{old} = 0.37$$

$$P_{b,old} = 495 \text{ hp} = 1258290 \text{ Btu/hr}$$

$$Q_{LHV} = 45 \text{ MJ/kg} = 19347 \text{ Btu/lb}$$

$$\rho = 0.8 \text{ kg/m}^3 = 49.8 \text{ lb/1000 ft}^3 \text{ (at 1 atm, 0}^\circ\text{C)}$$

To calculate the reduction in fuel consumption and cost associated with the reduction in friction power losses, the following assumptions were used:

- The rings are assumed to account for 20% of the total engine friction
- The increase in available energy resulting from the reduction in friction power losses is assumed to translate directly into lower fuel consumption for a given power output
- The lower heating value of natural gas is constant

- The price of natural gas was assumed to be \$8.50 per thousand cubic feet (estimated based on data from [25] for commercial use)
- An 80% capacity factor is assumed for the operation of the Waukesha engine to account for any maintenance that might be needed or downtime that might be experienced

The original fuel consumption of the engine can be determined from the above data:

$$\dot{m}_{f,old} = \frac{P_b}{\eta_{old} Q_{LHV}} = \frac{1258290}{(0.37)(19347)} = 175.78 \text{ lb/hr}$$

Information from the calculation presented in Appendix C.1 will be used here as well. In particular, the improvement in efficiency that is achievable from a 35% reduction in friction will be assumed to be 0.5%, for a conservative estimate.

Since $P_b = \text{const.}$, and $Q_{LHV} = \text{const.}$, the following relationship can be used to determine the reduction in fuel consumption:

$$\dot{m}_{f,improved} = \dot{m}_{f,old} \frac{\eta_{old}}{\eta_{new}} \quad (\text{C.3})$$

Therefore, the improved engine fuel consumption for this case is:

$$\dot{m}_{f,improved} = (175.78) \frac{0.37}{0.375} = 173.43 \text{ lb/hr}$$

Therefore, the reduction in the amount of fuel used per year is:

$$\Delta \dot{m}_f = (2.35 \text{ lb/hr})(24 \text{ hrs/day})(365 \text{ days/year})(0.8) = 16470 \text{ lb/year}$$

In terms of volume, this corresponds to the following reduction of natural gas used per year:

$$\Delta V_f = \frac{(16470 \text{ lb/year})}{49.8 \text{ lb}/1000 \text{ ft}^3} = 330723 \text{ ft}^3 / \text{year}$$

The reduction in cost associated with the 2.35 lb/hr reduction in natural gas consumption over a one year period is:

$$\Delta \text{Cost} = \frac{(\$8.50 / 1000 \text{ ft}^3)(2.35 \text{ lb/hr})(24 \text{ hrs/day})(365 \text{ days/year})(0.8)}{(49.8 \text{ lb}/1000 \text{ ft}^3)} = \$2800 / \text{year}$$